
On Noise and Single-Cell Expression Dynamics in Toxin-Driven Bacterial Competition

Alexandra Götz



Munich 2020

On Noise and Single-Cell Expression Dynamics in Toxin-Driven Bacterial Competition

Alexandra Götz

PhD thesis
at the Faculty of Physics
at Ludwig-Maximilians-Universität
Munich

handed in by
Alexandra Götz
from Ravensburg

Munich, Februar 26th 2020

Corrector: PD Dr. Madeleine Opitz

2nd Corrector: Prof. Dr. Erwin Frey

Tag der mündlichen Prüfung: 19.05.2020

**Über den Zusammenhang zwischen
stochastischer
Einzelzell-Toxinproduktionsdynamik und
bakteriellem Populationsfortbestand**

Alexandra Götz



München 2020

Zusammenfassung

Komplexe mikrobielle Gemeinschaften bestehen aus vielen verschiedenen Bakterienstämmen die eine Vielzahl an Interaktionsmöglichkeiten miteinander besitzen. Vor allem in Umgebungen die vielen Schwankungen ausgesetzt sind, ist die Stabilität eines solchen Ökosystems ein wichtiges Überlebenskriterium. Es ist jedoch noch kaum bekannt welche Faktoren die dynamischen Prozesse der bakteriellen Interaktion beeinflussen und wie sich die dadurch veränderten Prozesse auf den bakteriellen Wettbewerb auswirken. Die Interaktion von verschiedenen Bakterienstämmen kann z.B. durch die Produktion und Abgabe von allgemein nutzbaren Substanzen (z.B. Proteine,...) erfolgen. Daher ist es wichtig die Produktionsdynamiken solcher Substanzen in einzelnen Zellen (mikroskopische Interaktionsebene) zu untersuchen um ihren Einfluss auf die Zusammensetzung komplexer Ökosysteme (makroskopische Interaktionsebene) verstehen zu können. Dabei ist eine quantitative Analyse spezifischer Interaktionsparameter von besonderem Interesse, wie z.B. ihre Produktionsmenge und ihr Abgabezeitpunkt, um zu verstehen wie sich Änderungen dieser Parameter auf das Wettbewerbsergebnis zwischen den Interaktionspartnern auswirken. Ein weiterer wichtiger Faktor, der diese Parameter und damit den bakteriellen Wettbewerb beeinflussen kann ist stochastisches Rauschen.

In dieser Arbeit wird das plasmidkodierte ColicinE2 System von *Escherichia coli* als Modellsystem genutzt um oben genannte Aspekte zu studieren. Ein wichtiger Faktor der Interaktionen bei denen ein solcher Stamm beteiligt ist, ist die Produktion und Abgabe eines Toxins (Colicin genannt), das nahe verwandte Bakterien tötet. Daher wird in dieser Arbeit in einer Kombination aus experimenteller und theoretischer Analyse untersucht welchen Einfluss Einzelzellparameter wie der Zeitpunkt der Toxinabgabe und die Menge des abgegebenen Toxins auf den makroskopischen bakteriellen Wettbewerb (Populationsebene) haben. Des Weiteren wird analysiert welche regulatorische Mechanismen des ColicinE2 Systems das Rauschen von Toxinproduktionsmenge und Abgabezeitpunkt des Toxins kontrollieren. Abschließend wird der Wettbewerb zwischen einem toxinproduzierenden C-Stamm und einem toxinsensitiven S-Stamm untersucht und wie sich die zuvor untersuchten Expressionsdynamiken der einzelnen

Zellen und Stochastizität der Genexpression auf den Wettbewerb zwischen dem C-Stamm und dem S-Stamm auswirken.

Anhand dieser Untersuchungen konnte ich zeigen, dass die Toxinexpressionsdynamik und deren Rauschen im ColicinE2 System hauptsächlich durch globale Regulatoren wie die Proteine LexA oder CsrA kontrolliert werden. Im Bezug auf CsrA sind vor allem die Verfügbarkeit von freiem CsrA und welche Regulationskomponenten diese Verfügbarkeit steuern wichtig. Dabei konnte ich einzelsträngige DNA, die bei der Replikation des Colicinplasmids entsteht, als neuen Regulationsfaktor für freies CsrA identifizieren. Außerdem konnte ich zeigen, dass sich der Metabolismus der Bakterienzelle auf die Dynamiken der Toxinproduktion auswirkt und der Abgabezeitpunkt des Toxins mit der abgegebenen Colicinmenge korreliert. Des Weiteren konnte ich zeigen, dass sich die Toxinexpressionsdynamiken auf das Resultat des bakteriellen Wettbewerbs auswirken und dass sowohl die abgegebene Toxinmenge als auch eine zeitlich heterogene Toxinabgabe wichtig für den Wettbewerbserfolg der colicinproduzierenden Population sind.

Summary

Complex microbial communities are composed of a multitude of bacterial strains that interact with each other in many different ways. Stability of such systems is crucial for their long-term survival, especially in fluctuating environments. It is still largely unknown what factors influence bacterial interaction dynamics and how they affect bacterial competition. But, the interaction of strains can be driven by the production of toxins or public goods. Therefore, it is crucial to get further insight into the gene expression dynamics of these compounds in order to understand the development of such complex ecosystems. Factors affecting bacterial competition such as the timing of release of interacting components and the amount being released into the environment have to be studied in order to determine their influence on competition outcome. Additionally, it is unknown how noise in gene expression dynamics of interacting compounds and the resulting release distributions influence bacterial competition.

In this study, the plasmid encoded toxin producing ColicinE2 system of the well-known organism *Escherichia coli* was used as a model system. Bacterial interactions involving this strain are driven by the production and release of a toxin called colicin which kills closely related competitors. Therefore, in this combined experimental and theoretical study, toxin expression dynamics were investigated and how they determine the timing and amount of toxin being released. Additionally, mechanisms of noise control of both, toxin production and release in the ColicinE2 expression system were analyzed. Finally, the influence of stochasticity in single-cell expression dynamics and toxin production on bacterial competition outcome between a colicin producing strain and a toxin sensitive strain were investigated.

Using this analysis, I was able to show that both toxin expression dynamics and noise in the ColicinE2 system are mainly controlled by globally acting regulatory proteins such as LexA and CsrA. Regarding CsrA, factors affecting the availability of free CsrA play an important role. Furthermore, I was able to identify single-stranded DNA produced by replication of the toxin producing plasmid as a new, previously unknown regulatory component influencing CsrA abundance in the cell. In addition, I could show that the metabolism of the bacterial cell influences the timing of toxin

Summary

release, which is in turn correlated to the actual amount of released toxin. Finally, I could show how these toxin expression dynamics affect competition outcome for colicin driven bacterial interaction and could determine the importance of high toxin amounts as well as heterogeneity in toxin release timing for the competitive success of the colicin producing population.

Contents

Zusammenfassung	vii
Summary	ix
Publicationlist	xiii
1. Introduction	1
2. Background Information	5
2.1. SOS Response and Toxin Expression	5
2.1.1. ColicinE2 System and Regulation Mechanisms	6
2.2. Stochasticity and Noise in Gene Expression	10
2.2.1. Quantification of Noise	13
2.3. Bacterial Interaction	16
2.3.1. Colicin Driven Competition	18
3. Material and Methods	21
3.1. Cloning	21
3.1.1. Construction of Fluorescent Reporter Plasmid	21
3.1.2. Mutant Overview	24
3.2. Single-Cell Expression Dynamics	26
3.2.1. Measurement Procedure	26
3.2.2. Analysis	28
3.2.3. Gelelectrophoresis	31
3.3. Population Experiments	34
3.3.1. Measurement Procedure	34
3.3.2. Analysis	37
3.4. Simulation	39
3.4.1. Two-strain Interaction Model	39
3.5. Additional Software	44

4. Results: Single-cell Expression Dynamics in the ColicinE2 System	45
4.1. Toxin Expression Dynamics in Single Bacterial Cells	45
4.1.1. Control of ColicinE2 Expression Dynamics	45
4.1.2. Post-transcriptional Regulation by CsrA Controls the Time- point of Toxin Release	49
4.1.3. How Metabolism Affects Toxin Expression Dynamics	57
4.2. Effects of Toxin Release Dynamics on Population Fate	59
4.2.1. Population Growth is Dependent on Switching of Cells into the ON State	59
4.2.2. Toxin Amounts Being Released Depend on Toxin Release Time	63
4.3. Discussion	65
4.3.1. Single-cell Toxin Dynamics	65
4.3.2. Single-cell Dynamics Determine Single-strain Population Behavior	67
4.3.3. Summary	68
5. Results: Toxin Expression Dynamics Shape Two Strain Bacterial Compe- tition	71
5.1. Competition Success of Toxin Producers is Coupled to Toxin Expression Dynamics	71
5.2. The Importance of Toxin Release Time and Toxin Amount on Bacterial Competition	76
5.2.1. Competition with Similar Single-strain Growth of S and C Strains	76
5.2.2. Competition of a C Strain with a Faster Growing S Strain . . .	79
5.3. Introduction of Time-fluctuations/ Increased Stochasticity in Two-strain Competition Model	82
5.3.1. Implementation of Noise in the Two-strain Bacterial Interaction Model	82
5.3.2. Influence of Noise in Toxin Release on Bacterial Interaction . . .	84
5.4. Discussion	88
6. Results: Noise Generation in the Toxin Expression System	91
6.1. Quantification of Noise in Toxin Production and Release	92
6.2. Noise Control in the ColicinE2 System	99
6.2.1. How Transcriptional Regulation Affects Noise Generation	100
6.2.2. How Post-transcriptional Regulation Affects Noise Generation .	101
6.3. How Global Factors Influence Noise Generation	104

6.4. Discussion	106
7. Conclusion	111
8. Outlook	115
A. Media and Buffers	117
A.1. M63 Medium	117
A.2. Buffers	118
A.2.1. TAE Gel Electrophoresis	118
A.2.2. Gel Shift Binding Assay	119
B. Simulation Parameters	121
C. Details for Significance Analysis	123
C.1. Significance Analysis for Chapter 4	123
C.2. Significance Analysis for Chapter 6	125
Acronyms	129
List of Figures	131
List of Tables	133
Bibliography	135

Publicationlist

Publications related to results sections of this thesis

- AG1 **A. Götz**, M. Lechner, A. Mader, B. von Bronk, E. Frey, M. Opitz (2018), CsrA and its regulators control the time-point of ColicinE2 release in *Escherichia coli*. *Scientific Reports* 8, 6537.
- AG2 **A. Goetz**, A. Mader, B. von Bronk, A. S. Weiss, M. Opitz (2020), Gene expression noise in a complex artificial toxin expression system. *PLOS ONE* 15, e0227249 (2020).
- AW1 Anna S. Weiß¹, **Alexandra Goetz**¹, Madeleine Opitz (2020), Dynamics of ColicinE2 production and release determine the competitive success of a toxin-producing bacterial population. *Scientific Reports*. (*accepted for publication*)

Some of the figures presented in this thesis are adapted from the above listed first author publications under the CC BY 4.0 license. The corresponding figure captions specify the related publication.

Publications supplementing the work presented in this thesis

- SK1 S. Kesel, B. von Bronk, C. Falcón García, **A. Götz**, O. Lieleg, M. Opitz (2017), Matrix composition determines the dimensions of *Bacillus subtilis* NCIB 3610 biofilm colonies grown on LB agar. *RSC Adv.* 7, 31886-31898.
- BB1 B. von Bronk, S. A. Schaffer, **A. Götz**, M. Opitz (2017), Effects of stochasticity and division of labor in toxin production on two-strain bacterial competition in *Escherichia coli*. *PLOS Biology* 15, 1-25.
- BB2 B. von Bronk, **A. Götz**, M. Opitz, Complex microbial systems across different levels of description (2018). *Physical Biology* 15: 051002.
- BB3 B. von Bronk, **A. Götz**, M. Opitz (2019), Locality of interactions in three-strain bacterial competition. *Physical Biology* 16(1):016002.

¹contributed equally

- CFG1 C. Falcón García, F. Stangl, **A. Götz**, W. Zhao, S. A. Sieber, M. Opitz, O. Lieleg (2019), Topographical alterations render bacterial biofilms susceptible to chemical and mechanical stress. *Biomaterials Science*.
- MK1 M. Klotz, M. Kretschmer, **A. Goetz**, S. Ezendam, O. Lieleg, M. Opitz (2019), Importance of the biofilm matrix for the erosion stability of *Bacillus subtilis* NCIB 3610 biofilms. *RSC Advances* 9, 11521-11529.

1. Introduction

In nature, the stability of a microbial ecosystem is a key factor for its resilience and long term survival. To understand how such highly diverse, long-term stable systems of complex microbial compositions interact with each other, it is important to understand which mechanisms drive population fate of competing or cooperating single bacterial strains with each other. Starting with single-cell level interaction, the genetic regulation and environmental influences coordinating cell response play a vital role in determining the fate of a population. Stochastic fluctuations determine many processes both inside and outside of the cell, leading to variations in interaction dynamics over time. In order to understand or even predict the fate of such complex ecosystems, it is crucial to get further insight into the intricate processes driving gene expression dynamics (GED) of compounds produced by the single players within the ecosystem. These compounds can for example be toxins or public goods and the aim is to understand how their expression dynamics shape the formation of stable ecosystems.

In this study, the plasmid encoded ColicinE2 system of the well-known bacterial organism *Escherichia coli* was chosen as a model system. The ColicinE2 operon produces and releases a toxin called colicin that drives its own competition success by killing of closely related bacteria via the colicin (expressed by the *cea* gene). However, the cost for colicin release is cell lysis as a way to release the toxin into the environment. This mechanism is encoded by the gene *cel* of the ColicinE2 operon. The release of toxin by cell lysis benefits the population as a whole, but not the single toxin producers themselves. The ColicinE2 system has a complex, multi-layered regulation of gene expression on both the transcriptional and post-transcriptional level. Expression of the ColicinE2 operon is under the control of the SOS response of the cell by transcriptional repression via the protein LexA. SOS response is an important mechanism controlling expression of numerous genes in response to DNA damage within a bacterial cell [1–3]. Post-transcriptional regulation of the gene leading to cell lysis (*cel* gene) is mainly controlled by the global carbon storage regulator protein CsrA [4, 5], which also regulates a plethora of other genes in a cell [6, 7] and is part of the central carbon metabolism of the cell [7–9]. The presence of transcriptional and post-

transcriptional regulatory modules controlling colicin production and release in the ColicinE2 system is an ideal model system to investigate toxin expression dynamics (TED) and how TED is controlled by these regulatory units in order to increase the competitive success of the toxin producing strain. From previous studies it is known that stochastic processes in cell positioning and heterogeneity within gene expression of toxin producing genes can change competition results [10, 11]. The main question of this thesis is how the noisy GED of the interacting compound colicin determines competition outcome between a colicin producing and a sensitive strain (Figure 1.1). To answer this question, a quantitative experimental and theoretical analysis over a broad range of interaction levels was performed. Levels of investigation start with GED on the single-cell level over the single-strain population level and formation of different phenotypes within this population to the multi-strain interaction level and formation of complex colonies (see Figure 1.1). In this thesis, the underlying biological and theoretical background information concerning the ColicinE2 system, noise in gene expression and basic interaction mechanisms for colicin driven competition are introduced in Chapter 2. In Chapter 3 the used biophysical techniques ranging from single-cell time-lapse microscopy up to two-strain interaction range-expansion experiments are explained and model parameters of the theoretical model accompanying the experimental findings are introduced. Starting with a quantitative investigation on the gene expression level, single-cell TED are investigated in Chapter 4. In particular, an analysis of the noisy gene expression of toxin production and release is performed, and the impact of extracellular components such as nutrient availability and stress affecting above described regulatory components and thus TED is investigated. Furthermore, how these changes in TED shape the single-cell response and the formation of phenotypes within the population is analyzed. Additionally, it was studied how the formation of such phenotypes, e.g. existence of producers and reproducers within the population caused by TED variation shapes the fate of the toxin producing population (C strain, see Figure 1.1, green). A single-strain population can be composed of different phenotypes from one genotype, e.g the formation of toxin producers and reproducers in the C strain population (Figure 1.1). In Chapter 5 the knowledge of the ColicinE2 expression dynamics is used to further investigate how TED shape the interaction of the toxin-producing strain with a toxin-sensitive S strain (Figure 1.1 red). Starting from single-cell interaction up to macroscopic range expansion competition outcome, a combined experimental and theoretical analysis is used to identify main interaction mechanisms and their impact on competition outcome.

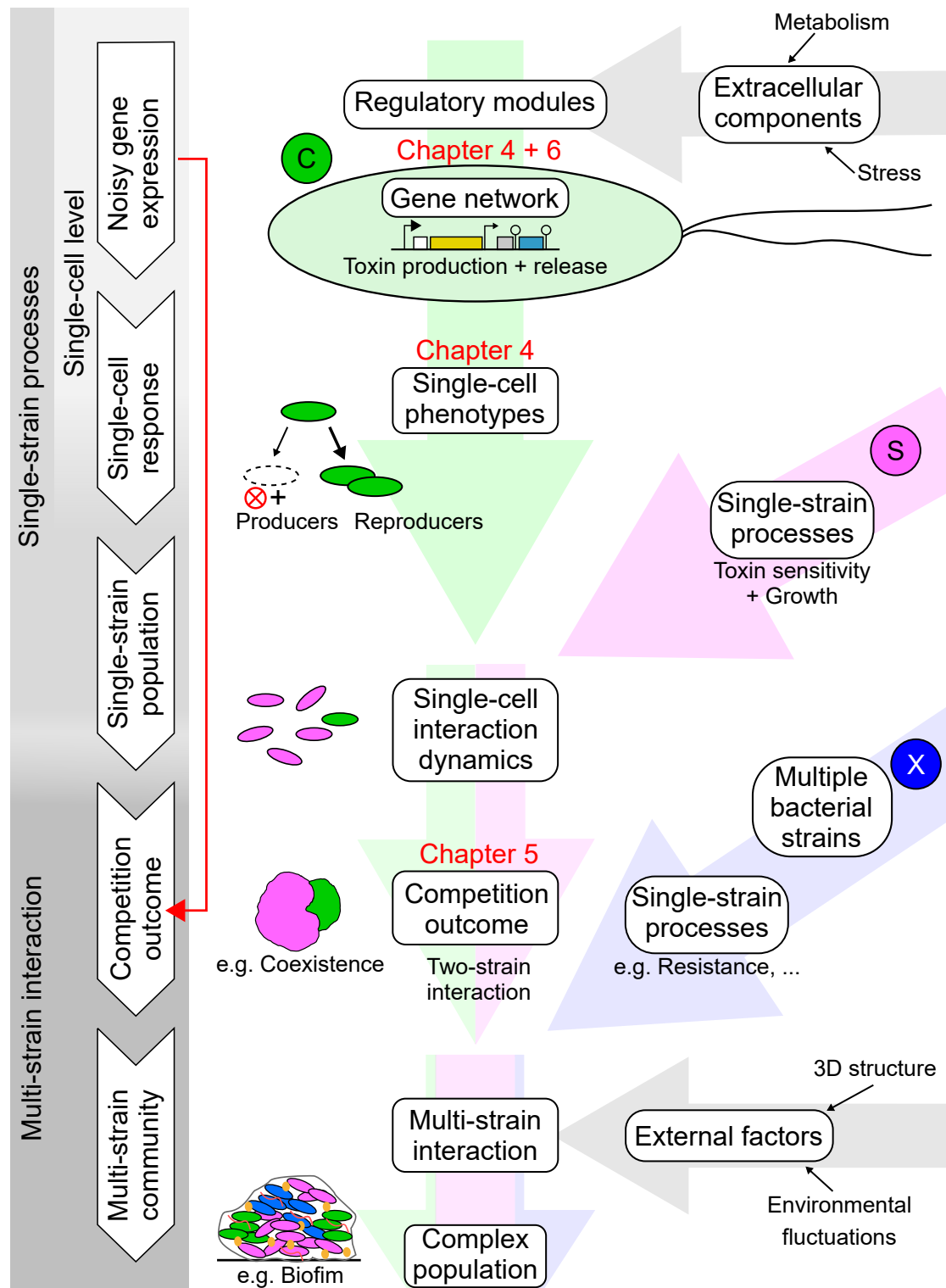


Figure 1.1

How single-cell gene expression affects multi-strain dynamics. Bacterial strains contributing to competition are marked in different colors (C: colicin producers, green; S: sensitive strain, magenta; X: additional strain, blue). Levels of interaction are marked by bold arrows (left). All strains contributing to interactions C, S and X are controlled by their own single-cell response which can result in single-cell phenotypes with different growth, toxin sensitivity (e.g. for S strain) or even toxin resistance. Multi-strain communities are created by interactions between multiple strains and can create complex populations such as biofilms, which can consist of many bacterial strains and their various produced interacting compounds (gray, orange and red in sketch). 3

In the following Chapter 6, single-cell analysis of GED within the ColicinE2 operon is performed in order to identify the regulators controlling noise generation in both toxin production and release of the ColicinE2 operon.

Subsequently, conclusions on how gene expression dynamics determine toxin driven two-strain interaction are made in Chapter 7 (Figure 1.1) and the importance of noise and stochasticity in TED for the competitive success of the toxin producing population are explained.

Finally, in Chapter 8 the findings of the ColicinE2 system are used to formulate their possible impact on complex microbial ecosystems such as bacterial biofilms (Figure 1.1) which can be created by interaction of multiple strains which can produce different interacting components. In these multi-strain interactions, the single-strain processes of each strain, such as different growth rates or variation in toxin sensitivity contribute to multi-strain interaction dynamics (Figure 1.1). Combining these cell interactions with environmental factors like 3D structure or environmental fluctuations, complex microbial populations can arise that can be stable in a multitude of conditions. However, detailed knowledge on composition and formation of these systems facilitates targeted disruption of unwanted microbial populations. This outlook for complex populations demonstrates the significance of understanding GED of interacting compounds produced by all players contributing to multi-strain interaction.

2. Background Information

To better understand the formation of complex multi-strain systems, it is important to understand underlying mechanisms driving interaction within these systems. For this, the underlying gene expression dynamics (GED) of interacting compounds between strains have to be elucidated and how they shape single-strain fate. However, the GED for the ColicinE2 system are inherently noisy and they are under the control of complex regulation mechanisms. To better understand how processes on the genetic level or determined by the environment affect competition outcome and GED, the following chapter explains basic mechanisms of gene regulation for the ColicinE2 system and introduces background information for interaction processes between strains. Additionally, fundamental information for the interaction parameters of the theoretical model are explained and methods for quantification of noise in the toxin expression system are introduced.

2.1. SOS Response and Toxin Expression

Many bacteria have developed the production of a toxin as natural defense mechanism against intruders into their habitat or other strains inhabiting the same environment [12, 13]. Among the many classes of killing agents produced by different bacterial strains are the bacteriocins, which are produced by a broad range of bacteria including the well known organisms *Escherichia coli* and *Pseudomonas aeruginosa* [12].

Bacteriocins that are produced by *Escherichia coli* are called colicins and are mostly plasmid encoded [12]. Their categorization into two groups is performed according to their uptake mechanism into the competitor cell [12, 14]. For example, group A colicins are colicins that are imported through the Tol system, whereas B group colicins are imported via the TonB system [14].

Most bacteriocins are specific for closely related strains e.g. *E. coli* colicins can kill other *E. coli* strains or varying members of *Enterobacteriaceae* [15]. However, according to mechanisms like their various modes of action of the colicin and different release and uptake mechanisms into target bacteria, colicins can be divided into a

multitude of categories [14]. Generally, the production of colicins is regulated by an SOS promoter which is under the control of the SOS response system in a bacterial cell. The SOS system of *E. coli* can switch between the states OFF and ON and thus constitutes a bistable system that is regulated with a double-negative feedback loop [16, 17]. In the OFF state transcription of the operon is repressed by LexA. In the ON state, when DNA damage is detected in the cell, the SOS response is triggered causing high expression of the genes in the colicin operon.

Furthermore, it is important to note, that genes under the induction of SOS promoters are known to be heterogeneously expressed [18]. The same was found in previous studies on colicins and specifically the ColicinE2 system [13]. The degree of heterogeneity was found to be dependent on the level of induction. Gene expression in the operon ranges from heterogeneous timing at low stresses, where the cells switch into the ON state over the time-course of the whole measurement, to a synchronous response at high stress induction, where cells switch almost simultaneously early on [13]. Applying this knowledge to bacterial interactions, von Bronk *et al.* [10, 11] have described how heterogeneity in the intermediate regime of induction gives the colicin producing strain an advantage in competition with other, sensitive strains.

2.1.1. ColicinE2 System and Regulation Mechanisms

In Chapters 4 and 6 of this thesis the mechanisms controlling single-cell expression dynamics as well as noise control of the ColicinE2 operon will be investigated. However, to get a better insight into the controlling mechanisms and identify regulatory modules, it is necessary to know the exact genetic details of the ColicinE2 operon contributing to toxin expression and release. Therefore, in the following the underlying genetic network of the ColicinE2 operon and main known regulator will be described in more detail.

Transcriptional Regulation In Figure 2.1 A the transcriptional regulation level of the colicin operon is shown. The ColicinE2 operon contains gene sequences for a colicin (*cea*), an immunity gene (*cei*) and gene whose expression leads to cell lysis (*cel*). The operon is under the control of an SOS promoter that is repressed by LexA when no external stress is present. Induction with stress leads to cleavage of LexA by RecA and thus transcription of the ColicinE2 operon. The transcriptional terminators T_1 and T_2 stop transcription. In the case of transcription stop at T_1 , transcription only happens for a fraction of transcription events, leading to a smaller probability

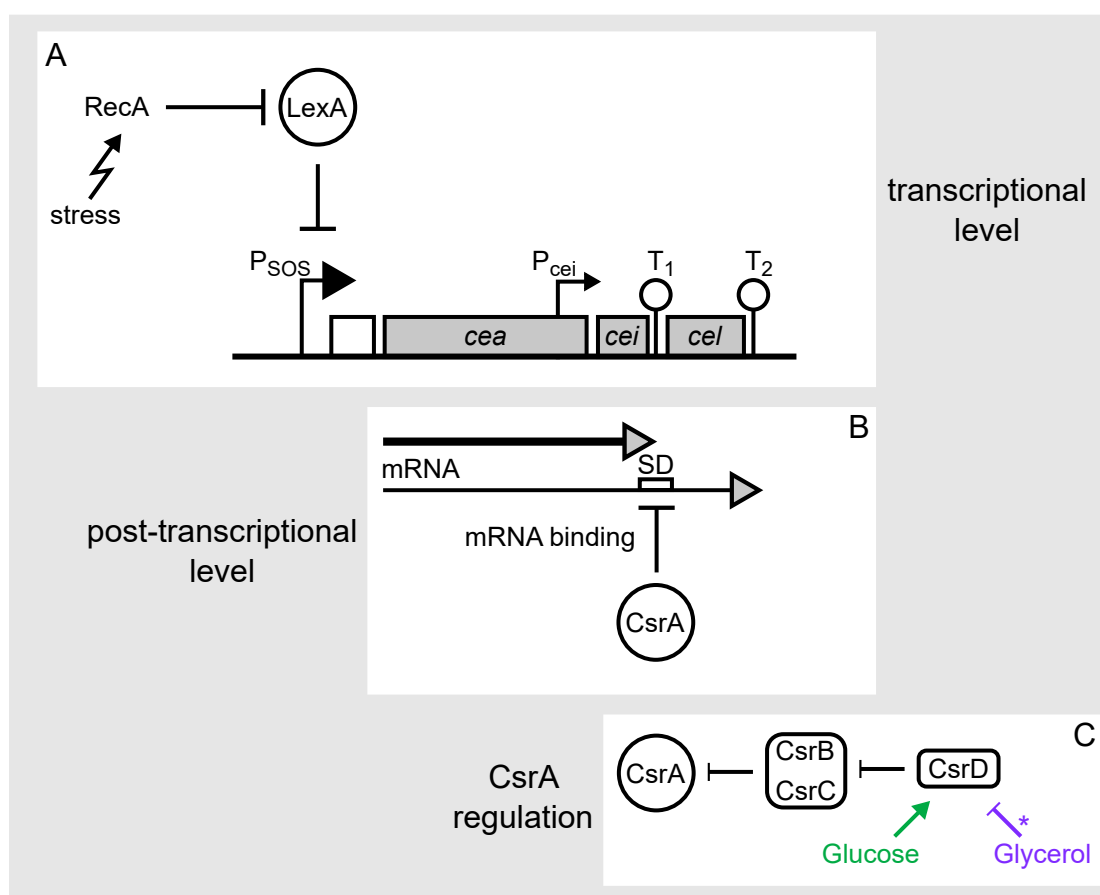


Figure 2.1

Gene regulation of the ColicinE2 system. A) Transcriptional level: The ColicinE2 operon contains gene sequences for a colicin (*cea*), an immunity gene (*cei*) and a gene leading to cell lysis (*cel*). The operon is under the control of an SOS promoter that is repressed (\top) by LexA when no external stress is present. Induction with stress leads to cleavage of LexA by RecA and thus transcription of the ColicinE2 operon. P_{cei} is an additional constitutive promoter for the immunity gene to facilitate toxin resistance even without stress. The transcriptional terminators T_1 and T_2 stop transcription. In the case of T_1 only for a fraction of transcription events. B) Post-transcriptional level: Upon SOS induction long and short mRNA are transcribed. Short mRNA is always produced when the SOS response is triggered and long mRNA is produced with a fixed probability leading to lower levels of long mRNA in the cell. Additionally, translation of the *cel* gene is repressed post-transcriptionally by binding of CsrA to long mRNA. CsrA is in turn regulated by CsrA binding partners like long mRNA or the sRNAs CsrB and CsrC. C) CsrA regulation: The sRNAs CsrB and CsrC repress the abundance of free CsrA inside a cell. In turn, they are repressed by the protein CsrD whose regulation is connected to the carbon system of the cell. If glucose (green) is the main carbon source, the production of CsrD is increased. In comparison to that, when glycerol (purple) is the main carbon source, less CsrD is present in the cell, indirectly affecting the abundance of free CsrA. * Denotes indirect action as no active CsrD repression takes place for glycerol supplemented medium.

of the *cel* gene to be transcribed. Thus, more short mRNA (*cea* and *cel* gene) is produced than long mRNA, that contains all three genes of the operon.

Post-transcriptional Regulation On the post-transcriptional level, further regulation of expression takes place (Figure 2.1 B). Upon SOS induction long and short mRNA are transcribed. Short mRNA is always produced and long mRNA is produced with a reduced probability leading to lower levels of long mRNA in the cell. Consequently, reducing the translation of the *cel* gene that leads to cell lysis. Additionally, translation of the *cel* gene is repressed post-transcriptionally by binding of CsrA to long mRNA. The mechanism of CsrA inhibiting *cel* translation will be discussed in more detail below.

CsrA Regulation The Carbon storage regulation (Csr) system consists of many components that interact with each other on multiple regulation levels and plays a role in the regulation of a multitude of target genes [6, 7, 19]. To reduce the complexity of the biological system, only the main components relevant for this thesis will be briefly described in the following. CsrA controls the translation of the *cel* gene in the ColicicnE2 operon by binding to long mRNA. Therefore, its regulation mechanisms are important for cell lysis in colicin producing cells. CsrA abundance is regulated by binding partners like the sRNAs CsrB and CsrC, which have multiple high affinity binding sites for CsrA [20, 21] and thus are in competition with the long mRNA for binding to free CsrA molecules. Furthermore, the sRNAs are inhibited by the protein CsrD which stimulates the degradation of the sRNAs when bound to one another [22]. Additionally, CsrD is connected to the carbon metabolism of the cell, which means that for different carbon sources in the medium, CsrD levels change [7, 9, 22]. While glucose as main carbon source increases the amount of CsrD in the cell (Figure 2.1 C: green), glycerol and other more complex sugars lead to reduced CsrD abundance (Figure 2.1 C: purple) and thus weaker sRNA degradation. As CsrA is a major player in post-transcriptional regulation of the *cel* gene, the regulatory components contributing to CsrA control will be investigated in Chapter 4 of this thesis.

Regulation of the Time-point of Cell Lysis A sketch for the repression mechanism of *cel* gene translation by CsrA is shown in Figure 2.2 A. The long mRNA forms a double hairpin structure including the Shine-Dalgarno (SD) sequence for binding of the ribosome in the second, looser hairpin [5, 23]. Thus CsrA and the ribosome are in direct competition for binding to this sequence. When no CsrA is present, the SD sequence of the mRNA is open for binding of the ribosome and translation of the *cel* gene can take place. Opposed to that, when a CsrA dimer is bound to the double

hairpin structure of long mRNA ribosome binding is blocked and no translation of the *cel* gene is possible (Figure 2.2 A). This indicates the importance of tight regulation of CsrA in a cell for fine tuning of cell lysis.

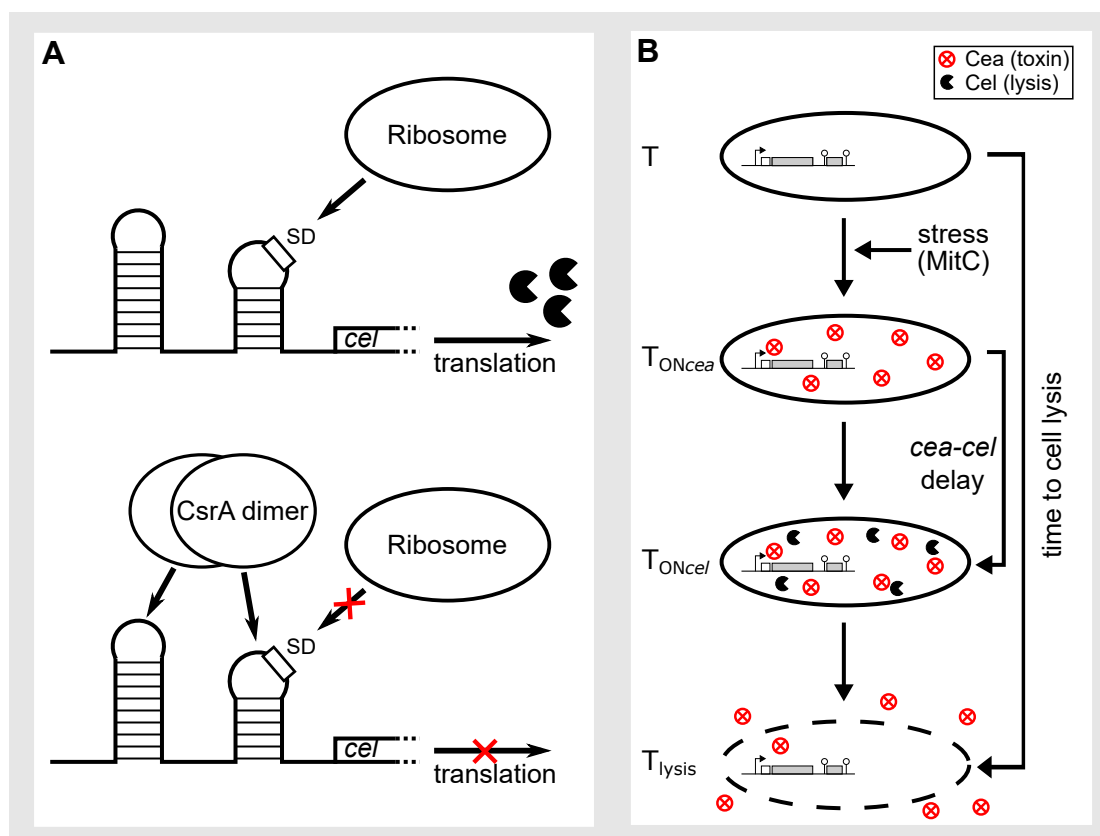


Figure 2.2

CsrA binding modulates *cel* gene translation and time-point of cell lysis. A) Double hairpin structure of long mRNA preceding the *cel* gene. Top: If no CsrA is present, the ribosome can bind to the Shine-Dalgarno (SD) sequence and translation is initiated. Bottom: CsrA dimer is bound to mRNA double hairpin, blocking the ribosome and thus translation. B) Predicted time-course of toxin production and release of the ColicinE2 operon. Time-points of gene expression start for *cea* and *cel* are marked as $T_{ON_{cea}}$ and $T_{ON_{cel}}$, respectively. Cell lysis is the final step in the expression cascade at T_{lysis} and leads to toxin release into the environment.

Altogether, there are multiple steps that regulate *cel* translation, which could lead to a delay in expression and lysis times for cells containing the pColE2-P9 plasmid which is sketched in Figure 2.2 B. Cells containing the ColicinE2 operon that are induced with a stressing agent, such as Mitomycin C (MitC) [24], first show production of the toxin at time-point $T_{ON_{cea}}$. Some time after that, at $T_{ON_{cel}}$, *cel* gene production is started. Finally, when enough lysis agent has accumulated in the cell, lysis takes place (T_{lysis}) and the toxin is released into the environment where it can kill closely related

bacteria. As toxin release is facilitated by cell lysis and death, the time-point of cell lysis limits the toxin expression time within a cell. A main goal of this thesis is to understand the expression dynamics of this bistable and heterogeneously expressing operon. Furthermore, regulatory modules for toxin expression and release dynamics as well as noise control need to be identified to understand the underlying mechanisms of bacterial competition from the single-cell phenotype level to competition outcome.

2.2. Stochasticity and Noise in Gene Expression

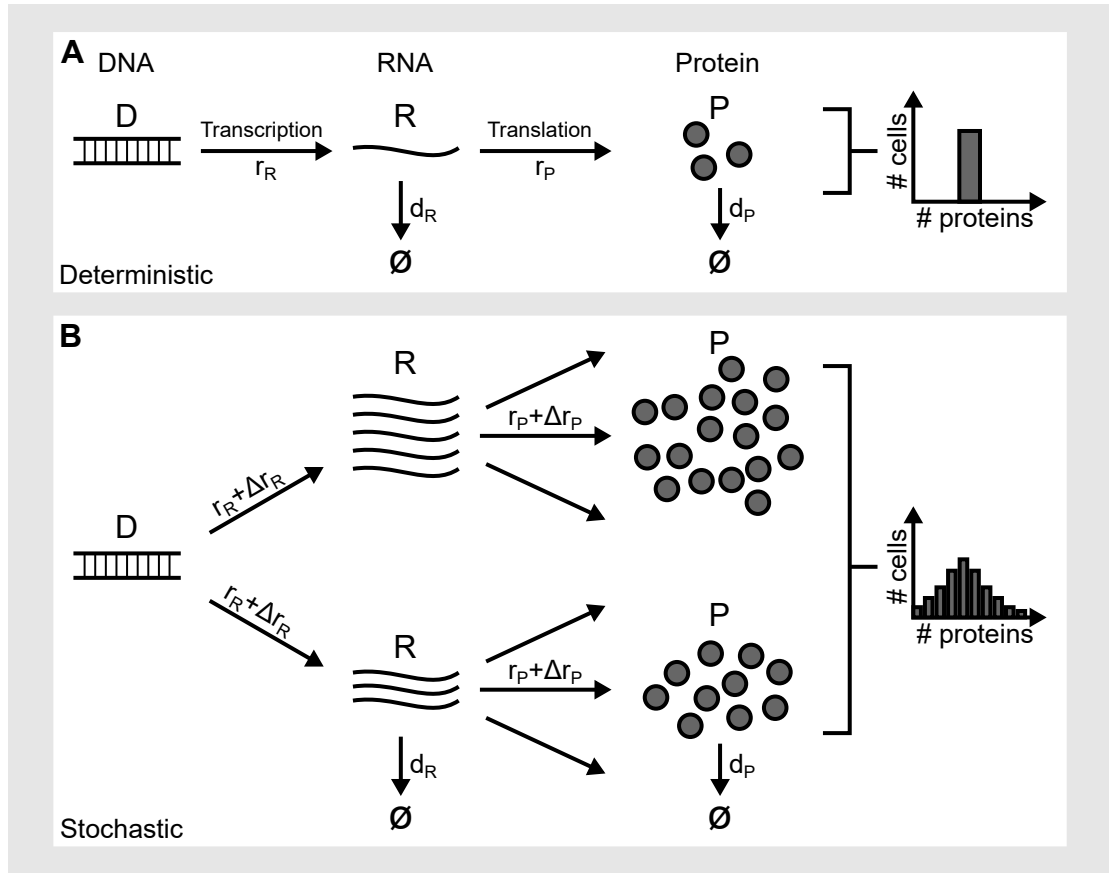
Previous work by Mader *et al.* 2017 showed heterogeneous timing in toxin expression dynamics at low induction levels of the ColicinE2 operon [13] which were possibly caused by stochastic fluctuations in protein availability of the SOS response system [16] or in repair mechanisms of DNA [25]. Furthermore, von Bronk *et al.* 2017 showed the importance of heterogeneity in toxin expression and release and stochasticity in cell positioning for competition outcome [10]. In Chapter 6 of this thesis, the regulatory elements controlling noise in toxin expression and release will be investigated. Additionally, how these stochastic fluctuations in toxin dynamics influence competition outcome will be explored in Chapter 5. For better understanding, basic elements of noise control relevant for the ColicinE2 system will be presented in this section.

In Figure 2.3 A, the production of a protein from a DNA sequence is shown for a deterministic case. DNA is transcribed to mRNA which then in turn, via translation, produces a fixed amount of proteins inside a cell. As the histogram on the right side shows, all individuals of the population show exactly the same amount of proteins per cell. This only holds true, if all steps of the expression dynamics are deterministic. The events of this reaction cascade can be described with rate equations like the following:

$$\begin{aligned}\partial R_t &= r_R \cdot D - d_R \cdot R \\ \partial P_t &= r_P \cdot R - d_P \cdot P\end{aligned}\tag{2.1}$$

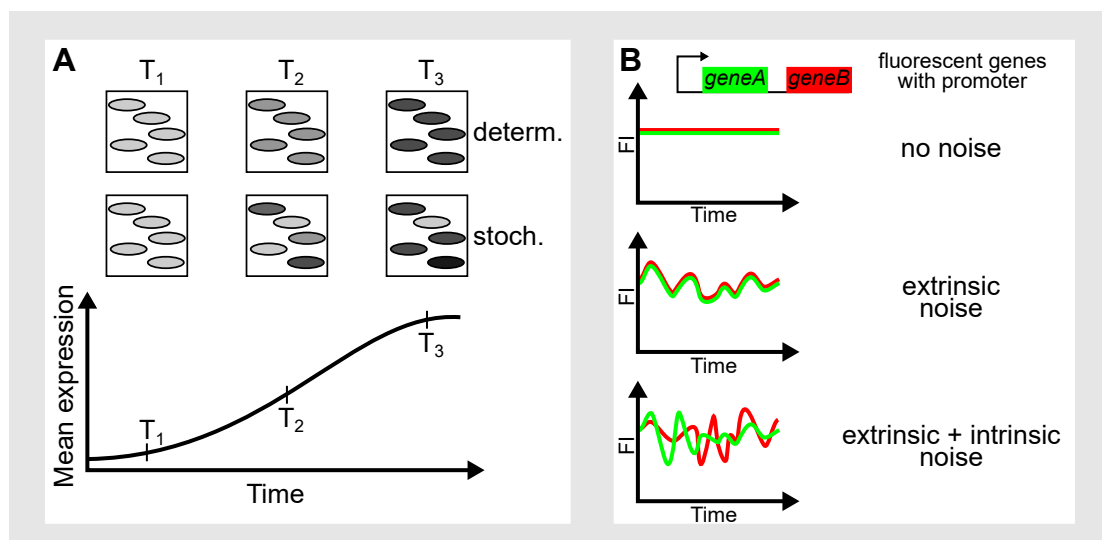
Where D, R and P are the number of DNA, RNA and Protein. ∂R and ∂P are the changes of RNA and protein number over time. Transcription rate is defined as r_R , RNA translation to proteins as r_P and degradation of RNA and proteins with d_R and d_P respectively.

In most cases the binding kinetics of two binding partners (e.g. polymerase to DNA) are defined by stochastic probabilities for encountering binding partners, diffusion,


Figure 2.3

Illustrations of deterministic and stochastic gene expression. A) Deterministic gene expression where DNA (D) is transcribed to RNA (R) with rate r_R , which is then translated to proteins (P) with rate r_P leading to a fixed number of proteins in each cell as shown in the sketched histogram. Degradation of RNA and proteins happens with rates d_R and d_P , respectively. B) Stochastic gene expression where one DNA can be transcribed to fluctuating numbers of RNA. RNA is then translated to varying numbers of proteins. Both processes are under the control of stochastic fluctuations that are marked with fluctuating terms for both transcription and translation rates (Δr_X). This noise in both processes leads to varying protein distributions in different cells as sketched in the histogram.

uptake of resources and brownian motion [26]. This makes the expression of the system more random as shown in Figure 2.3 B. One DNA sequence can be transcribed to various amounts of RNA due to stochastic fluctuations in transcription rate, similar fluctuation in translation rate can then lead to a big variety of protein numbers in a cell. In contrast to deterministic expression, a population that expresses proteins under the influence of random processes will have a broad distribution of protein numbers between individuals of the cell population (see Figure 2.3 B histogram). Thus, it is important to incorporate stochastic fluctuations into the differential equations shown above (Equation (2.1)) to better describe many natural systems.

**Figure 2.4**

Noise types and influences. A) Sketch for fluorescent protein production in a deterministic and stochastic case. Both possibly leading to same mean Fluorescence Intensity (FI) over time with diverse single cell responses. B) Production of two fluorescent proteins in green (GFP) and red (RFP) under the same promoter. No noise: both FPs expressed at constant rate leading to steady FI. Extrinsic noise: both FPs have FI fluctuating at the same interval. Extrinsic and intrinsic noise: both FPs with fluctuating FIs over time at different times. B) adapted from [27].

A number of steps in an expression process can contribute to the noise in protein numbers of a system. When only population averages of protein amounts within the cells are observed, information on noise between individuals of the population might be lost. An example for this is shown in Figure 2.4 A. A sigmoidal mean protein expression over time can be observed for the deterministic production of a protein with a constant production rate and the protein accumulates in all cells of the population in the same way. Comparable mean expression levels over time can be caused by stochastic processes that lead to differences between cells, where only some cells express the protein at high levels and others express the protein at low levels (see Figure 2.4 A). This behavior can only be separated in single-cell analysis such as single-cell time-lapse microscopy. To facilitate observation of the expression dynamics of the ColicinE2 system with fluorescence time-lapse microscopy, a reporter plasmid with all essential regulation mechanisms of the ColicinE2 operon was used. The genes *cea* and *cel* coding for the toxin and cell lysis were exchanged with genes coding for the fluorescent proteins YFP and CFP, respectively.

As noise can be generated by variation in many different processes inside and outside of cells, their influence can be separated into two categories: extrinsic and intrinsic noise [28–31]. How these can be differentiated was studied by Elowitz *et al.* [27] and

is shown in a schematic in Figure 2.4 B. A model system with two genes coding for fluorescent proteins (FPs) expressed under the same promoter was studied and the mean FI of the complete population was observed over time [27]. Without noise, both FPs are produced at a constant mean level over time (Figure 2.4 B top). In contrast to that, if external noise is present this can lead to fluctuations in FI over time with both FPs fluctuating at the same rates. This could be due to external noise such as availability of inducer for the production of the FPs in the environment, different levels of polymerases or cell size [32]. Adding intrinsic noise, both FPs show fluctuating mean intensities over time which lose their strong correlation if both intrinsic and extrinsic noise are present (Figure 2.4 B bottom). Intrinsic fluctuations typically arise from inherent stochastic fluctuations in biological processes e.g in transcription and translation. Comparing this to regulation in the more complex ColicinE2 operon reveals some similarities and deductions. For the ColicinE2 system, both genes are expressed with the same promoter. Gene expression is triggered as a consequence of the SOS response. This means that extrinsic noise could be caused by local variations in inducer concentration or different uptake of the DNA damaging agent into the cell over time. If this would be the only cause of noise in the system both the *cea* and the *cel* gene would show expression patterns similar to Figure 2.4 B with different expression levels (only long mRNA contains *cel* gene) but with strong correlation in time. As intrinsic noise source for the ColicinE2 system, a variety of components could come into play due to the multi-layered regulation of the different genes in the operon. First, factors influencing noise of transcription and translation such as the availability of both polymerase and ribosome would affect both genes [29, 30]. Second, the additional post-transcriptional regulation of the *cel* gene by CsrA and all its regulators could pose an additional noise source only affecting *cel* gene expression. All of these extrinsic and intrinsic noise factors could lead to expression patterns of *cea* and *cel* comparable to the two genes shown in Figure 2.4 B (bottom), with fluctuating, non correlated expression patterns of both genes.

2.2.1. Quantification of Noise

As seen before, many factors contribute to the expression noise of the ColicinE2 system. In this thesis, the main goal is to analyze the noise of toxin production and release between different individuals of a population at various times and to investigate how noise is controlled in the ColicinE2 system. In order to facilitate comparison between the noise levels of the two genes (*cea* and *cel*) at different time-points a fixed

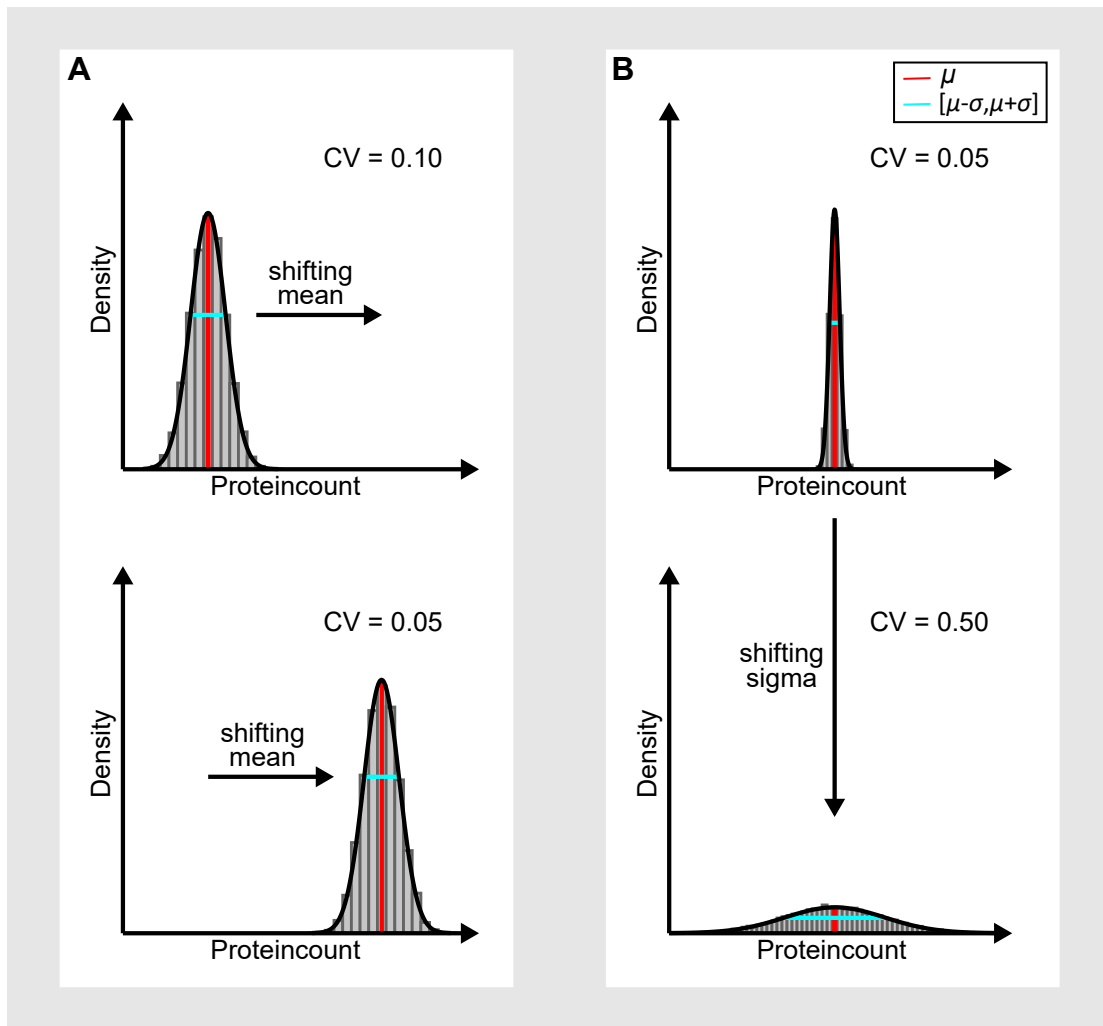


Figure 2.5

Quantification of noise. Sketches of distribution histograms of protein numbers (grey bars) with the density function of a fitted normal distribution (black line) are shown for various distributions. Red lines: μ ; Cyan line: $[\mu - \sigma, \mu + \sigma]$. A) A distribution with shifted mean μ but constant standard deviation σ . Leading to a change in coefficient of variation (CV). B) A distribution with a constant μ but shifting σ leading to a change in CV.

parameter for noise quantification has to be chosen. In the used reporter plasmid that contains all major regulatory modules of the ColicinE2 operon, these genes were replaced with a *yfp* and *cfp* gene, respectively. Thus, gene expression patterns including noise between cells can be compared by fluorescent intensity distributions over all measured cells. Two well known properties that are characteristic for a measured fluorescent distribution are the mean fluorescent intensity μ and the corresponding standard deviation σ which evaluates the distribution spread. Using these, the coefficient of variation (CV) is a way to quantify noise of a system compared to its mean.

It is calculated as follows:

$$CV = \frac{\sigma}{\mu} \quad (2.2)$$

where CV denotes the coefficient of variation, σ denotes the standard deviation and μ the mean of the distribution. Thus, the noise of a system is considered in relation to its mean. If the CV of a system changes this can be due to a change in μ or σ or both. Examples for changes in CV of an expression pattern of a fluorescent protein in a cell population is sketched in Figure 2.5. Two possible CV shifts are shown when only one of the parameters changes at a time.

When only the mean protein level within a population changes but the standard deviation stays the same (Figure 2.5 A) the CV changes accordingly. For example $\sigma = 1$ might be big for $\mu = 10$ but not for $\mu = 20$. In contrast to only looking at the standard deviation which does not change, the CV is reduced by a factor of 2. The opposite behavior is shown in Figure 2.5 B. Here, the standard deviation changes while the mean stays constant. For a constant $\mu = 10$ the distributions can either be narrow ($CV = 0.05$ and $\sigma = 0.5$) or broad ($CV = 0.5$ and $\sigma = 5$).

Many factors can contribute to noise generation in a complex gene regulation network. The different steps in regulation (transcription and translation) influence noise differently depending on the transcription and translation rates of the protein observed [33]. Furthermore, effects such as transcriptional bursting [34] and the presence of global factors in regulation [35] can change noise dynamics significantly. Global factors influence many genes within a cell and for example the ribosome density within the cell [36]. This makes disentangling the impact of regulation mechanisms of a complex regulatory network, such as the ColicinE2 system, difficult and experimental analysis requires step-by-step introduction of mutations on the various levels responsible for the tight control of toxin production and release. Especially since stochastic fluctuations adding to multiple levels can increase or sometimes reduce noise at the end of the cascade [33, 37].

2.3. Bacterial Interaction

In nature, bacteria normally do not live in a habitat by themselves but have to share space and nutrients with a multitude of other competitors. In such a crowded environment there are various ways that bacteria can interact with one another. The interactions of two-player interaction are divided in two main categories: cooperation and competition [38, 39] (Figure 2.6).

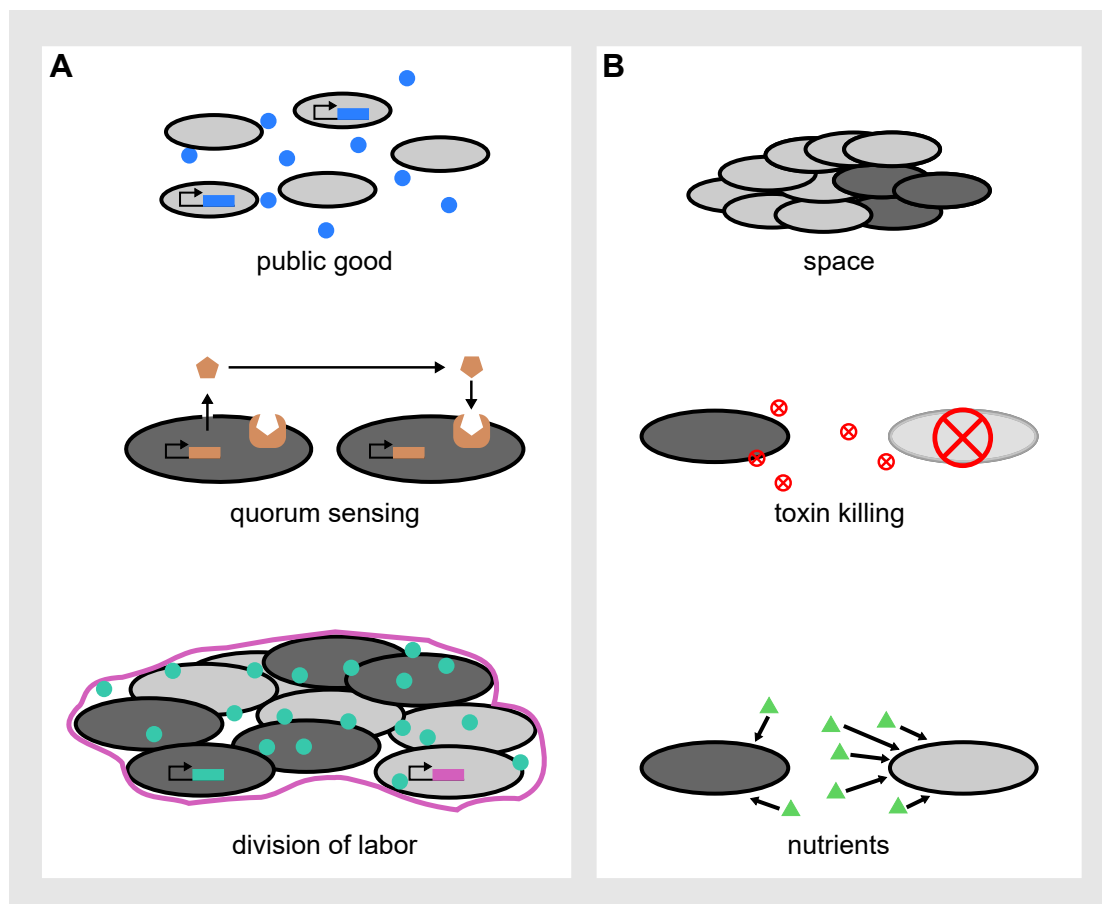


Figure 2.6

Bacterial interaction mechanisms. A) Cooperation mechanisms versus B) competition mechanisms. A) Positive interaction (cooperation) types can be: Public good production for all cells of a population (top), quorum sensing (middle) between cells by production and sensing of a signaling molecule and division of labor (bottom) as shown here by production of different elements for a biofilm of different phenotypes in a community. B) Competitive interactions can be: Limitation of space (top) by faster growth, active killing of unrelated cells via toxin secretion (middle) or resource limitation by faster uptake of nutrients from the surrounding (bottom).

Positive interactions that benefit all bacteria within the habitat are classified as cooperative interactions [39–41]. Some examples for cooperation are shown in Figure 2.6 A. The first case is the production of a public good, which comes at a metabolic cost

for the producers but benefits the population as a whole e.g. giving them a growth advantage. This public good could be an enzyme that helps predigest nutrients in the environment [42]. A second cooperation mechanism of bacteria is called quorum sensing [43]. Here the interaction includes production and release of signaling molecules that can be detected by all individuals of the population (Figure 2.6 A). If a sufficient level of these signaling molecule is detected, population response is triggered by e.g. production of a certain protein [43]. Finally, due to stochastic fluctuation between individuals of one population, different phenotypes can be active, producing different beneficial components which in combination increase success of the population. Such a process can happen in communities like biofilms [44] and is called division of labor. In contrast to these actions, competitive interactions only benefit some players in a population by active killing or repression of others [39, 45]. Schematics for some competition mechanisms are shown in Figure 2.6 B. One way of bacteria to increase success in competition is to limit the competitors access to resources such as space or nutrients. In the case of space this might be done by faster growth [46, 47] or active spreading [48]. For nutrient access, one way could be use of nutrients from the environment [49]. A more active way of repression is the production and release of a toxin that kills competitors (Figure 2.6 B). This leads to better conditions for the toxin producing strain by an increase in nutrition and space for their own growth [50]. Including more players into the competition, indirect interactions can affect competition outcome. This means that the interaction of two players with one another can have a combined effect on a third player within the system. This is called higher order interaction [11]. For example, von Bronk *et al.* 2019 studied the impact of higher order interactions on competition outcomes of a three strain interaction where one strain that produces a toxin can clear space for growth of a resistant strain [11]. In recent years Friedman *et al.* 2017 [38] used a bottom up approach to quantify sub-populations of two player competitions of a collection of multiple players. In a next step they increased the number of players in the competition to see if predictions from the lower level interactions hold true [38]. They found that some competition outcomes of three players could not be explained by their two player counterparts. This highlights that in order to understand higher order interactions it is essential to elucidate the underlying GED of interacting compounds within the system and apply this knowledge to increasingly complex systems.

In this study, the ColicinE2 system of *Escherichia coli* was chosen as model system due to its multi-layered regulation of gene expression on the transcriptional and post-

transcriptional level. Main controlling modules are the global proteins LexA and CsrA. The underlying single-cell GED and their contribution on bacterial competition will be analyzed in this thesis. Interaction mechanisms between the strains and conditions used in this study will be introduced in the following.

2.3.1. Colicin Driven Competition

In case of colicin driven competition of multiple strains, previous studies investigated conditions where coexistence of all strains was possible. For this, Weber *et al.* 2014 [46] studied a three strain interaction of a colicin producer (C), a sensitive strain (S) and a resistant strain (R). Modification of strain properties, like growth rate was shown to change the interaction dynamics, depending on the scenario that was observed. It can be (i) cyclic, where S inhibits R, R inhibits C and C inhibits S, (ii) hierarchical, where two strains inhibit the third and one of the inhibiting strains dominated the other, or (iii) intermediate, where some of the interactions are neutral. Observation of three strain competition for different mixing ratios and strains with varying growth rates combined with theoretical simulations revealed possible coexistence regimes for three strain interaction in a small range of parameters [46]. This means in order to facilitate coexistence in such a competition scenario, fine tuning of interaction dynamics is essential. For colicin driven two-strain competition of a ColicinE2 producing strain with a sensitive strain, von Bronk *et al.* 2017 [10] set up a model system that is shown in Figure 2.7.

In this system, competition between strains is achieved by two mechanisms. First, the colicin strain (C) produces its toxin and releases it into the environment. When a sensitive S strain encounters a colicin, it dies with a probability depending on the colicin concentration of the surrounding medium. Second, the sensitive strain is initially present with a $100\times$ higher amount than the C strain. This gives the S strain an advantage in the competition for space thus enabling spacial exclusion of the C strain. This scenario poses a cyclic scenario, where both strains inhibit each other. Additionally, the C strain shows cooperation within its own population. This is done by division of labor between cells that replicate and cells producing the toxin and releasing it via cell lysis (see Figure 2.7).

For this system, it was shown that the C strain can dominate competition mostly in a regime where switching into the toxin producing ON state is heterogeneous in time [10, 13] (heterogeneous timing of toxin expression described above). The division of labor between colicin production and replication (cooperation shown in Figure 2.7), as well

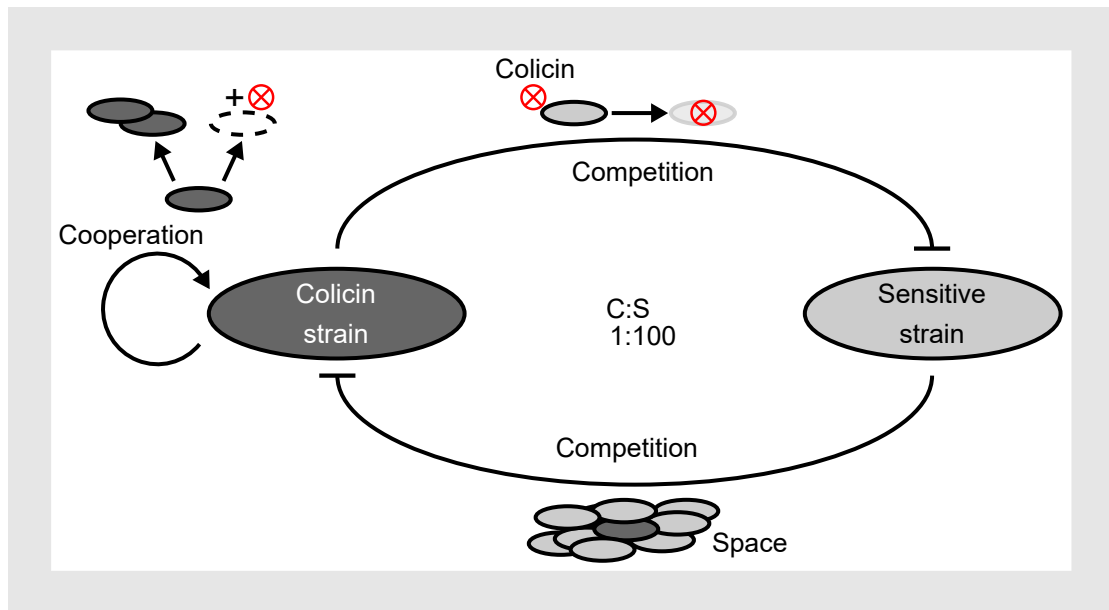


Figure 2.7

Colicin driven two-strain interaction. \uparrow indicates interaction, whereas \top indicates inhibition. A colicin producing strain (C) interacts with a sensitive strain (S) via toxin action. The C strain population shows cooperation within the population by division of labor between replicators and toxin producers. Competition with S strain is facilitated by colicin action leading to S cell death. Due to increased initial amounts of S cells ($C : S = 1 : 100$) the sensitive strain competes with the C strain via spacial exclusion. Figure adapted from [51]

as the high stochasticity in toxin release times gives the C strain a major advantage at intermediate induction [10]. Additionally, stochastic positioning of bacteria during initial growth and production plays a key role for the success of the C strain that is outnumbered by S cells [10]. Using a stochastic 2D lattice based model for bacterial interaction dynamics of the C and S strain, the importance of different components for competition outcome can be studied. As described in Chapter 1, a main goal for this thesis is to analyze how changes in GED and noise of the ColicinE2 system shape single-strain population behavior as well as the competition outcome for colicin driven interaction (Figure 1.1). Using the lattice based model, dependence on factors that are biologically connected like the amount of toxin being released into the environment and the timing of release can be analyzed separately. Additionally, changes in the different growth and production rates within the system can help to identify major players for interaction. In order to understand and model population behavior of increasingly complex systems and habitats, it is crucial to understand the GED of the major interacting components. For example, using a bottom up approach, Friedman *et al.* 2017 showed that it can be hard to predict the outcome of a three strain liquid

2. *Background Information*

competition even when the outcomes of all sub-groups of two-strain competitions are known [38]. Thus the goal of this thesis is to understand how toxin expression dynamics (TED) of the ColicinE2 system determine toxin driven bacterial competition by gaining further knowledge on various levels of abstraction, starting from single-cell level and its impact on the single-strain response. Following this it will be elaborated, how these changes on the single-strain level shape two-strain bacterial competition.

3. Material and Methods

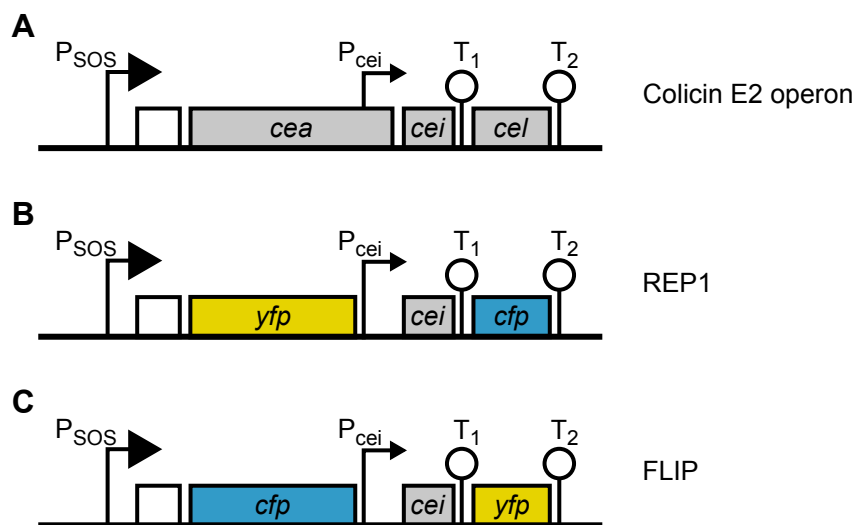
In this chapter, all methods used for data acquisition of this thesis will be introduced. Starting with the creation of a fluorescent reporter plasmid and various mutations regarding GED in the ColicinE2 system. In the next step, single-cell experiments and analysis methods are illustrated which were used to elucidate single-cell and single-strain expression dynamics for Chapters 4 and 6. Following that, the methodology of data acquisition of single-strain populations as well as competition is presented in unison with the respective analysis tools. The results of this will be presented in Chapters 4 and 5. The chapter concludes with the introduction of the theoretical model used for two-strain competition simulations in Chapter 5.

3.1. Cloning

3.1.1. Construction of Fluorescent Reporter Plasmid

In order to observe the temporal expression dynamics of the ColicinE2 operon, specifically the timing of toxin production and release, a fluorescent reporter plasmid was constructed in previous studies by Mader *et al.* 2015 [13].

The genetic schemes are shown in Figure 3.1 and depict the operon of the ColicinE2 system and two fluorescent reporter strains. In Figure 3.1 A, the colicin operon is shown as described in Chapter 2 including the SOS box and all regulation mechanisms (transcriptional and post-transcriptional). In the first fluorescent reporter strain (REP1) the genes coding for the toxin (*cea*) and cell lysis (*cel*) are replaced by the sequences coding for the Yellow Fluorescent Protein (YFP; mVenus) and Cyan Fluorescent Protein (CFP; mCerulean) (Figure 3.1 B, Table 3.1). This reporter plasmid retains all major regulation mechanisms of the wild-type operon, but enables observation with fluorescence microscopy to study expression dynamics in the system. The Fluorescent Proteins (FPs) were chosen for their stable characteristics in protein folding, bleaching and fluorescence [52–54]. The multi copy pBAD24 backbone was used for construction of the REP1 reporter plasmid to mimic the expression of the

**Figure 3.1**

Reporter plasmids configuration. A) Genetic scheme of the colicin E2 operon of the wild-type (WT) ColicinE2-P9 plasmid carrying the colicin gene (*cea*), the immunity gene (*cei*) and the lysis gene (*cel*). B) the REP1 reporter plasmid [13], where the *cea* and the *cel* gene are replaced by sequences coding for the fluorescent protein mVenus and mCerulean, respectively, whose production can be measured using fluorescence microscopy. C) FLIP reporter plasmid with flipped fluorescent genes compared to REP1.

multi copy pColE2-P9 wild-type (WT) plasmid. It contains the pBR322 origin of replication (ORI) with an approximate measured plasmid copynumber of ~ 55 copies per cell as compared to ~ 20 copies for the pColE2-P9 plasmid (Table 3.1).

Another fluorescent reporter strain FLIP was constructed here to test the influence of the fluorescent protein on expression, specifically on the noise in the ColicinE2 system. In this FLIP mutant, the FPs are interchanged compared to REP1, which means the genes *cea* and *cel* of the wt operon are replaced with *cfp* and *yfp* respectively (Figure 3.1 C and Table 3.1). This change is particularly interesting for analysis of noise control in the operon, as variation in FPs and their intrinsic heterogeneity in mean fluorescence its variation might have an effect on noise in the system. The created plasmids are integrated into different strains for observation. First, a toxin sensitive S strain of *Escherichia coli* S_{WT} that does not contain any plasmids and second, the toxin producing C strain C_{WT} that contains the colicin plasmid pColE2-P9 [50] (see Table 3.1). Only cells containing the ColicinE2 wt plasmid are able to produce toxin and release it into their surroundings via cell lysis. This will be further discussed in Section 3.2. Additional strains were created by genetic mutations of the S_{WT} .

Name	Strain - Plasmid	Modification/Information	Copies Col. Rep.	ssDNA	Ref.
S _{WT}	BZB1011	Wild-type strain without any plasmids	-	-	[50]
C _{WT}	BZB1011 E2C	Wild-type strain with pColE2-P9 plasmid	~20	+	[50]
S _{REP1}	BZB1011 - pMO3	Reporter strain (sensitive) ColE2 operon with exchanges: <i>cea-yfp cel-cfp</i>	-	~55	[13]
C _{REP1}	BZB1011 E2C- pMO3	Reporter strain (colicin producer) ColE2 operon with exchanges: <i>cea-yfp cel-cfp</i>	~20	~55	[13]
LexA1	BZB1011 - LexA1	Modified LexA binding to SOS box	-	~55	[55]
LexA2	BZB1011 - LexA2	Modified LexA binding to SOS box	-	~55	[55]
Δ LexA	BZB1011 - Δ LexA	SOS box deletion; no LexA binding	-	~55	[56]
CsrA1	BZB1011 - CsrA1	Stronger CsrA binding	-	~55	[55]
CsrA2	BZB1011 - CsrA2	Weaker CsrA binding	-	~55	[55]
Δ LexA/CsrA2	BZB1011 - Δ LexA/CsrA2	No LexA binding, weaker CsrA binding	-	~55	[56]
CsrB	CsrB - pMO3	No CsrB (genetic deletion)	-	~55	[55]
CsrC	CsrC - pMO3	No CsrC (genetic deletion)	-	~55	[55]
CsrBC	CsrBC - pMO3	No CsrB and no CsrC (genetic deletion)	-	~55	[55]
S _{REP2}	BZB1011 - pMO8	Reporter plasmid with reduced copy number	-	~13	[55]
C _{REP2}	BZB1011 E2C- pMO8	Reporter plasmid with reduced copy number	~20	~13	[55]
C _{AMP}	BZB1011 E2C- pMO9	Plasmid with Amp resistance, no CsrA binding sites, no ColE2 operon	~20	~55	[51]
S _{FLIP}	BZB1011 - pMO11	Reporter strain with interchanged FPs ColE2 operon with exchanges: <i>cea-cfp cel-yfp</i>	-	~55	[56]
S _{RFP}	BZB1011 - RFP	Plasmid pBAD24, RFP Arabinose inducible Amp resistance; no ColE2 operon	-	~55	[51]

Table 3.1

Overview of the strains used in this study with genetic modifications and information on expected effect on the strain. The approximate plasmid copynumbers of pColE2-P9 and a reporter plasmid in a strain are given with Col. and Rep. respectively and the presence of single-stranded DNA ssDNA are marked with + in strains containing the wt plasmid. ssDNA numbers are given as it represents a new regulatory element that was found during this work and is will be discussed in Chapter 4. The origin of the strains are given with the respective Ref.

3.1.2. Mutant Overview

In order to elucidate the various factors influencing expression in the ColicinE2 system as described in Chapter 4, it is important to methodically change expression dynamics by introducing mutations that have impact on different regulation levels. An overview over all mutants used for this study with genetic modification, strain information and copynumber of plasmids is shown in Table 3.1. If not marked otherwise, all plasmids were created by mutations on the reporter plasmid pMO3. For detailed information on cloning steps please see the publications listed in Table 3.1. All mutations were verified by sequencing analysis.

Transcriptional Mutations

Three different mutations on the transcription level were constructed that change the LexA binding to the SOS box. Strains LexA1 and LexA2 were created to have different binding strengths of LexA to the SOS box. According to literature LexA1 should have stronger LexA binding to the SOS box [57, 58], leading to stronger repression. In contrast to that, LexA2 should have weaker LexA binding [57, 58] and thus less repression of the operon. However, it was found that both mutants show weaker expression of the ColicinE2 operon under stress conditions, which will be shown in Chapter 4. A third transcriptional mutant was created where the SOS box sequence was deleted, leading to constitutive expression of the operon.

Post-transcriptional Mutations

As described for the wild-type ColicinE2 operon, post-transcriptional repression of the lysis gene is achieved by CsrA binding to the long mRNA transcript of the operon, thus repressing *cel* gene translation. Two mutants were created that change the binding affinity of CsrA to the long mRNA, which leads to different repression strengths. For CsrA1 an optimal CsrA binding motif [4] was chosen to increase CsrA repression of *cfp* translation. In contrast to that, the changes to mutant CsrA2 caused the loss of the second hairpin structure in the T1 repressor region of the RNA leading to significantly decreased CsrA binding to mRNA [4, 59].

Genome Modifications

Another way to alter translation of the *cel/cfp* gene is by not directly changing CsrA binding affinity to mRNA, but to adjust free CsrA levels in the cell by modifying the

amount of sRNAs (CsrB and CsrC) that sequester CsrA. This is done by introducing genetic deletion mutants that do not contain either CsrB, CsrC or both CsrB and CsrC (CsrBC) as described in Table 3.1. For these mutants the genomic sequences coding for CsrB and CsrC were replaced with antibiotic resistance cassettes. The absence of these sRNAs in the cell should lead to an increase in free CsrA levels and accordingly to higher repression of *cfp/cel* (see Chapter 2).

Plasmid Copynumber

When SOS response is triggered, transcription of short and long mRNA of the operon takes place. The amount of long mRNA as a binding partner for CsrA in turn tunes the amount of free CsrA and the expression of *cfp/cel* in the system. A mutation that changes the plasmid copynumber and hence the amount of long mRNA created when stress is present should thus lead to changes in CsrA abundance. REP2 is genetically very close to REP1 but has less reporter plasmid per cell with ~ 13 compared to ~ 55 copies for REP1 (see Table 3.1). This is achieved by replacing the pBR322 origin of replication (ORI) of REP1 with the p15A ORI that has a reduced copynumber [60]. This reduction leads to a decreased likelihood of *cel/cfp* gene expression due to a higher fraction of long mRNA being bound to the repressor CsrA.

Reduced Amount of CsrA Binding

For mutants with reduced copynumber the key mechanism reducing *cfp/cel* gene expression is the reduction of CsrA binding sites when less long mRNA is produced. Expanding on this principle a strain without additional binding sites for CsrA on the reporter plasmid should lead to the highest repression of *cel* by CsrA. As all C_X strains will be used for long-term competition experiments the use of an antibiotic in the medium is crucial to prevent cross-contamination by other bacteria. This prevents the use of the C_{WT} strain for competition experiments. Therefore, a resistance plasmid AMP was created with the same backbone as REP1 but without any part of the ColicinE2 operon and transformed into the C_{WT} strain, creating the C_{AMP} mutant. It is genetically closest to the colicin producing wild-type strain, as it contains the pColE2-P9 plasmid and the ampicillin resistance plasmid without any CsrA or LexA binding elements.

3.2. Single-Cell Expression Dynamics

One main goal of this thesis is to elucidate the role of single-cell toxin expression dynamics (TED) for bacterial competition. The production and release of toxin in the ColicinE2 system is a heterogeneous process regulated on various factors including the gene network and extracellular components (see Chapter 2). To study the importance of TED for the population level, it is crucial to understand the response of the system to stress on the single-cell level as explained in Chapter 1. Therefore the above described mutants (see Table 3.1) are studied with fluorescence time-lapse microscopy and various parameters are analyzed to characterize the stress response of the ColicinE2 system and its regulation.

3.2.1. Measurement Procedure

Growth Conditions

As the ColicinE2 system is a complex regulated system, it is important to minimize external fluctuations by setting reproducible growth conditions. In this study cultures were always grown on M63 minimal medium with either glycerol or glucose as carbon source and with additional 100 µg/ml ampicillin for selection, if not indicated otherwise (for detailed ingredient list of the growth medium see Appendix A). Cultivation steps for single-cell time-lapse experiments were fixed as follows:

1. An overnight culture of each strain was grown for approximately 16 h at 37°C shaken at 300 rpm (rounds per minute).
2. Overnight cultures were diluted to an optical density of $OD_{600} = 0.05$ or $OD_{600} = 0.1$ and grown under the same conditions as described above until $OD_{600} = 0.2$ was reached, which is the beginning of exponential growth.
3. 50 µl of diluted cultures were then incubated for 7.5 min in an ibidi slide (VI^{0.4}, Ibidi GmbH, Germany) pre-coated with poly-L-lysine (BIOCHROM, Germany) for better attachment to the channel bottom.
4. Channels were then rinsed with medium to remove free floating bacteria from the channel and transferred to the microscope.
5. Time-lapse measurements were started and stress was applied after the first image by flushing a channel with medium supplemented with various concentrations of the antibiotic Mitomycin C (MitC).

Fluorescence Time-lapse Microscopy

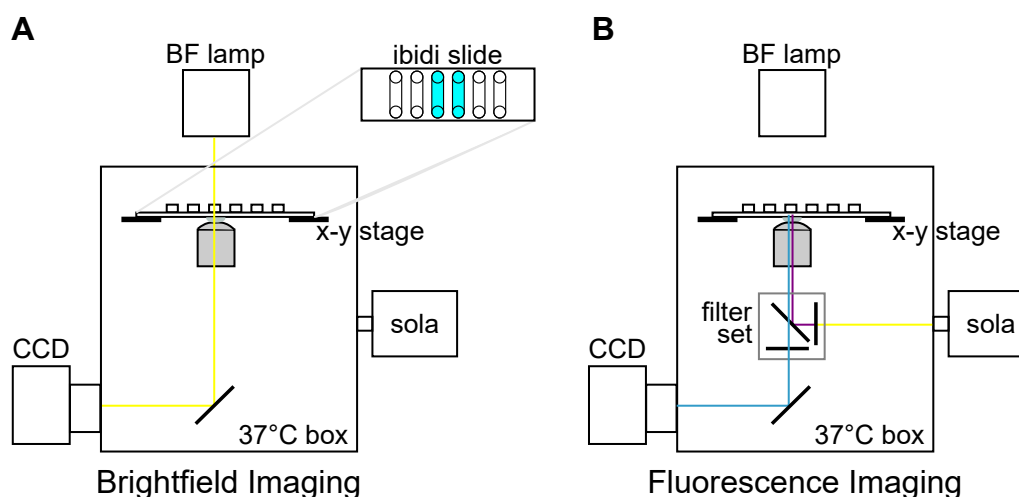


Figure 3.2

Time-lapse microscopy setup and light path. A) Brightfield (BF) imaging with ibidi measurement slide (two channels with different induction levels). B) Fluorescent imaging sola LED as light source. Filter set consisting of excitation filter, beam splitter and emission filter. Image acquisition with CCD camera for both images.

For fluorescence time-lapse experiments, the slides with two channels prepared for simultaneous measurements were transferred to the inverse microscope Axiovert 200M (Carl Zeiss, Germany) shown in Figure 3.2. The setup further contains a CCD camera (Andor Technology, Ireland), a Zeiss EC Plan-Neofluar 100x/1.3 oil-immersion objective and a heat chamber with temperature set to 37 °C. Brightfield (BF) images were taken with top illumination by a halogen lamp (Figure 3.2 A). Fluorescence images were taken with an external illumination by LED (SOLA, Lumencor, USA) and addition of a filter set consisting of a beam splitter BS520, an excitation bandpass HC500/24 and an emission bandpass HC 542/27 for YFP images and of a beam splitter BS520, an excitation bandpass HC500/24 and an emission bandpass HC 542/27 for CFP images (see Figure 3.2 B). The open source software Micromanager Version 1.3 was used for imaging [61]. Depending on the measured strain, images were taken every 10 min or 15 min for a total length of 5 h. Induction with MitC was performed at three different stress levels of 0.10 $\mu\text{g/ml}$, 0.25 $\mu\text{g/ml}$ and 0.40 $\mu\text{g/ml}$.

3.2.2. Analysis

Cell Tracking and FI Data

Single-cell traces were obtained using the ImageJ plug-in Cell Evaluator [62]. Cells were traced in BF images as shown for 30 min and 135 min in Figure 3.3 A and C for all analyzed cells and the traces were then transferred to fluorescent images. The extracted data was then plotted over time for all cells in YFP and CFP (Figure 3.3 B,D) . Combined data sets for each induction level were merged from at least two data sets and a minimum of 64 cells per condition. For background correction the program ImageJ [63] was used. The modal gray value for each image was subtracted from each image and stacks over time were created. Time traces for all cells were then analyzed using the Cell Evaluator plug-in [62] for ImageJ.

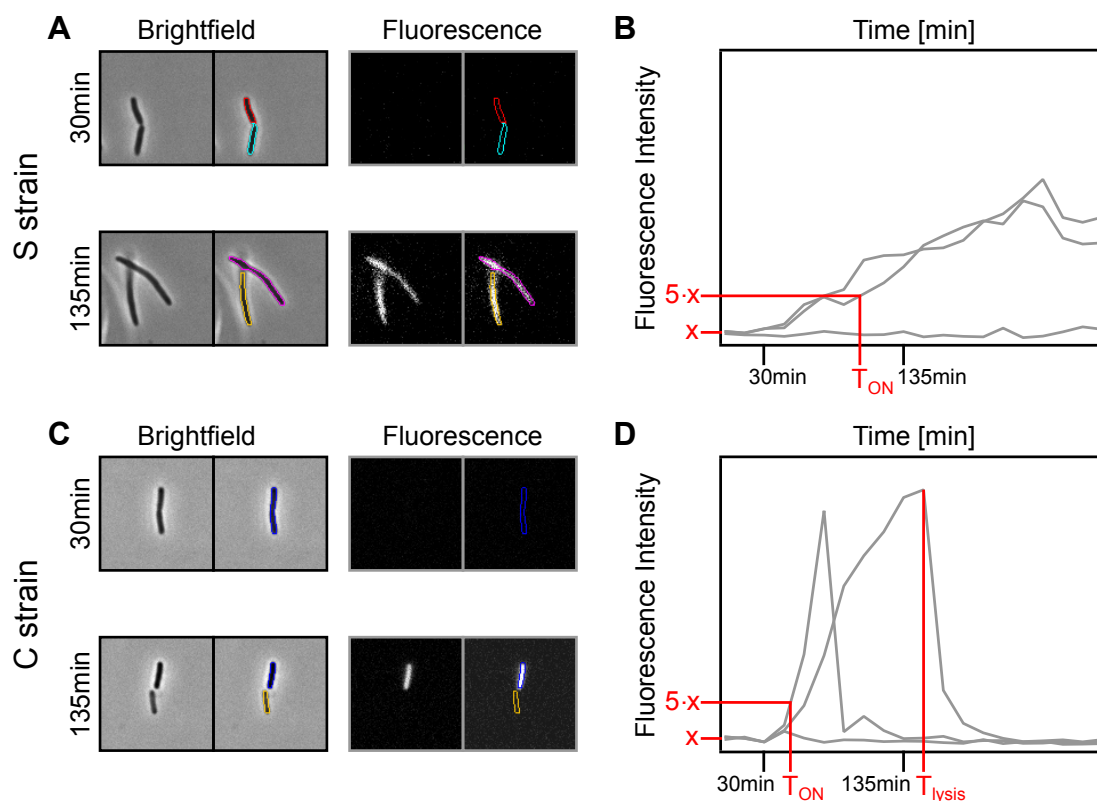


Figure 3.3

Comparison of S strain (A,B) and C strain (C,D) data. A,C) Brightfield (BF) images with colored marks for identified cells at 30 min and 135 min at induction level of $0.1 \mu\text{g/ml}$ MitC. Cell traces from BF images are transferred to fluorescent images and in the defined areas FI per area is extracted for each cell. The FI data for the marked cells is plotted in B) and D) for the S and C strain. Onset times (T_{ON}) are marked when the threshold $5 \cdot x$ is overcome. For C cell, the lysis time (T_{lysis}) is marked for a sharp drop in FI and visible in loss of contrast in the BF image.

Comparing S and C Strain Data Traces

Distinct differences between data obtained for the two cell types S (sensitive) and C (colicin producing) are visible in fluorescence intensity data independent from reporter plasmid added to the strain. This is due to the fact, that the C strain carries the wild-type pColE2-P9 plasmid, enabling cells to produce toxin and release it via cell lysis. C cells with a fluorescent reporter plasmid carry two plasmids, the pColE2-P9 plasmid and the reporter plasmid (Table 3.1).

First, observing the time development of fluorescence in the S strain (Figure 3.3), it is obvious that in the absence of stress or for low stress there are two cell populations: cells that produce FPs and cells that do not. This is due to heterogeneity in the SOS response. Cells start to visibly produce fluorescent proteins around 1 h after induction with MitC. They seem to reach a maximum of fluorescence at the end of the measurement, going into a steady state.

Comparing the data of the S strain with that of the C strain (Figure 3.3 B and D) the same heterogeneity can be observed in both strains. Some cells do not produce fluorescent proteins in both strains. The C strain however does not show a steady state of fluorescence intensity (FI) at the end. In contrast, C cells reach their maximum FI sooner and then show a sharp drop in FI. Comparing this behavior to the single-cell traces in Figure 3.3 C it becomes clear that this drop is caused by cell lysis and release of not only the toxin, but also the FPs inside the cell. Therefore, one characteristic parameter of the C strain (that is not observable for S strains) is the time-point of cell lysis (T_{lysis}).

Parameter Definition

Analyzing the single cell behavior several parameters for characterization arise (Figure 3.4). First, as described before, not all cells of the population produce fluorescent proteins. Therefore, the population is divided into the two states OFF and ON according to their FI (Figure 3.4 A). This separation is defined by a threshold that has to be reached for a cell to fall into the ON category. It is set for each cell separately depending on their basal fluorescence in the first three time-points [13], before visible increase of FI. If the basal FI of a cell is defined as x then the threshold of $5 \cdot x$ has to be overcome for a cell to be counted as a producer (Figure 3.4 B). The time when cells exceed this threshold is defined as T_{ON} , for each fluorescence channel separately.

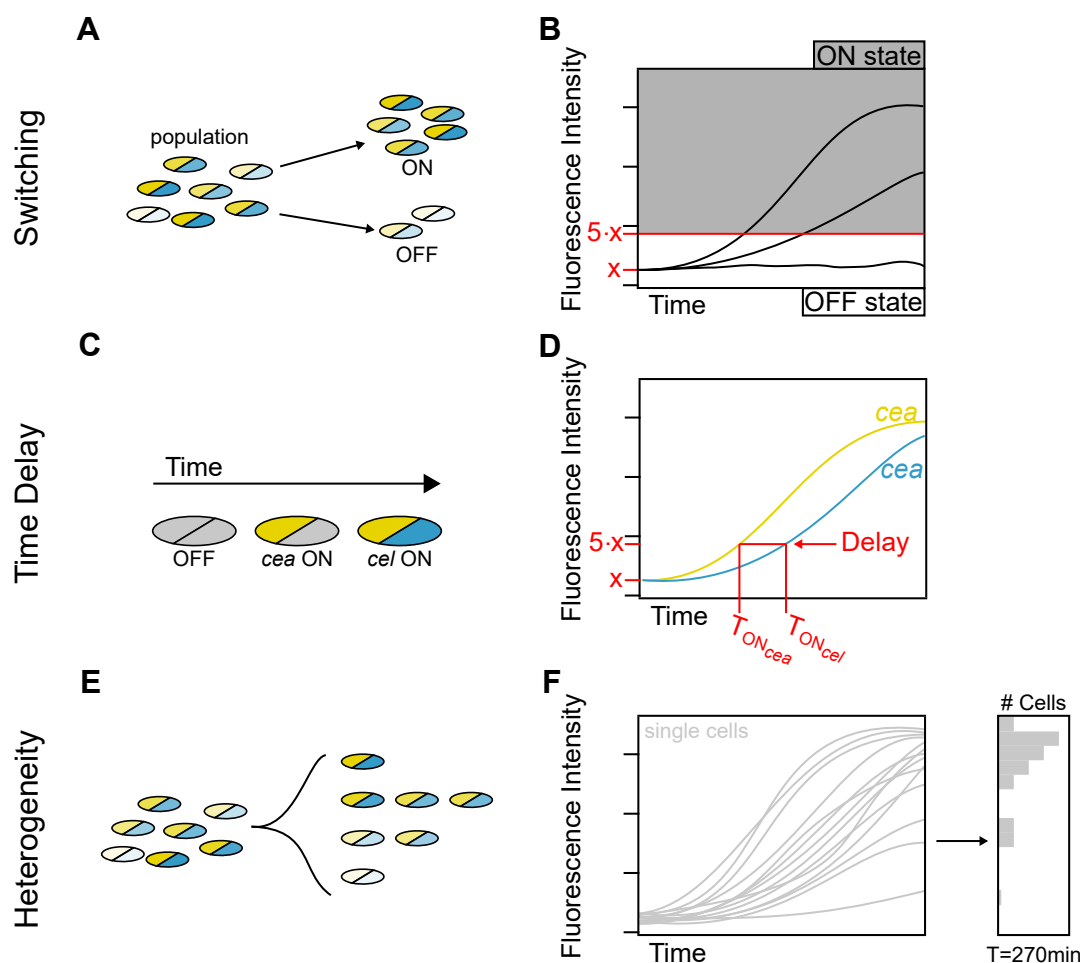


Figure 3.4

Analyzed parameters in single cell measurements. A,C,E) Sketches for possible cell dynamics. B,D,F) Sketches of corresponding data curves and analyzed parameters. A,B) Population of cells is divided into ON and OFF state according to their FI. ON cells express FPs over a threshold value which is called switching. C,D) Time delay between switching into the ON state of the two FPs. E,F) Cells express FPs heterogeneously over time and in intensity leading to a broad distribution of intensities over all cells.

A second characteristic of the ColicinE2 system is the presence of a time-delay between *cea/cfp* and *cel/ypf* expression. This means, that the onset of YFP expression is earlier than that of CFP expression in the REP1 strain (Figure 3.4 C). The delay is calculated as the time between onset of YFP expression ($T_{ON_{cea}}$) and CFP expression ($T_{ON_{cel}}$) in each cell (Figure 3.4 D).

Finally, the heterogeneity of the system is an important characteristic of toxin production and release. Single cell traces show broad FI distributions at all measured time-points (Figure 3.4 E,F). This behavior is also known as noise which quantifies the spread of the data compared to their mean. The coefficient of variation (CV)

is used to quantify the noise of the FI distributions at different time-points in our measurements with $CV = \sigma/\mu$ [64].

3.2.3. Gelelectrophoresis

Detection of single-stranded DNA

In recent years, Morales *et al.* 2015 detected the accumulation of ssDNA in cells containing the pColE3-CA38 plasmid [65] and identified the genetic sequences responsible for ssDNA production. With this plasmid, ssDNA is produced as an intermediate of rolling circle plasmid replication. Thus, sequencing of the complete pColE2-P9 plasmid was performed and the sequence was deposited at GenBank with the accession number KY348421. Comparing the genetic sequence of the wild-type pColE2-P9 plasmid with that of the pColE3-CA38 sequence, homologies were detected in multiple regions of the plasmid, including the one responsible for ssDNA formation (for details see Götz *et al.* 2018 [55]).

To test for accumulation of ssDNA in C cells (see Chapter 2), bacterial overnight cultures were induced with 0.25 $\mu\text{g}/\text{ml}$ MitC for 75 min. Using the QIAprep Spin Miniprep Kit (Qiagen, Germany) the total DNA was extracted from the cell suspension and cleaved with the enzyme PvuI (New England Biolabs (NEB), Germany) to cut the plasmid double stranded DNA. A 1% agarose gel with TAE buffer (see Appendix A) stained with EtBr was used to separate the different DNA types by fragment lengths from a cell extraction. Various markers and ladders were applied to the gel with the DNA extracts to verify the presence of ssDNA in C strains, specifically two phage ssDNA (M13mp18 and Phi174, NEB, Germany) were used for comparison. The Gel image is shown in Figure 3.5 with red boxes marking the ssDNA present in the C_{WT} strain. Its length corresponds to that of ~ 6800 basepairs of the pColE2-P9 plasmid, confirming the presence of ssDNA in the C strain which is only produced by the wild-type plasmid but not the reporter plasmids.

Binding Assays of CsrA to RNA and ssDNA

To determine the binding affinity of various RNA and ssDNA constructs to CsrA gel shift assays were performed. For detailed components of the buffers and tables for CsrA concentrations please see Appendix A. RNA and ssDNA sequences comparable to the CsrA binding regions of the plasmids of REP1, CsrA1 and CsrA2 (Table 3.1) were used to investigate binding strength of CsrA to RNA and ssDNA with differ-

3. Material and Methods

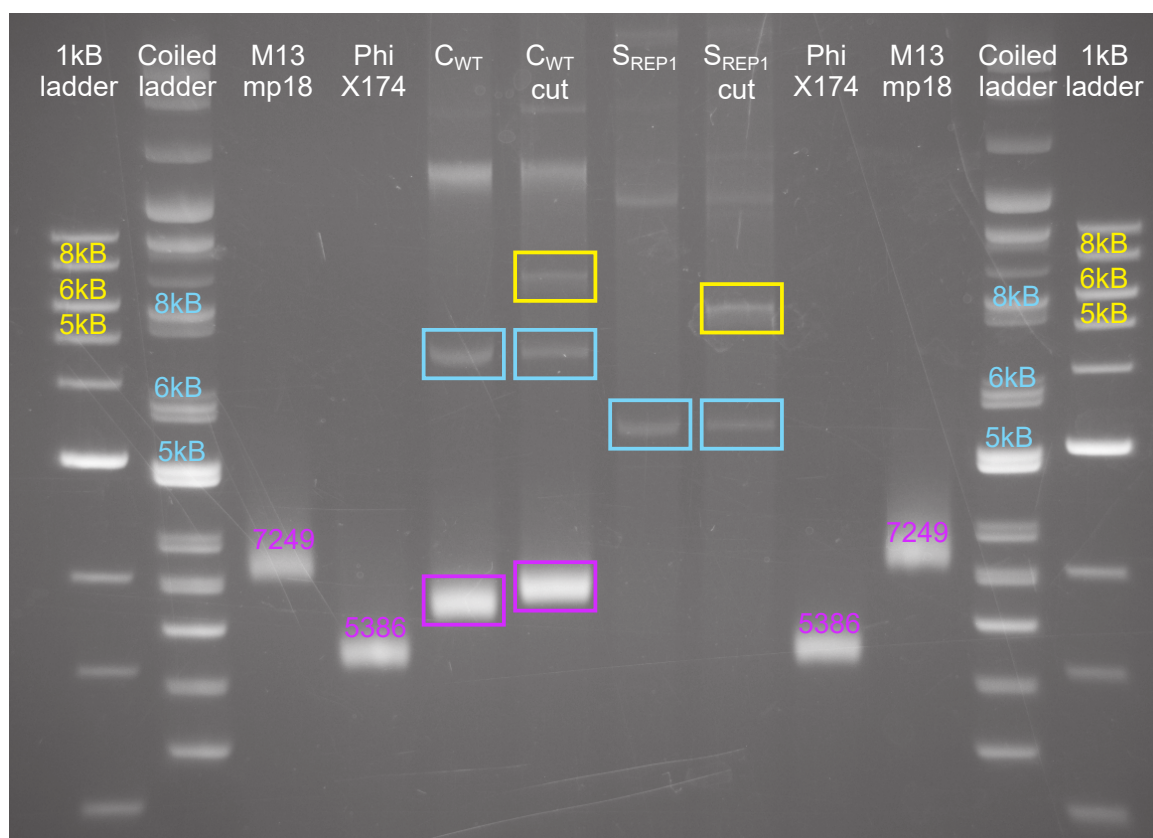
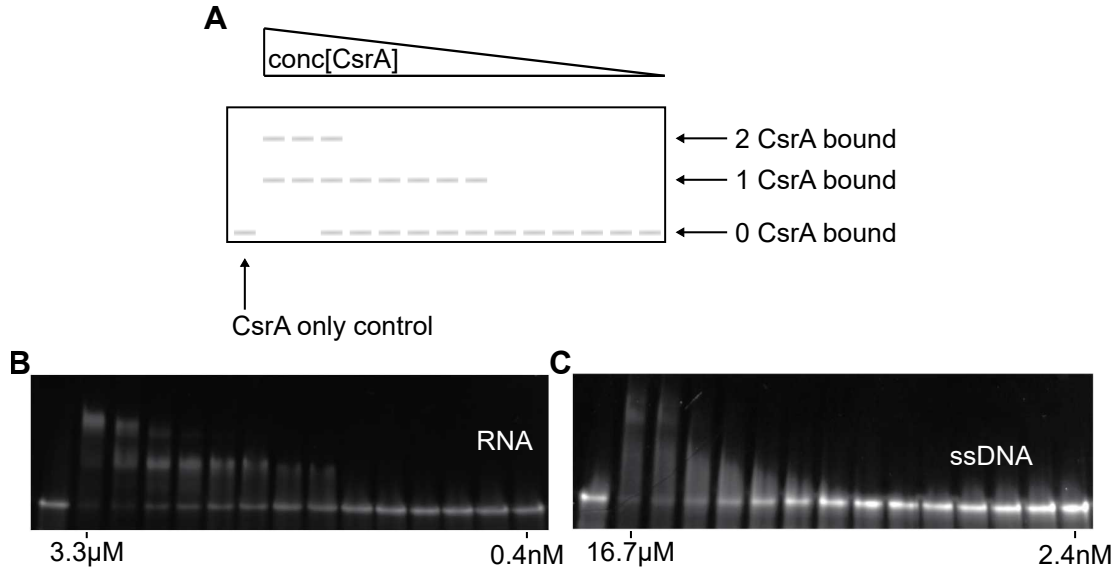


Figure 3.5

Agarose gel for ssDNA detection. DNA extracted from the bacterial cells was run before and after addition of a cutting enzyme (cut). Different length markers (ladder) were added for comparison to fixed DNA length scales. Yellow boxes correspond to cut plasmids of each strain, while blue boxes mark the uncut plasmid. Purple box marks the ssDNA present only in the C strain in length fitting a single-stranded DNA ring of the the plasmid size. For comparison two single-stranded phage plasmid DNAs were added (M13mp18 and PhiX174). Figure adapted from [55].

ent sequences. First, Cy5-labeled RNA and ssDNA fragments were heated to 85 °C and 90 °C respectively and slowly cooled in a folding buffer (see Appendix A). A N-terminal 6xHis-tagged CsrA protein (Biozol, Germany) was added to folded RNA and ssDNA in decreasing concentrations to analyse shifting of Cy5-labeled RNA/ssDNA fragments in the gel when CsrA is bound. As shown in Figure 3.6 A, RNA/ssDNA fragments with bound CsrA run slower in the gel, leading to bands further up. Gel shift measurements were performed at room temperature at 85 V for 1 h using precast 4-20 % gels (Mini-PROTEAN TGX Protein Gels, bio-rad) and Tris/Glycine buffer (Bio-Rad Laboratories, USA). Binding reactions of Cy5-labeled fragments with constant RNA/ssDNA concentration were incubated at 37 °C for 30 min (protocol adapted from [4, 5]). Gel shift images were made using a Cy5 filter set and the ChemiDoc MP

**Figure 3.6**

Protein binding assay to RNA and ssDNA. A) Schematic of the gel shift assay for CsrA binding to RNA/ssDNA. Grey: Cy5-labeled ssDNA/RNA bands. B,C) Fluorescence images of gelshift for CsrA binding to Cy5-labeled RNA (B) or ssDNA (C) fragments, respectively.

Imaging System (Bio-Rad Laboratories, USA). Images of the gel shifts for REP1 RNA and ssDNA are shown in Figure 3.6 B) and C), respectively. The unbound fraction of RNA/ssDNA was determined using ImageJ by detection of remaining FI in the band and fitted in IgorPro 7.04 (Wavemetrics, USA) using Equation (3.1):

$$FI = m - (m - b) \times \left[\frac{R + P + K_D - \sqrt{(R + P + K_D)^2 - 4RP}}{2 \cdot R} \right] \quad (3.1)$$

adapted from Pagano *et al.* 2011 [66], where FI is the Fluorescence Intensity of the unbound RNA/ssDNA band, m and b are the maximum and basal FIs for each band, R is the RNA/ssDNA concentration used (constant), P is the concentration of CsrA in each lane and K_D is the dissociation constant. Data of three independent measurements was fitted to calculate the mean binding strength of CsrA to the three RNA and ssDNA sequences. The calculated K_D values are discussed in Chapter 4 to analyze the effect of CsrA binding for GED in the ColicinE2 system.

3.3. Population Experiments

In order to investigate the impact of TED on the population level for a colicin producing population and the competition with a sensitive S strain, various C_X strains were used due to their different TED (see Table 3.1). In order to differentiate between the C strains and S strain in competition experiments, the strain S_{RFP} was used. Its plasmid contains the pBAD24 backbone and carries a gene encoding for a red fluorescent protein (mCherry/RFP) whose fluorescence can be induced by addition of arabinose to the growth medium, leading to constitutive expression of RFP.

3.3.1. Measurement Procedure

Growth Conditions

In this study bacterial cultures were always grown on M63 minimal medium with either glycerol (GLY) or glucose (GLU) as carbon source and with addition of the 100 $\mu\text{g}/\text{ml}$ of ampicillin to prevent cross-contamination and 2% arabinose for RFP induction in the S_{RFP} strain (for detailed ingredient list see Appendix A). Cultivation steps for liquid cultures were:

1. An overnight culture of each strain was grown for approximately 16 h at 37°C shaken at 300 rpm.
2. Overnight cultures were diluted to an optical density of $OD_{600} = 0.1$ and grown under previous conditions until $OD_{600} = 0.2$ was reached, which is the beginning of exponential growth.
3. C strain cultures were filtered with Amicon Ultra 100K-filter (Merck KGaA, Germany) for 8 min at 4500 rpm in order to remove toxin from pre-lysed cells from the medium.
4. Cells were removed from the filters in a second centrifugation step with 5 min at 4500 rpm and after that, 300 μl medium was added to the cells.
5. Optical density for both S and C strain was adjusted to $OD_{600} = 0.1$ and then mixed in a ratio of 100:1 (S:C).
6. 40 μl of each control (S and C unmix) and the mixture was applied into separate wells of a 384-well plate (Greiner Bio One, Austria) that was used as source plate in the next steps.

Spotting Bacteria

For competition experiments extremely low volumes of cell suspensions were chosen, to enable single-cell interaction. Adapted from von Bronk *et al.* 2017 and 2019 [10, 11], a pipetting robot (Echo 550, Labcyte, USA) was used to apply these small sample volumes in high replicate numbers on a one well plate with nutrients (see Appendix A, plates: Nunc OmniTray, ThermoFisher scientific, USA). In this study, 5nl sample were chosen for control spots and bacterial mixtures and were spotted onto the M63+Agar plates on three plates (see Figure 3.7 A). To keep fluctuations from medium composition and temperature fluctuations at a minimum, all three C strains (C_{REP1} , C_{REP2} , C_{AMP}) and their competitions with S_{RFP} were spotted on the same plates. Each plate contained 75 or 76 spots with all of them being monitored in parallel at the same time steps.

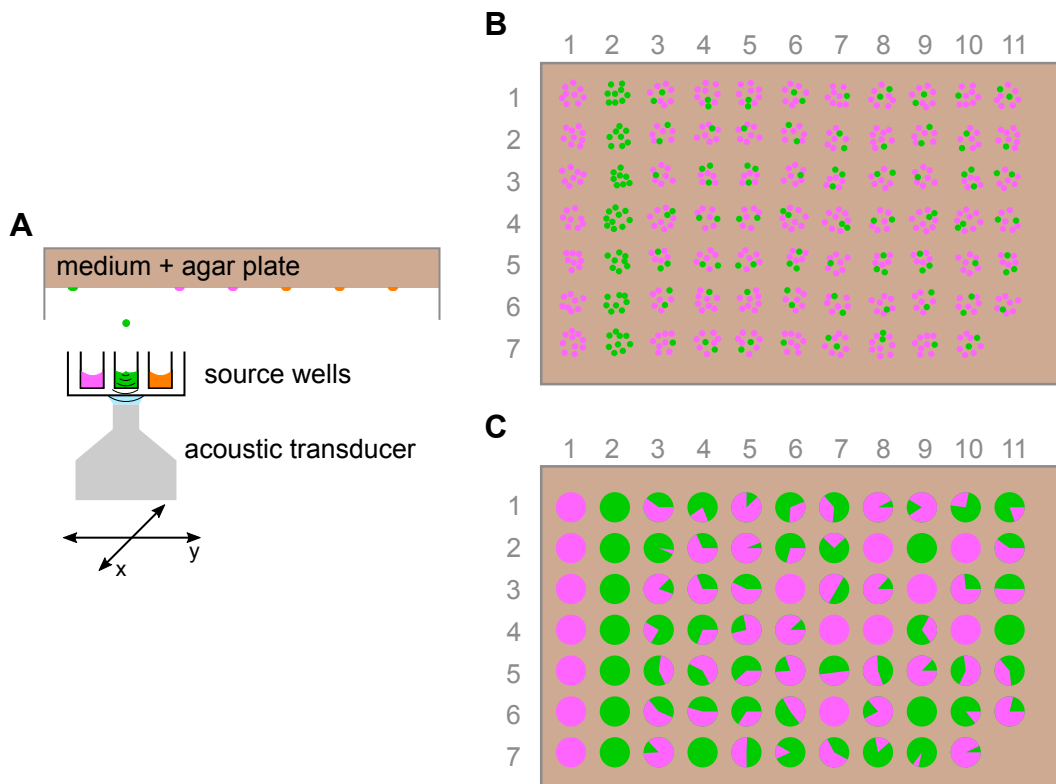


Figure 3.7

Bacteria spotting and competition. A) Sketch of bacterial application with Echo 550 pipetting robot. B,C) Plate setup with bacteria for 76 spots multi-spot acquisition with the stereo microscope (B) $t = 0h$ and C) $t = 48h$).

Multi-scale Microscopy

For analysis a reference image of all plates was taken at $t = 0h$ and also used to identify and exclude incorrectly spotted clusters (Figure 3.7 B). Two of the three replicates were then grown in an incubator for 48 h with 80 % humidity at 37 °C. The third plate, containing the control spots of unmixed C and S strains was grown in a transparent heat chamber (ibidi, Germany) and observed with a stereo microscope (SMZ 25, Nikon) in intervals of 1 h, which will be called SMZ setup from now on. Growth conditions in the heat chamber were the same as for plates grown in the incubator. After 48 h images of all three plates (grown in setup and in incubator) were taken again to record competition outcomes (Figure 3.7 C). Experiments were repeated 2-3 times for each medium composition (GLY or GLU) and induction level.

Toxin Production

Testing the influence of colicin on S strain growth requires two steps. i) Extraction of colicin from the medium of induced C strain cultures. ii) Apply the extracted colicin on pregrown S cells to determine the killing capacity of the extracted colicin.

C strains were grown similar to competition experiments (steps 1-5) and diluted to $OD_{600} = 0.1$. After that, they were incubated for 160 min at an induction level of 0.25 µg/ml to ensure that most cells released their produced toxin into the medium. To remove lysed cells from the medium, cultures were centrifuged at 13 000 rpm for 15 min. 500 µl of the supernatant was filtered (10K-filters, Amicon Ultra) and diluted 1000-fold.

During colicin extraction, S cells were prepared for toxin testing. They were grown according to steps 1-2 in competition experiments and diluted to $OD_{600} = 0.1$. Pre-heated M63 agar plates were then inoculated with 500 µl evenly spread on the plate. After incubation of these plates for at least 1.5 h at 37 °C, 50 nl of the diluted colicin suspensions were spotted onto the plate using the pipetting robot. For analysis, images of the plates were taken at $t = 0h$ and $t = 16h$ in RFP channel and BF mode using the SMZ setup described in the competition experiments.

Live-Dead Staining

For competition experiments it is important to have a better insight into the switching dynamics of the cells, especially for comparison with simulation results. This is done by live-dead screening of induced cells at fixed time-points. C strain cultures were

grown as for competition experiments steps 1-5 and then diluted cultures were induced with MitC concentrations of 0.00 $\mu\text{g/ml}$, 0.01 $\mu\text{g/ml}$ and 0.10 $\mu\text{g/ml}$ for up to 3 h. Every hour 50 μl were extracted and stained with the LIVE/DEAD BacLight Bacterial Viability Kit (ThermoFisher scientific, USA). For staining 0.5 μl of dye was used in a 1:1 ratio of SYTO 9 and propidium iodide and incubated for 15 min in the dark. For analysis of dead and living cells with fluorescence microscopy, 0.5 μl of stained cells were pipetted onto an agar plate and dried for a few minutes until the liquid evaporated. Then fluorescence images for all induction levels and at each time-point were taken with a 90i Nikon upright microscope (Nikon, Japan) and the DS-Qi1MC digital camera (Nikon, Japan) using filter sets for RFP and GFP detection. Analysis was performed with the software ImageJ by manually counting red and green cells.

3.3.2. Analysis

Growth Rate Evaluation

A crucial information for competition evaluation is how fast the strains grow on different media and induction levels. Growth rates were obtained from the control spots grown on the same plates as competition experiments to keep the conditions as similar as possible. Analysis was performed on BF images of microscopy between 11 h and 48 h. Due to contrast problems with shadows at the edge of bigger colonies, the images were analyzed manually in ImageJ by marking the area covered by the colony at each time-point as shown marked in red in Figure 3.8 A. The growth curves were then plotted using IgorPro Version 7.04 (WaveMetrics Inc., USA) and fitted with a linear fit function between 20 h and 48 h as this regime showed linear area growth for all conditions observed. This time regime contains a shift of zoom factor in images of growth, thus for better comparison images of areas at 23 h and 48 h are shown in Figure 3.8 A as the zoom level remained unchanged between them.

Area Detection in Competition Experiments

Image analysis for competition outcome was performed using BF and RFP images for 48 h of bacterial mixed colonies. An overlay of all channels in a C_{REP1} with S_{RFP} competition is plotted in Figure 3.8 B. Area detection was performed for BF and RFP images using a Matlab script from von Bronk *et al.* 2018 [39] and Matlab Version R2017b (Mathworks, USA). The complete area covered by bacteria is extracted from the BF image (Figure 3.8 B gray area BF) and the area covered by S strain is extracted

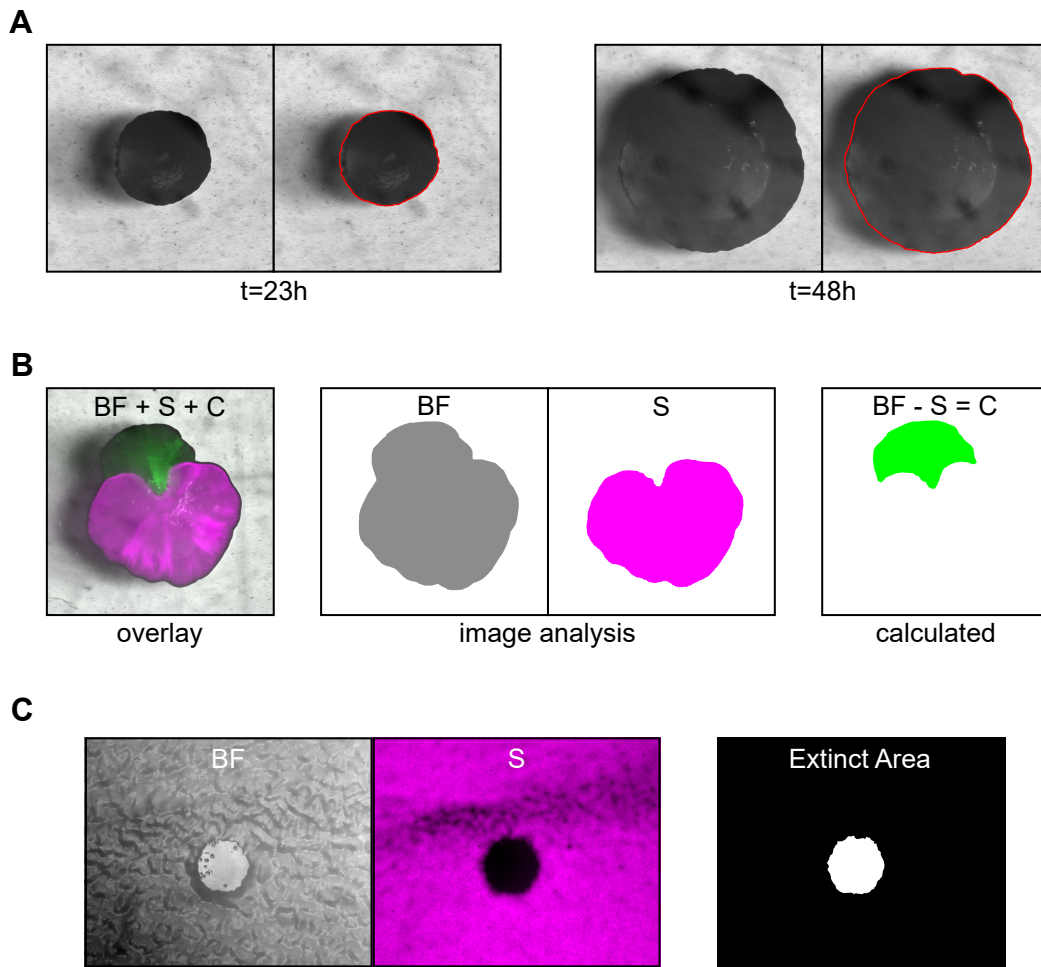


Figure 3.8

Area detection for population experiments. A) Colony image and overlay of BF image with detected area (red) used for growth rate (GR) fitting at 23h and 48h. B) Area detection for competition experiments. Overlay of all measured channels at 48h (left). Extrapolated areas from BF and RFP (S strain) image. C) strain area is calculated as relative complement of S in BF, as not all C_X strains express a fluorescent protein. C) Detection of extinct area in toxin production experiments. BF and S channel images (left) and corresponding extinct area detected (right).

from the RFP image (Figure 3.8 B magenta area S). As not all C strains used in competition experiments contain a fluorescent reporter plasmid (Table 3.1), C strain covered area is calculated from BF and RFP images as $C = BF - S$ (Figure 3.8 B green area C).

The minimal area detectable for bacterial colonies was set as $2.4 \times 10^4 \mu\text{m}^2$, below which the outcome was classified as extinction. Competition outcomes were calculated as fractions of total area and then classified by C fraction as follows:

Outcome	S_{wins}	Coexistence	CS_{wins}	Extinction
C fraction	<10%	10-90%	<90%	no bacteria detected

Table 3.2

Classification of competition outcomes depending on the fraction of C strain area covering the final detected area.

Extinct Area by Toxin

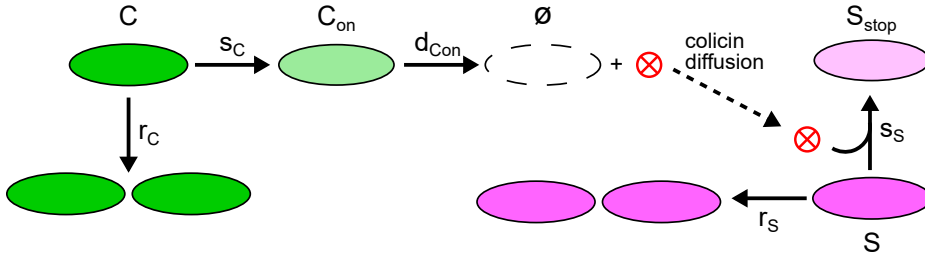
Tests measuring the amount of toxin being produced by different C_X strains were analyzed with pictures taken after 16 h in BF and fluorescence channels (example shown in Figure 3.8 C) left). The extinct area was analyzed manually with ImageJ using adjustment of intensity threshold and the wand tracing tool. A combination of a traced extinct area of a C_{REP1} produced colicin area is shown in Figure 3.8 C).

3.4. Simulation

3.4.1. Two-strain Interaction Model

In nature, many biological processes are connected to one another, e.g the time-point of cell lysis for cells containing the ColicinE2 operon, is connected to the amount of toxin being released, which will be discussed more closely in Chapter 4. Theoretical modeling of the competition makes it possible to disentangle the influence of those factors and allows for variations of parameters like production rates, stochasticity and toxin sensitivity. For experiments on competition between a sensitive (S) strain and a colicin producing (C) strain according to the interaction conditions described in Chapter 3 a simulation was used that was previously described by von Bronk 2017 *et al.* that is constructed as shown in Figure 3.9 (adapted from [10]).

For a large number of cells, where the influence of stochastic fluctuations can be neglected, a set of linear ordinary differential equations (ODE) can describe the dynamics shown in Figure 3.9. This ODE include the following deterministic rate equations that are dependent on the transition rates adding individuals to a state or the ones for cells leaving a state:


Figure 3.9

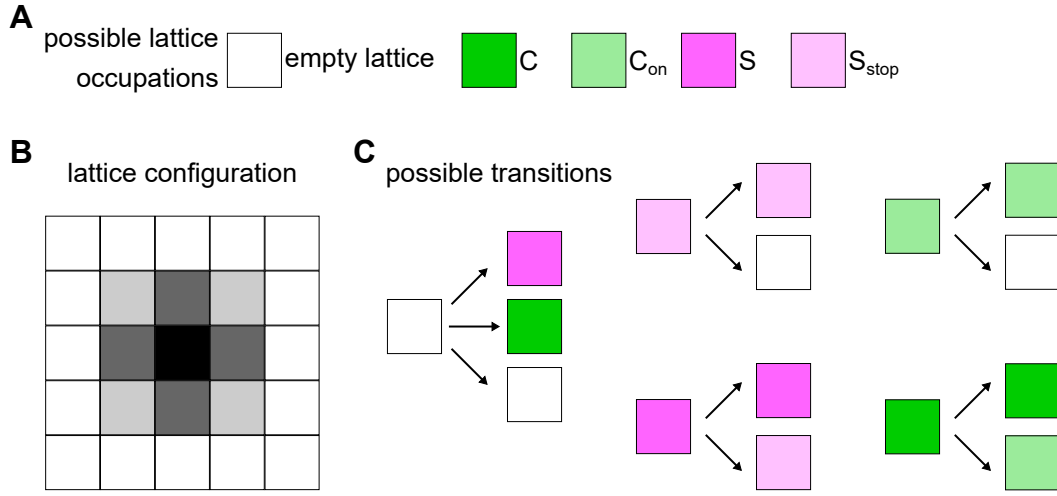
Two-Strain Interaction Parameters adapted from [10]. r_X replication rate of strain X (C or S), s_C switching rate of C into the state C_{on} , and $d_{C_{on}}$ degradation rate of C_{on} with subsequent cell lysis and toxin release. s_S switching of S into the S_{stop} state when encountering a colicin in the environment, making switching into S_{stop} dependent on the concentration of colicin ($[col]$) in the environment. Figure adapted from [51].

$$\begin{aligned}
 \partial_t C &= r_C \cdot C - s_C \cdot C \\
 \partial_t C_{on} &= s_C \cdot C - d_{C_{on}} \cdot C_{on} \\
 \partial_t S &= r_S \cdot S - s_S \cdot [col] \cdot S
 \end{aligned} \tag{3.2}$$

Where each strain S or C, can reproduce with a rate r_X . The C strain has the ability to switch into the ON state with a constant switching rate s_C depending on the stress level. When this happens, it can release toxin via cell lysis with the rate $d_{C_{on}}$. This rate is dependent on the expression of the gene *cel* in the cell and is the inverse of the lysis time T_{lysis} measurable in single cell time-lapse microscopy. When colicin is released into the environment it diffuses in the surrounding, which is implemented into the simulation with an exponential gradient from the point where C cell lysis occurred [46]. A S strain encountering colicin in the environment can switch into the S_{stop} state with a switching rate of s_C . Switching thus depends on the concentration of colicin in the environment ($[col]$).

The two strain interaction parameters were implemented into a simulation by von Bronk *et al.* [10, 11, 67]. In the following the basic principles of this model will be explained.

For expansion in 2D a 250x250 lattice was chosen. A space in the lattice can be empty or contain any of the states described in Figure 3.9 and shown in Figure 3.10 A. A spot in the lattice has 8 neighbors that are considered in each simulation step and influence the occupation of an empty site (see Figure 3.10 B). Interaction is possible for the 8 neighbors (Moore neighborhood) [68] and is weighed depending on distances as shown in Equation (3.3), which is comparable to the neighbors shown in Figure

**Figure 3.10**

Lattice configuration and transitions for simulation. A) Definition of possible lattice occupations corresponding to states shown in Figure 3.9 and Chapter 2. B) Lattice configuration for considered lattice space (black) and its neighbors (dark grey: Neumann neighbors, lightgrey: Diagonal neighbors, light and dark grey: Moore neighbors) in a Moore neighborhood used for simulations (Equation (3.3)). C) Possible transitions for all lattice occupations described in A) depending on the environment. Probabilities are given in Equations (3.4, 3.5, 3.6). Simulation adapted from [10].

3.10 B. Here direct neighbors (Neumann neighborhood) [68] are marked in dark gray while diagonal neighbors are shown in light gray.

$$\begin{aligned}
 N_{Moore} &= N_{Neumann} + N_{Diagonal} \\
 &= 4 \cdot 1 + 4 \cdot \frac{1}{\sqrt{2}}
 \end{aligned} \tag{3.3}$$

Each lattice site has a defined probability for switching into another state or staying in its current one, depending on occupation of their Moore neighborhood. Possible transitions are shown in Figure 3.10 and depend on the lattice site under consideration. Probabilities p for all transitions are listed in Equations 3.4-3.6.

$$\begin{aligned}
 p_{empty,S} &= N_S \cdot r_S \cdot \Delta t \\
 p_{empty,C} &= N_C \cdot r_C \cdot \Delta t \\
 p_{empty,stay} &= 1 - (N_S \cdot r_S + N_C \cdot r_C) \cdot \Delta t
 \end{aligned} \tag{3.4}$$

With N_X : number of neighbors of type X in the surrounding (with distance factor shown in Equation (3.3)) and r_X : replication rate of X strain. Switching of an empty state thus depends on the number of S or C cells in the environment. Each state can

either switch into another state according to the transitions shown in Figure 3.9 or stay in its current state.

$$\begin{aligned} p_{S,switch} &= [col] \cdot s_S \cdot \Delta t \\ p_{S,stay} &= 1 - [col] \cdot s_S \cdot \Delta t \end{aligned} \quad (3.5)$$

With $[col]$ being the concentration of colicin in the surrounding, s_S switching rate of the S strain into the S_{stop} state and Δt the time step size in the simulation. S cells switch into S_{stop} depending on the colicin concentration in their environment. Which, as described above, is simulated with an exponential decay from its point of origin.

$$\begin{aligned} p_{C,switch} &= s_C \cdot \Delta t \\ p_{C,stay} &= 1 - s_C \cdot \Delta t \\ p_{Con,switch} &= d_{Con} \cdot \Delta t \\ p_{C,stay} &= 1 - d_{Con} \cdot \Delta t \end{aligned} \quad (3.6)$$

Where s_C describes the switching rate of the C strain into the ON state (C_{on}) and d_{Con} the rate of degradation of a C_{on} cell and thus emptying a lattice space. The rate d_{Con} with which the C_{on} cells release toxin is limited by the minimal time to cell lysis that is set for the system to react to encountered stresses.

Initial positioning of cells on the lattice is random in a circular pattern (resembling experimental conditions) but kept at a ratio of approximately 1 C cell for 100 S cells. Furthermore, in order to decide which switching takes place, all probabilities for a space are summed up and a random number between 0 and 1 is chosen. Depending on this number and its position in the probability sum, the new state of this lattice space is determined. This is repeated for all lattice sites occupied or neighboring an occupied space for each time-point.

When a filled lattice space 'touches' a border of the defined lattice, rescaling of the current lattice occupation as well as all rates (growth, switching etc.) takes place. Detailed parameters that are fixed for all simulations are given in Table 3.3.

The switching rate s_C was varied between 1 % and 99 % representing induction levels from low to very high external stress. Analytical solution of the ODE system (Equation (3.2)) was performed by von Bronk and steady state solutions were obtained for the fractions of switching C cells [10, 67]:

Parameter	Definition	Size
N	lattice sites in x and y dimension	250
Δx	initial lattice spacing	2 μm
Z	factor used for rescaling of lattice	5
Δt	time step size	1.5 min
t_{end}	complete simulation time	2790 min
C:S	mean initial ratio of C to S strain	1:100

Table 3.3

Fixed parameters for competition model were adapted from von Bronk [10, 67]

$$Frac(t) = \left[\frac{C_{on}(t)}{C_{on}(t) + C_{off}(t)} \right]_{t \rightarrow \infty} = \frac{s_C}{r_C + d_{C_{on}}} \quad (3.7)$$

Other parameters, such as lysis time, growth rate, toxin effectivity and toxin amount have to be adjusted by extraction from measurements as follows:

- **GRs**: Growth rates for all strains S and C_X were extrapolated from linear fits of control measurements as described above. The conversion factor from area growth rate to simulation growth rate was chosen as in Bronk *et al.* [10, 11].
- **$d_{C_{on}}$** : Degradation rates for all C_X strains were calculated from their median time to cell lysis (T_{lysis}) determined in single-cell time-lapse microscopy.
- **n_{tox}** : Toxin amounts were determined in experiments as described in Section 3.3 and inserted as factors depending on the lowest toxin amount, which was set to factor 1. More detailed information is given in Chapters 4 and 5.
- **σ_S** : Toxin sensitivity of the competitor (S) is a factor that was determined by adjusting simulation to experimental results over broad ranges, as it cannot be measured easily. In previous studies by von Bronk *et al.* [10, 11], s_S was chosen as 1500. Here, this also fits for the C_{REP1} strain over a broad range of stresses.
- **s_S** : Toxin effectivity fo toxin to the S strain is calculated as $s_S = \sigma_S \cdot n_{\text{tox}}$, making it dependent on both the S strain sensitivity to toxin and the amount of toxin being released by C_X .
- **[col]**: The colicin concentration is determined by the position of the observed lattice space compared to that of C strains releasing toxin. For each cell lysis of a C cell, an exponential decaying profile of toxin in the lattice is calculated [10, 46]. This leads to a decrease in [col] the farther the distance between the observed lattice cite and a lysed C lattice site.

In summary, this model facilitates theoretical analysis of bacterial interaction over a broad time-scale from single cell interaction to macroscopic competition outcome. For detailed description of the model and all its components, please see von Bronk 2018 [67]. The key components driving ColicinE2 driven interaction are implemented including stochasticity in gene expression as well as positioning, toxin production and sensitivity, growth rates and switching of the C strain into the toxin producing strain. This theoretical approach enables investigation of the different components separately, even if they are biologically linked. Selective variation of parameters is supported by the framework.

3.5. Additional Software

Data Plots and Sketches All sketches and multi-panel figures were made using the open-source vector graphic software Inkscape Version 0.92.4.

Data plots were created using the statistical programming language R (Version 3.5.2) in combination with R studio (Version 1.1.463) and various R packages like 'ggplot2'. Boxplots that are shown in the result section are composed as follows: Boxes depict the interquartile range (IQR) (25-75th percentile) with the line within the box for the median. Whiskers (lines perpendicular to boxes) range from $1.5 \cdot IQR$ above and below each box. Dots depict outliers in the distribution that are below and above these whiskers [69].

Significance Analysis Significance analysis was performed using the statistical programming language R (Version 3.5.2) in combination with R studio (Version 1.1.463) and the 'stats' library. First, distributions were tested for normality using the 'shapiro.test' function. Accordingly, normal distributions were tested with a two sample t-test ('t.test' function). Non-normal distributions were tested for significance using the 'wilcoxon.test' function, performing a Mann-Whitney-Wilcoxon test.

4. Results: Single-cell Expression Dynamics in the ColicinE2 System

The results discussed in this chapter are published in Götz *et al.* 2018: *CsrA and its regulators control the time-point of ColicinE2 release in Escherichia coli* [55] and Weiß *et al.* 2020 (accepted): *Dynamics of ColicinE2 production and release determine the competitive success of a toxin-producing bacterial population* [51].

4.1. Toxin Expression Dynamics in Single Bacterial Cells

4.1.1. Control of ColicinE2 Expression Dynamics

To understand the underlying mechanisms that in the end determine outcome of the C-S interaction it is important to investigate the toxin expression dynamics (TED) of the C strain at the single-cell level. More importantly, how these TED are controlled e.g. by regulatory modules. To investigate this, a combination of experimental and theoretical analysis was performed. Fluorescence time-lapse microscopy of single cells at different induction levels with the antibiotic mitomycin C (MitC) is used to test strains with transcriptional and post-transcriptional mutations. For this, a reporter plasmid containing *cfp* and *yfp* as replacements for toxin gene *cea* and gene *cel*, causing cell lysis (details on mutations see Table 3.1), and their fluorescence traces are investigated.

The regulation of the ColicinE2 system consists of two major steps. First, the transcriptional regulation via LexA, which is coupled to the SOS response of the bacterial cells. And second, the post-transcriptional regulation of *cel* gene translation controlled by production of long mRNA (less than short mRNA) and an additional repression of translation via the global protein CsrA which is part of the carbon storage regulatory (Csr) system of bacteria. Starting with characterization of the created reporter plasmid (REP1, see Table 3.1 and Chapter 3), the S strain was used in order to be able

4. Results: Single-cell Expression Dynamics in the ColicinE2 System

to investigate fluorescence over long times without cell lysis. The created strain with the reporter plasmid REP1 is called S_{REP1} . Comparable to the wild-type pColE2-P9 system the REP1 plasmid is a multi-copy plasmid and contains all major regulation elements of the ColicinE2 operon (see Figure 3.1). Fluorescence-time lapse microscopy was performed (details see Chapter 3) to obtain information on expression strength in the ColicinE2 system which can be analyzed by the fluorescence intensities of the FPs YFP and CFP, respectively. After this, the time-point of expression start can be investigated using time-lapse data and the time of switching into the ON state as described in Chapter 3 Figure 3.4.

For the S_{REP1} strain, fluorescence intensity data show an increasing fluorescence over time where a steady state seems to be reached at the end of the measurement. This leads to final median fluorescence intensities (FI) of 2002 FU and 547 FU for YFP and CFP respectively (Figure 4.1).

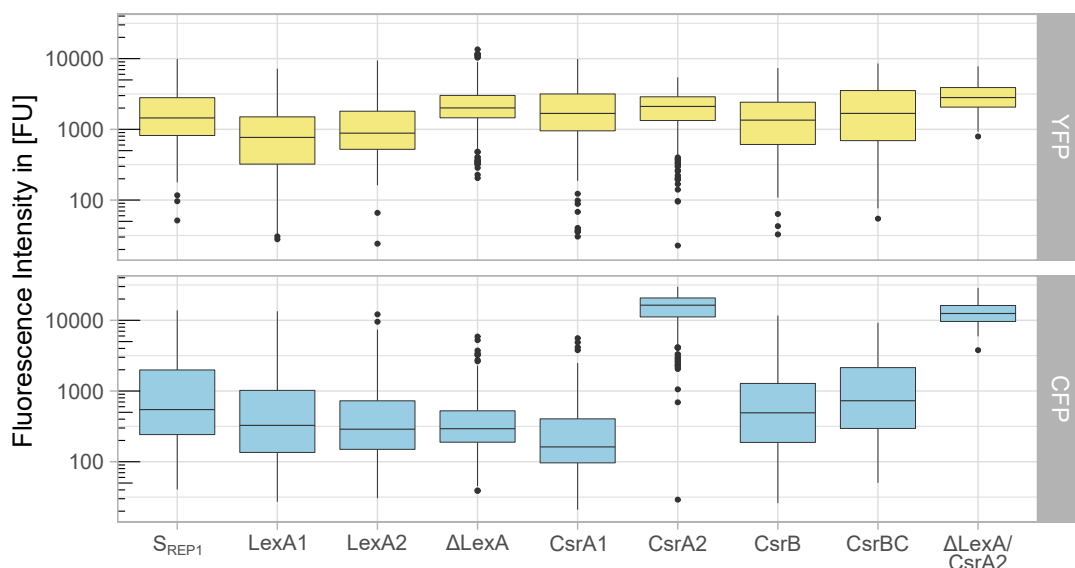


Figure 4.1

Expression of the FP from the reporter genes in several mutant strains. Final FI in fluorescent units [FU] for all S_X mutants of the REP1 strain measured. YFP (yellow; *cea*) in CFP (blue, *cel*) shown in top and bottom box plots respectively. The intensities were obtained at the end of measurements at 270 min for the three high induction levels of 0.1 $\mu\text{g}/\text{ml}$, 0.25 $\mu\text{g}/\text{ml}$ and 0.4 $\mu\text{g}/\text{ml}$ of MitC. (For detailed description of mutations see Table 3.1.)

To study the influence of transcriptional regulation in the ColicinE2 system, three mutants with changes in the binding strength of LexA to the SOS box on DNA were created (Chapter 3 Table 3.1). The mutants LexA1 and LexA2 were expected to have increased and decreased binding of LexA to the SOS box whereas in the ΔLexA the

complete LexA binding motive is deleted from the sequence which leads to constitutive expression of the operon (Methods and Table 3.1). As expected, the mutants LexA1 and Δ LexA showed decreased and increased YFP fluorescence according to their LexA mutations. However, LexA2 also shows reduced FI compared to the S_{REP1} strain which is opposed to the expected effects by weaker LexA repression. Changes in transcriptional repression have an effect on CFP expression as the amount of long mRNA that contains the *cfp* gene is dependent on the transcription rate. When YFP fluorescence is decreased in LexA1 and LexA2, CFP fluorescence decreased with it.

In a next step, various mutations on the post-transcriptional regulation level were introduced. These mutations can be grouped into two categories. First, changes on the DNA of the plasmid carrying the operon which lead to increased and decreased binding of CsrA to the resulting long mRNA for the mutants CsrA1 and CsrA2, respectively. The second category of mutations are chromosomally introduced genetic modifications in the S strain creating the strains CsrB and CsrBC which cannot produce the sRNAs CsrB or both CsrB and CsrC due to deletion of their gene sequences (Chapter 3). These mutations should increase the amount of free CsrA in the cells by reduction of CsrA sequestering elements, in this case sRNAs, that carry multiple CsrA binding sites each. The observed changes in YFP fluorescence, were as expected, rather small as post-transcriptional mutations should not have any major effects on transcription of the entire operon. However, only the mutations in CsrA binding strength in the mutants CsrA1 and CsrA2 led to significantly decreased or increased CFP expression, respectively. While the CFP fluorescence in CsrA1 decreases by a factor of 4, the increase for CsrA2 is much higher with a factor of 10. This is due to the increase of CsrA binding for CsrA1 which is much smaller than the reduction of CsrA binding in CsrA2 as the binding motive for CsrA on the wild-type long mRNA is almost optimal [70] (discussed in detail in the Chapter 3). In contrast to expectations, CFP fluorescence did not change significantly for both sRNA mutants even though a higher number of free CsrA was expected to be available. This could be due to compensatory effects that will be discussed later.

To confirm the effect of the CsrA2 mutation on the expression of FPs in the system, a double mutant with a combination of the deletion of LexA binding (Δ LexA) was combined with the highly reduced binding for CsrA creating the strain Δ LexA/CsrA2. This strain showed increased YFP fluorescence similar to Δ LexA as well as CFP intensities comparable to CsrA2, according to both single mutations.

Investigating the time dynamics of expression of the ColicinE2 system it is essential

to understand the timing of colicin production and release. For that, the time of switching into the ON state was analyzed for both the toxin (YFP) and production of protein leading to cell lysis (CFP) as the time when their respective fluorescence intensity crosses a threshold (see Chapter 3, Figure 3.4 D). The resulting switching times (T_{ON}) for all mutants are shown in Figure 4.2.

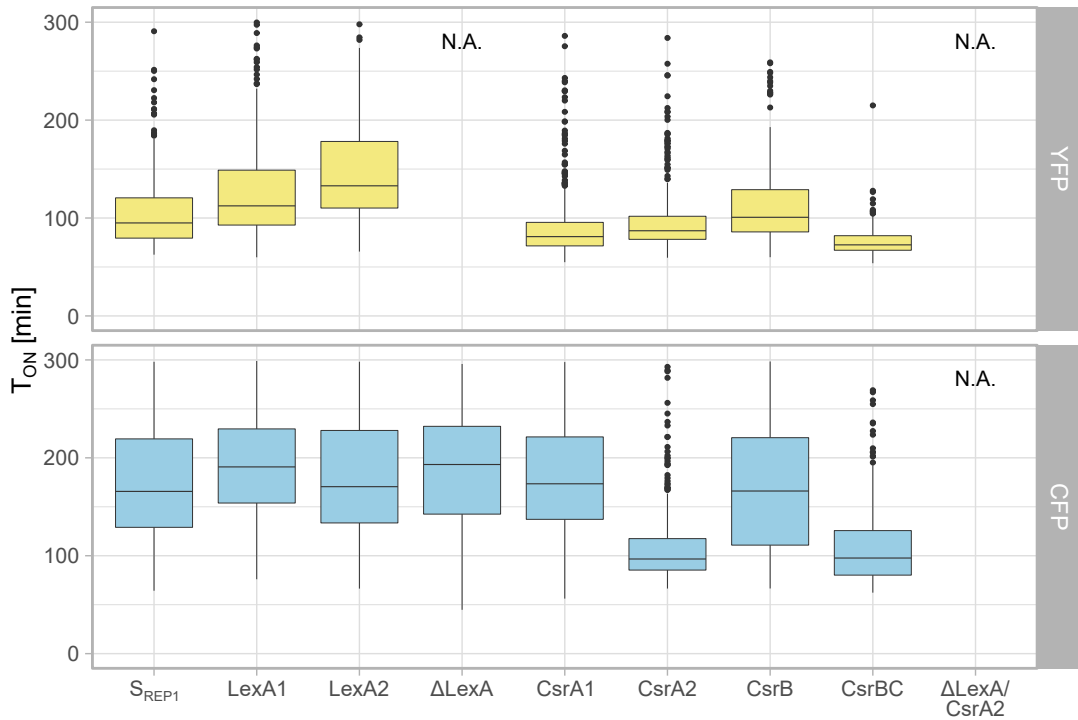


Figure 4.2

Times of switching into the ON state of both reporter genes in several mutant strains. T_{ON} in minutes after induction for all S_X mutants of the REP1 strain. YFP (*cea*: yellow) and CFP (*cel*: cerulean) shown in top and bottom box plots respectively. N.A. for non available data points when all cells are producing the FPs constitutively. The measured times were obtained for all three induction levels of 0.1 μ g/ml, 0.25 μ g/ml and 0.4 μ g/ml MitC. (For detailed description of mutations see Table 3.1.)

The data shows that for the S_{REP1} strain, which is genetically closest to the wild-type ColicinE2 operon, the median T_{ON} of YFP and CFP for all three measured MitC concentrations (0.10 μ g/ml, 0.25 μ g/ml and 0.40 μ g/ml) are 95 min and 166 min, respectively. This means that production time of toxin ($T_{ON_{cea}}$) starts before that of *cfp* which leads to a delay between toxin production and release in this strain. In the next steps the effect of several genetic modifications on timing of switching into the ON state of YFP and CFP are analysed for the single cell data over all induction levels. Mean T_{ON} for YFP were measured between 76 min and 147 min with corresponding mean CFP T_{ON} ranging from 110 min to 189 min. This shows again that in general,

the gene *cel* is expressed later than *cea* in the operon. For mutations varying the transcription of the operon by changing LexA binding (LexA1 and LexA2) the ON times of YFP are shifted to later times, supporting the assumption that both mutations lead to higher operon repression, which was shown by their FI traces. Accordingly, the ON times of CFP in these mutants shift to later time-points as well (Figure 4.2). This means that higher operon repression by LexA leads to later switching into the ON state in both YFP and CFP. The Δ LexA mutant in turn has no measurable switching time for YFP as it produces the FPs constitutively without SOS induction. However its ($T_{ON_{cfp}}$) is shifted to 184 min which is later than that of S_{REP1} . One reason for that could be the deletion of LexA binding to the SOS box. In this case many cells produce CFP without induction and thus have no measurable switching time for CFP and YFP. However, T_{ON} can only be calculated for cells switching into the ON state during the measurement but not the cells that are already in the ON state when the measurement started.

Observation of the S_X strains with mutations related to the post-transcriptional repressor CsrA shows that all of these mutants start switching of YFP slightly earlier or comparable to S_{REP1} (Figure 4.2 CsrA1-CsrBC). Additionally, CsrA mutants show higher variations in CFP switching times into the ON state. While both CsrA1 and CsrB show no significant shift in $T_{ON_{cfp}}$, CsrA2 and CsrBC show shifts in switching time at much earlier time-points. In case of CsrA1 this is due to the small change in binding strength of this mutation compared to S_{REP1} . For CsrB, the second sRNA (CsrC) has been shown to be able to compensate the effect of the single gene knock-out by increasing CsrC production [71]. In both mutants with significantly earlier CFP switching times, the mutations cause big changes in either CsrA binding strength (CsrA2) or in CsrA abundance inside the cells (CsrA2 and CsrBC). Their earlier mean $T_{ON_{cfp}}$ of 110 min for CsrA2 and 111 min for CsrBC is significantly earlier than in S_{REP1} and is comparable to $T_{ON_{yfp}}$ of 105 min for S_{REP1} . These findings indicate that CsrA binding and its abundance are a key player in the regulation of toxin release in the ColicinE2 system.

4.1.2. Post-transcriptional Regulation by CsrA Controls the Time-point of Toxin Release

In previous studies Lechner *et al.* [72, 73] performed a theoretical analysis to model the post-transcriptional regulation of the ColicinE2 system. In collaboration with

Matthias Lechner from the Frey group (LMU Munich), this model was extended to include all regulatory elements that will be discussed in the following. Those components include plasmid composition and abundances in the various strains and an overview over the main components is shown in Figure 4.4 B (adapted from [55]). The model was then validated using parameters from experimental data and reproducing experimental delay distributions of the S_{REP1} strain. Deterministic differential equations for the main regulatory components of the system were set and are shown in the following as described in [55].

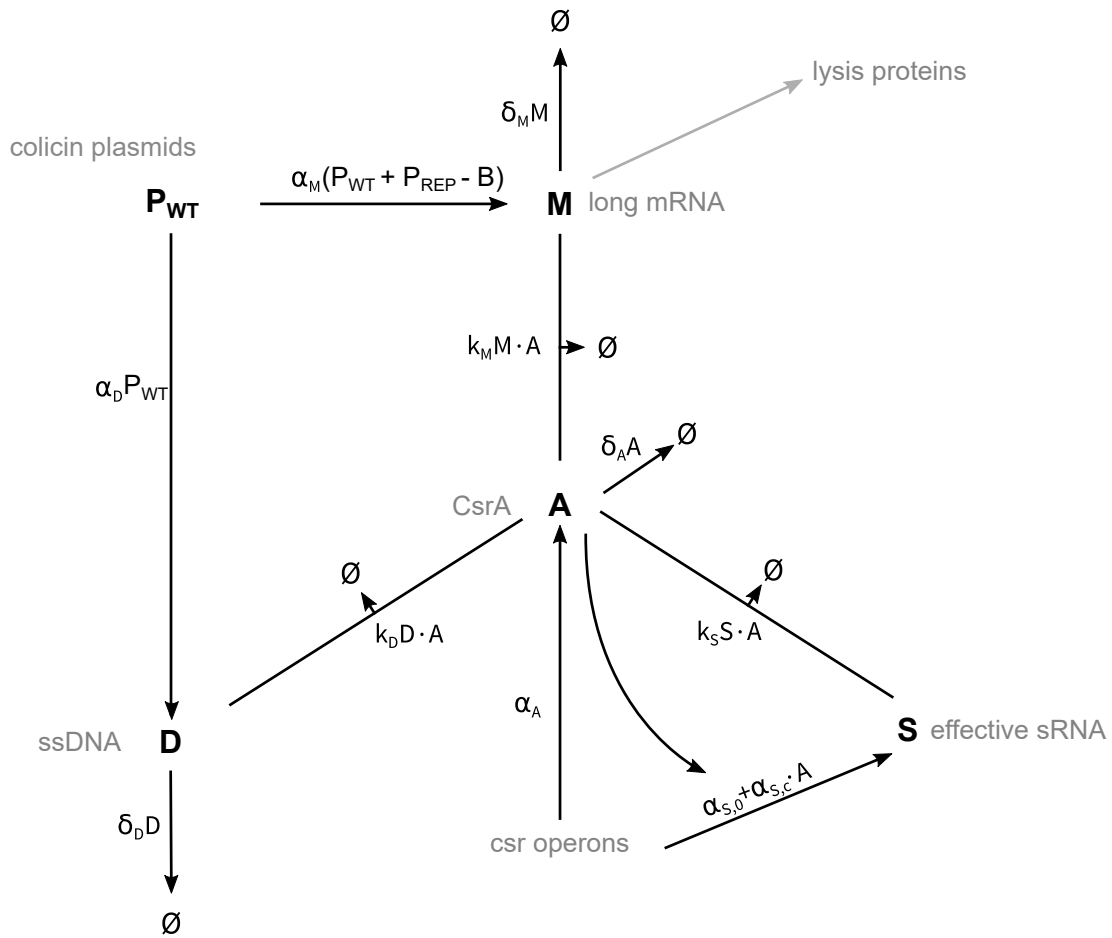


Figure 4.3

Biochemical network involved in the post-transcriptional regulation of ColicinE2. The complex description of the network can be reduced to the set of effective interactions shown here. The derivation of these effective descriptions is given in Götze *et al.* 2018 (Figure adapted from [55]). The abundances of free CsrA, long mRNA, effective sRNA and ssDNA are given by A , M , S and D . Degradation (δ_X), production (α_X) and binding rates (k_X) are given for each component X . The plasmid number of the wild-type pColE2-P9 plasmid is described with P_{WT} . (Figure adapted from [55]).

Starting with the abundance of long mRNA (M) that increases with production rate α_M depending on the total number of plasmids within the cell, specifically the wild-type ColicinE2 plasmid P_{WT} and the reporter plasmid P_{REP} . However, only when the promoter is not repressed transcription of the operon can happen and long mRNA can be produced. Thus, the number of repressed promoters B reduces the amount of mRNA. Decrease of long mRNA can happen in two processes (Figure 4.3): (i) spontaneous degradation with rate δ_M depending on mRNA number and (ii) coupled degradation of long mRNA by binding to CsrA (A). The resulting differential equation reads (adapted from [55, 72]):

$$\partial_t M = \alpha_M(P_{WT} + P_{REP} - B) - \delta_M M - k_M M \cdot A \quad (4.1)$$

Next, the differential equation for changes in abundance of the sRNAs (CsrB and CsrC) with different amounts of CsrA binding sites was combined into one parameter called effective sRNA [72]. The amount of effective sRNA S was given by [55]:

$$\partial_t S = \alpha_{S,0} N + \alpha_{S,c} N \cdot A - \delta_S S - k_S S \cdot A \quad (4.2)$$

Effective sRNA abundance is dependent on basal sRNA production from the carbon storage regulation (Csr) system with rate $\alpha_{S,0}$, and CsrA driven production with rate $\alpha_{S,c}$. Spontaneous degradation (rate δ_S) and complex formation by binding of CsrA to sRNA with rate k_S decrease the number of effective sRNA in the cell (Figure 4.3). As shown in Chapter 3, the wild-type plasmid pColE2-P9 can produce single-stranded DNA (ssDNA: D) by rolling circle replication of the plasmid. Replication with rate α_D depending on the number of colicin plasmids P_{WT} and accordingly, degradation with rate δ_D also depends on sDNA abundance (Figure 4.3). Another option for ssDNA degradation is the possible binding of CsrA to ssDNA that will be discussed in more detail in this section. The corresponding equation is [55]:

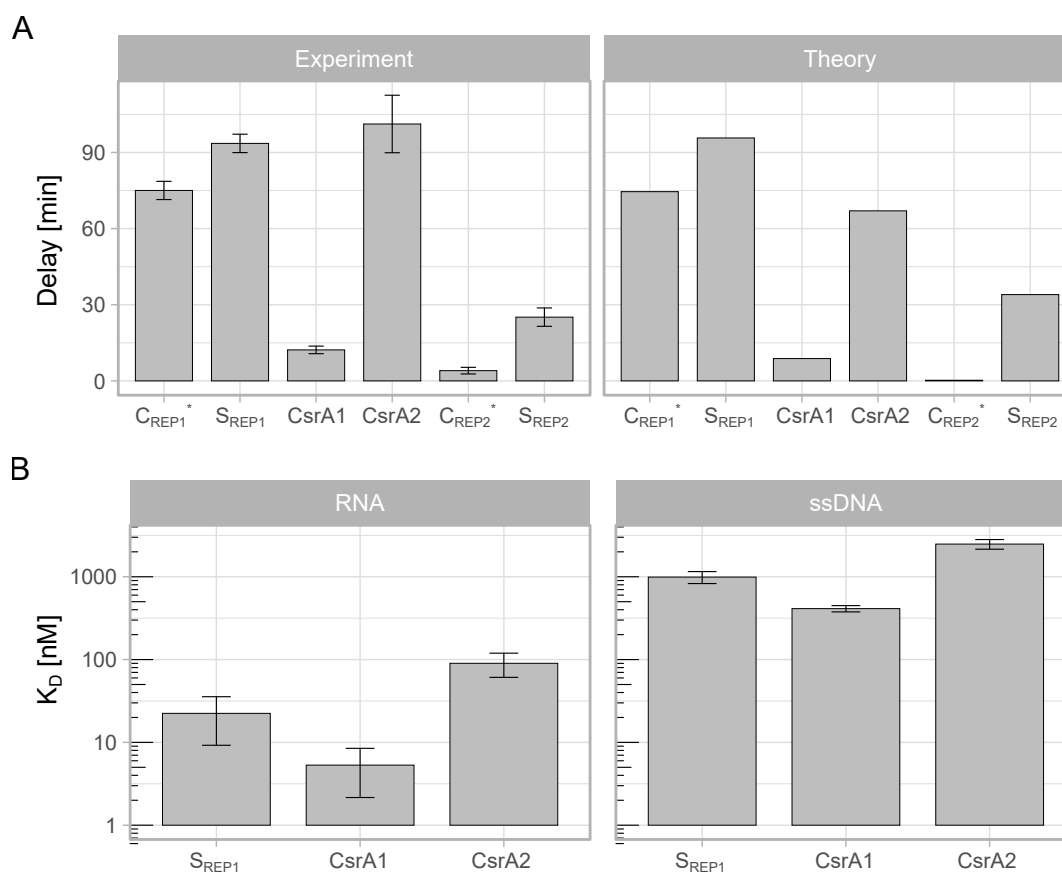
$$\partial_t D = \alpha_D \cdot P_{WT} - \delta_D D - k_D D \cdot A \quad (4.3)$$

Finally, the differential equation describing the changes in the abundance the global regulation protein CsrA (A) contains many coupled degradation processes due to binding to the various sequestering elements. It depends on the amount of long mRNA (M), effective sRNA (S) and ssDNA (D). Each of those lead to degradation with rate k_X (X : corresponding binding partner). Increase of CsrA numbers takes place when CsrA is produced by the Csr system with rate α_A (Figure 4.3). The resulting equation

is shown in Equation (4.4) [55].

$$\partial_t A = \alpha_A - \delta_A A - k_M M \cdot A - k_S S \cdot A - k_D D \cdot A \quad (4.4)$$

Combining all this, a theoretical analysis was performed with values adapted from experimental data and previous knowledge of the ColicinE2 system and its main regulating components. The model was validated with experimental data and then used to predict the expression behavior of the wild-type C_{WT} that can not be investigated with fluorescence time-lapse microscopy. Furthermore, the role of ssDNA as a regulating mechanism was evaluated. A more detailed description of the complex theoretical model can be found in Lechner *et al.* 2016 [72] for the basic model and in Götz *et al.* 2018 [55] and Lechner 2017 [73] for the new model that was extended to include different plasmid copynumber and presence of ssDNA as a new CsrA sequestering element. First however, a closer understanding of the expression dynamics of the ColicinE2 system has to be gained. For this, it is important to analyze not only the difference in mean times of switching into the ON state, but also the time delay between production and release of the toxin for each single cell due to the heterogeneity of the system. For this, the time delay between switching into the ON state in YFP and CFP was quantified as $\text{delay} = T_{ON_{cfp}} - T_{ON_{yfp}}$ for every cell that switches into the ON state in both fluorescent channels. Since the data for T_{ON} shown in Figure 4.2 revealed the importance of CsrA for control of T_{ON} times (especially $T_{ON_{cfp}}$), the effect on delay in the mutants CsrA1 and CsrA2 were tested for all cells switching into the ON state in both YFP and CFP. For these two mutants the same effects as for their T_{ON} times of YFP and CFP were observed. When CsrA has a stronger binding to mRNA, CFP switching is shifted to later times due to lower likelihood of translation and the delay becomes longer. In contrast, in the CsrA2 mutant, where much less CsrA binding to RNA takes place due to the lack of the second hairpin structure of the long mRNA, *cfp* translation takes place with reduced repression and the delay becomes very short with 12 min compared to 75 min in S_{REP1} . Changes in CsrA binding to long mRNA are quantified in the model by varying k_M . Corresponding to mutations in CsrA1 and CsrA2 k_M was adjusted for increased binding strength ($k_M = 0.0125$, CsrA1) or decreased binding strength ($k_M = 0.0018$, CsrA2). Here, the trends from experimental results were replicated with increasing delay for stronger repression by CsrA and vice versa (Figure 4.4 A). Hence, experiments as well as theoretical analysis show that the *cea-cel* delay in each cell is mainly regulated by the repression of long mRNA translation by CsrA and that CsrA plays a key role in TED.

**Figure 4.4**

Delay times and measured binding strengths for variations in CsrA binding efficiency. A) Delay times for mutants with varying CsrA binding strength or changing number of CsrA binding partners. B) Mean K_D in [nM] with standard error of the mean (SEM: error bar) for RNA and ssDNA corresponding to mutant strains derived from gel-shift assays. *: marks C_X strains measured under growth conditions without arabinose.

The ColicinE2 operon is encoded on a multi-copy plasmid with a copynumber of approximately 20 copies/cell for the wild-type plasmid. In contrast, the reporter plasmid REP1 has a mean copynumber of 55 copies/cell. This means that in general when the SOS response is triggered, more long mRNA is produced from the plasmid with more copies. As shown before, CsrA is a main player in regulation of the delay in the ColicinE2 system by binding to the long mRNA target and repressing translation of the *cel* gene and might be affected by the total number of long mRNA present in a cell. To test this hypothesis a second reporter plasmid was created that is similar to REP1 but has a reduced copynumber of 13 copies/cell and transformed into S strain to create S_{REP2} . Measurements and simulations of this strain confirmed that the amount of CsrA binding partners such as long mRNA in a cell directly influences delay time.

Specifically, for a plasmid with less copies and less long mRNA ($S_{\text{REP}2}$) a longer delay was observed (Figure 4.4 A). Even though the total number of CsrA in a cell is quite big, the amount of free CsrA was shown to be quite small [74]. Subsequently, free CsrA abundance might be crucial for the regulation of delay times.

Furthermore, experiments for $C_{\text{REP}1}$ and $S_{\text{REP}1}$, which carry the same reporter plasmid in a strain with or without the wild-type plasmid (C or S, see Table 3.1) revealed a big difference in time delays for the two strains. Similar to earlier studies by Mader *et al.* 2015 [13] there was only a small time delay between YFP and CFP in a toxin producing strain $C_{\text{REP}1}$ (Figure 4.4 A). However, the strain without the colicin plasmid had a mean delay of 75 min. The only difference between these two strains is the presence of the ColicinE2 plasmid in C cells. This means, that some additional regulation mechanism on the wild-type plasmid is responsible for the change in delay time. Earlier studies by Morales *et al.* 2015 [65] on the pColE3-CA38 plasmid revealed that single stranded DNA intermediates (ssDNA) produced by rolling circle replication of the plasmid can accumulate in the cells. Homology analysis of the pColE2-P9 and the pColE3-CA38 plasmid revealed that most of the genes involved in autonomous plasmid replication are present in both plasmids [55]. To confirm that ssDNA can indeed accumulate in cells carrying the pColE2-P9 plasmid, DNA of induced and uninduced $S_{\text{REP}1}$ and $C_{\text{REP}1}$ cells was extracted and run through an agarose gel. This revealed the presence of ssDNA in cells carrying the WT plasmid (Figure 3.5). The ssDNA could interact with the regulator CsrA by sequestering free CsrA binding partners and thus change the time delay in C_X cells. To address this hypothesis, gel shift analysis was performed with CsrA and RNA or ssDNA of the ColicinE2 sequence to prove that the mRNA binding protein CsrA can bind to both ssDNA and RNA (Figure 4.4 B). CsrA can bind to RNA corresponding to the long mRNA of the ColicinE2 plasmid with a K_D of (22 ± 13) nM, which is in good accordance with literature [5, 23]. Furthermore, the same experiments for CsrA binding to a corresponding ssDNA sequence revealed a K_D of (991 ± 164) nM, showing that the mRNA binding protein CsrA is also able to bind to ssDNA, but with a lower affinity. This is in accordance with previous studies revealing that proteins containing a KH domain can bind to mRNA and ssDNA [4, 75] and CsrA has been shown to contain a KH domain [76]. Further analysis on the binding behavior of CsrA was performed for RNA and ssDNA resembling the nucleotide sequences of the mutant strains CsrA1 and CsrA2. The binding affinities to RNA were measured and CsrA exhibits stronger (K_D of (5 ± 3) nM) and weaker binding (K_D of (90 ± 29) nM) to the RNA sequences of CsrA1 and CsrA2, respectively (Figure 4.4

B). These results confirm the predictions made for the binding of CsrA to changes RNA sequences of the mutants (see Chapter 3). The same trends for binding strength changes due to mutation were confirmed for the corresponding ssDNAs, indicating the specificity of CsrA binding to the same motifs on RNA ssDNA (GGA motif). Even though CsrA binding to ssDNA is less efficient than to RNA (factor ≈ 45), ssDNA can be a relevant component for CsrA sequestering in C cells because it is produced independently from SOS response and can accumulate to high numbers in a cell (Figure 3.5, Chapter 3). Experiments with C_{REP1} and C_{REP2} showed that the presence of the second plasmid and its ssDNA greatly lower their time delay in comparison to their corresponding S_X strains (Figure 4.4 A).

To elucidate the importance of ssDNA in the regulation of the *cel* gene in cells containing the wild-type plasmid, a detailed theoretical analysis was performed for the various strain configurations like their copynumbers and abundances for each strain, including the wild-type strain (C_{WT}) that does not carry any FPs or reporter plasmids (Figure 4.5 A).

A comparison of *cel* gene expression was performed in the absence ($\alpha_D = 0$) and presence ($\alpha_D = 7$) of ssDNA. For strains that contain ssDNA (C_X) free CsrA abundance is reduced and the delay times are lower than in corresponding S strains and also lower than in the absence of ssDNA (Figure 4.5 B,C). For high copynumbers in the C_{REP1} strain, the ssDNA can completely eliminate the time delay, which is in good accordance to experimental data. C_{REP2} which has a reduced copynumber is only able to release the toxin at high numbers if ssDNA is present. For the wild-type strain, where cell lysis only can be measured after at least 150 min, theoretical analysis predicts a time delay in the range of one hour and in the absence of ssDNA no cell lysis is happening within the time-scale of the measurements. Without ssDNA only a small number of C_{WT} cells are able to release the toxin which shows that for the natural system ssDNA is an important regulating mechanism for efficient toxin release.

4. Results: Single-cell Expression Dynamics in the ColicinE2 System

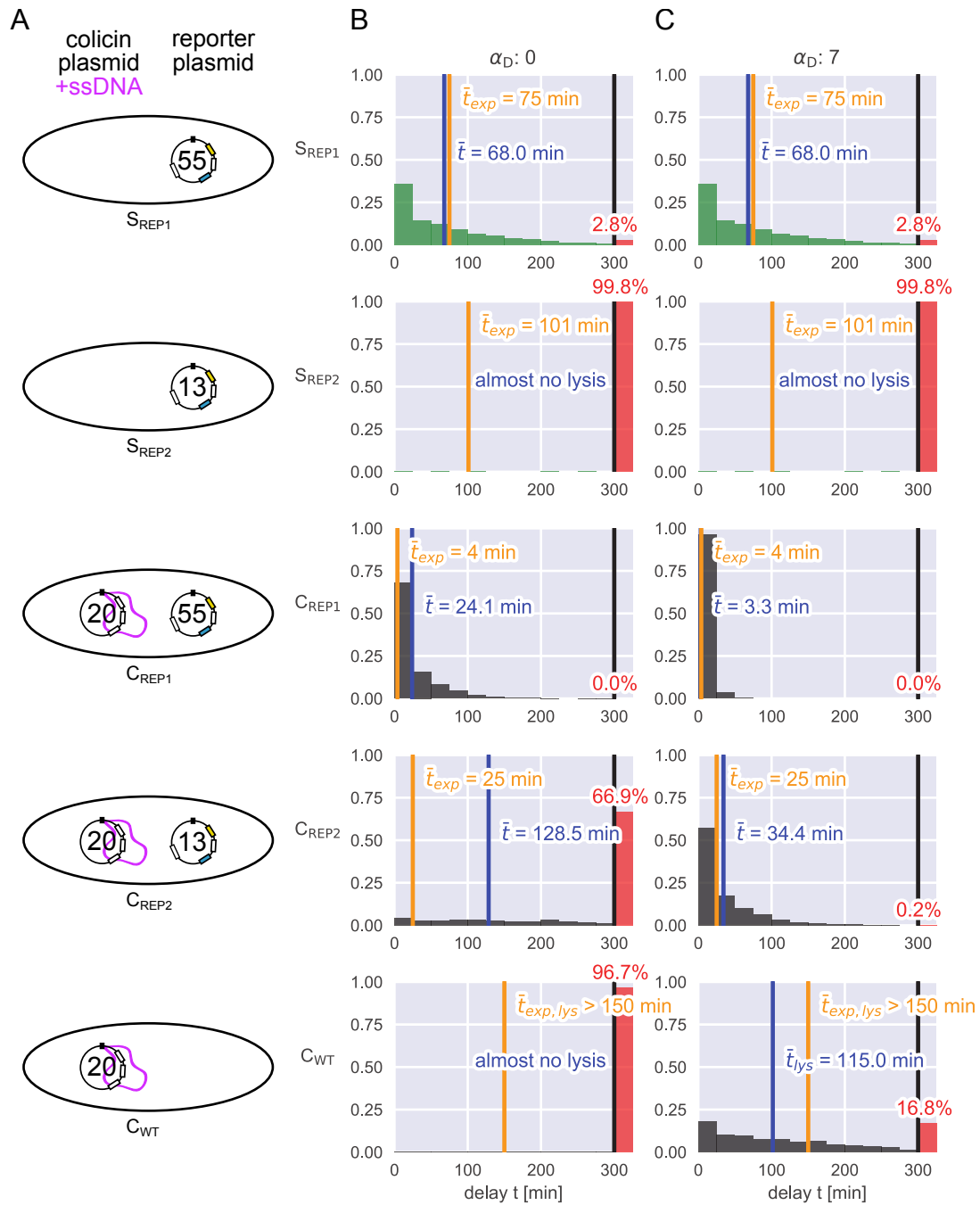
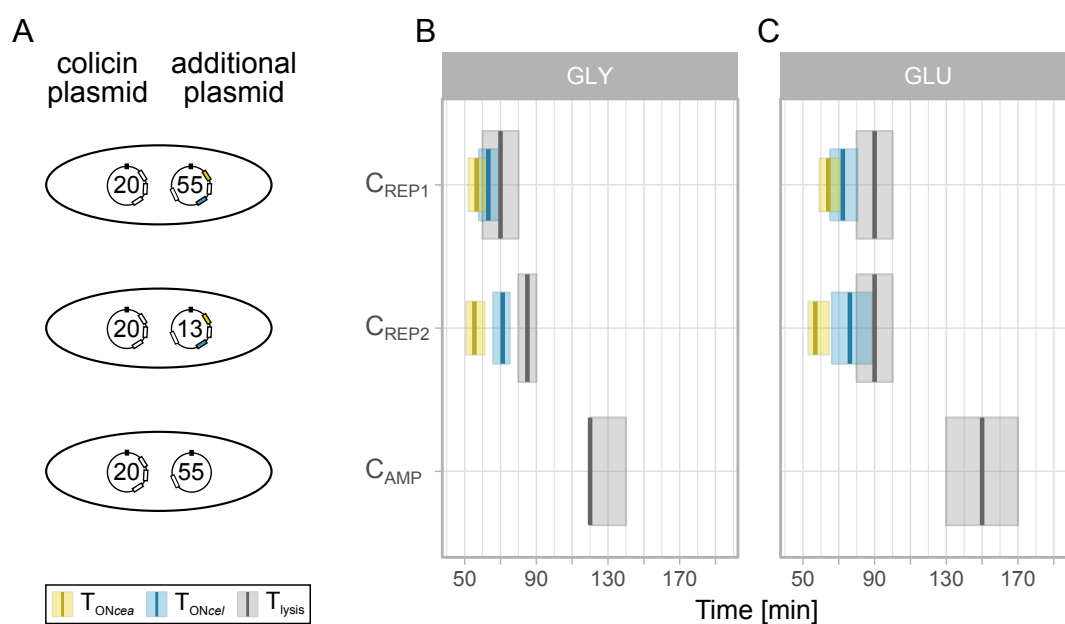


Figure 4.5

Theoretical modeling shows importance of ssDNA as binding partner for CsrA. A) Strains with included plasmids and their plasmid copynumber. The colicin plasmid produces ssDNA (purple) and is present in all C_X strains. B,C) Histograms of the *cea-cel* delay for all strains obtained by theoretical analysis. B) $\alpha_D = 0$ for no ssDNA present in cells. C) $\alpha_D = 7$ with ssDNA in cells. In each graph the mean experimental delay is included (orange line) and compared to the mean theoretical delay (dark blue line). The fraction of cells that do not lyse in the timescale of experiments (>300 min) are depicted on the right (red bar and fraction). For C_{WT} no experimental delay can be measured and instead the experimental lysis time is included (orange: $t_{exp,lys}$). For all S_X strains changes in α_D do not have an effect on simulations as the reporter plasmid does not produce ssDNA. Figure adapted from [55].

4.1.3. How Metabolism Affects Toxin Expression Dynamics

In the next set of experiments, the influence of external factors such as the carbon source for TED in the ColicinE2 system was analyzed. In Chapter 2, it was shown that the regulation in the Csr system is dependent on the main carbon source, changing free CsrA abundance for varying sugars (e.g. glycerol and glucose). The expression dynamics of multiple colicin producing strains under competition conditions (see Chapter 3 and Appendix A) were analyzed from experiments performed for two different main carbon sources: glycerol or glucose. In the previous section, it was shown that the abundance of CsrA plays a major role in the dynamics of toxin production and release of the ColicinE2 system. The abundance of the free global regulator protein CsrA is determined by the occurrence of its binding partners such as the sRNAs (CsrB and CsrC), the amount of long mRNA transcripts and the presence of ssDNA from pColE2-P9 replication. Furthermore, the central carbon metabolism of the cell is essential for the Csr system in general. As shown in Chapter 2 Figure 2.1, the type of carbon available for the metabolism shifts the main pathways in the Csr system and thus the abundance of free CsrA [9, 22]. When glycerol is the main carbon source, a small amount of CsrA is available and *cel* repression is expected to be small. The opposite happens for glucose as main carbon source where more CsrA is present which should lead to higher *cel* repression. Consequently, this leads to the hypothesis that toxin release for C cells grown with glucose takes place at later times than for glycerol supplemented medium. This hypothesis was tested with fluorescence time-lapse microscopy of the three colicin producing strains C_{REP1} , C_{REP2} and C_{AMP} at high induction levels of $0.25 \mu\text{g/ml}$ with M63 medium (M63-Competition Appendix A) supplemented with either glycerol or glucose. For strains containing a reporter plasmid (REP1 and REP2), switching in YFP and CFP as well as lysis times were measured. C_{AMP} was chosen as replacement for C_{WT} to gain further insight into natural ColicinE2 expression dynamics. It was chosen because it carries an antibiotic resistance on a second plasmid, preventing contamination in long-term experiments but not altering the toxin expression dynamics with any newly introduced CsrA binding sites (see Table 3.1). Thus, C_{AMP} is genetically closest to the C_{WT} strain (see Figure 4.6 A) and, due to the lack of fluorescent markers, only the lysis time can be analyzed for C_{AMP} . The expression dynamics of all measured strains are shown in (Figure 4.6) with their median time and corresponding interquartile ranges. Additionally, significance analysis was performed (Chapter 3) and results are given in Appendix C Table C.1.

**Figure 4.6**

Toxin expression dynamics are dependent on post-transcriptional regulation via CsrA. A) Schematic of the plasmid composition in the three C_X strains used. Numbers in circles indicate the copynumber of the different plasmids within a strain (details see Table 3.1). B,C) Onset times (T_{ON}) for *cea* and *cel* ($T_{ON_{cea}}$: yellow and $T_{ON_{cel}}$: cyan) and lysis time (T_{lysis} : gray) for toxin producers grown in glycerol (B:GLY) or glucose (C:GLU) supplemented medium. B,C) Thick lines with shaded boxes show the respective median with interquartile range for each time. Significance analysis performed as described in Chapter 3. For detailed results of significance analysis see Table C.1. Figure adapted from [51].

Median ON times for *cea* precede those of *cel* and lysis is the last step in toxin dynamics. C_{REP1} with glycerol showed the smallest *cea-cel* delay with about 6 min and subsequent lysis at 70 min after induction with MitC. C_{REP2} with glycerol has a longer delay of 19 min and cell lysis at 85 min. Accordingly, the latest median cell lysis on glycerol was measured for C_{AMP} with 120 min (Figure 4.6 B). These results support the findings for the S_X strains described above and shows that cell lysis takes place some time after $T_{ON_{cel}}$ depending on the strain and its plasmid composition. Free CsrA abundance can not only be influenced by the plasmid composition in a cell, but also by the regulation of the Csr system via carbon uptake. Hence, the experiments were repeated with glucose as main carbon source (Figure 4.6 C) and effects on TED were analyzed.

For glucose, all ON times for C_{REP1} show a significant shift to later times compared to glycerol. However, the *cea-cel* delay stays nearly constant with 5 min. This is not the case for C_{REP2} where the delay increases to 19 min even though $T_{ON_{cea}}$ stays the same but both $T_{ON_{cel}}$ and the T_{lysis} happen at significantly later time-points. The

same is true for C_{AMP} where the lysis time of 150 min for cells grown on glucose is significantly later than for cells grown on glycerol (for significance analysis see Table C.1). The late lysis times measured for C_{AMP} on both carbon sources are comparable to results for C_{WT} obtained in the theoretical and experimental analysis described above.

Comparing all this data shows for glucose containing medium that the toxin-producing strains undergo lysis significantly later than for cells grown on glycerol. Taken together, these measurements show that the type of carbon source influences the TED in the ColicinE2 system.

4.2. Effects of Toxin Release Dynamics on Population Fate

After the effects of genetic modification on the single-cell level for switching times and fluorescence intensities have been analyzed, the next step was to check what effects these changes in TED have on the population level of S_X or C_X strains. For example, changes on the single cell level like change in lysis time could lead to variations in growth. Another option would be, that when mutations are introduced the fraction of cells reacting to MitC induced DNA damage leads to different amounts of cells switching into the ON state. These factors will now be discussed further in detail.

4.2.1. Population Growth is Dependent on Switching of Cells into the ON State

Analysis of time-lapse experiments for various mutations in both YFP (*cea*) and CFP (*cel*) enable to determine the fraction of ON cells for both fluorescent channels from the amount of cells that cross the 5x threshold of their initial intensities (see Figure 3.4 A,B). The cumulative fraction of cells that have switched into the ON state after 270 min are shown in Figure 4.7 for both S_X and C_X strains.

In general, the fraction of cells that switch into the ON state in CFP never exceeded the one in YFP. This means that not all cells that are ON in YFP contribute to the delay as not necessarily all of them are ON in CFP. In S_{REP1} , when almost all cells switch into the ON state in YFP, only 77 % are in the ON state in CFP (Figure 4.7 A). In all S_X mutants the fraction of ON cells in YFP was higher than 85 %, which means that at high MitC induction levels of 0.1 $\mu\text{g/ml}$ to 0.4 $\mu\text{g/ml}$ almost all cells produce

4. Results: Single-cell Expression Dynamics in the ColicinE2 System

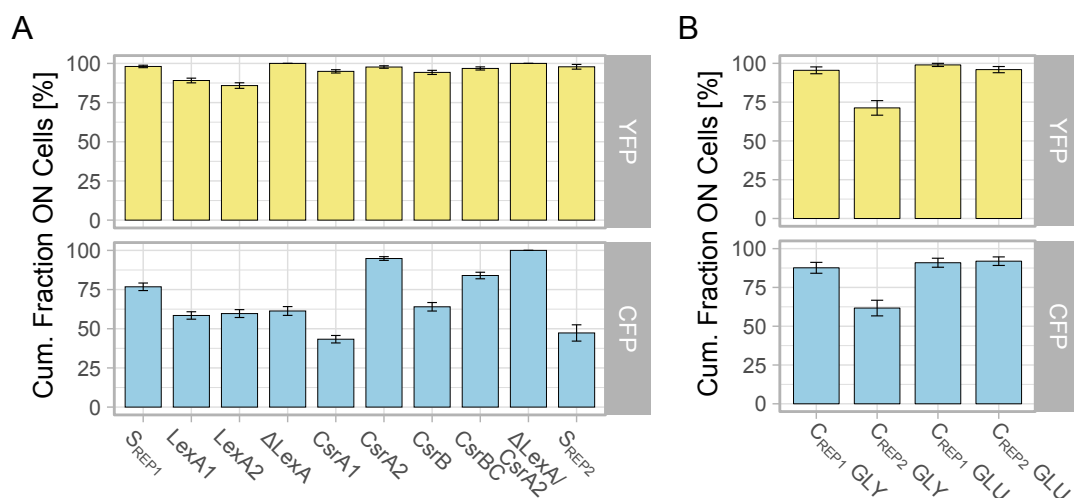


Figure 4.7

Fraction of cells switching into the ON state for YFP and CFP in various S_X and C_X strains. Cumulative fraction of ON cells for S_X (A) and C_X (B) populations. Bars depict the mean fraction of cells that switch into the ON state over the complete measurement duration of 5 h with SEM (standard error of the mean) as error bars. A) S mutants measured in medium supplemented with glycerol as carbon source and over three MitC concentrations from 0.1 μ g/ml to 0.4 μ g/ml. B) C mutants measured for either glycerol (GLY) or glucose (GLU) supplemented medium with 0.25 μ g/ml MitC.

the toxin, even for increased operon repression due to increased LexA binding (LexA1 and LexA2). A closer look at the *cel* expression confirms main observations for the $T_{ON_{cel}}$ times of the mutants. When either LexA or CsrA represses the expression of the operon more strongly, a smaller fraction of cells switch into the ON state in CFP (Figure 4.7 A). This was strongest for the mutations with increased CsrA binding to mRNA (CsrA1) or lowered copynumber (S_{REP2}). In contrast to this lower switching for mutations that lead to stronger operon repression, both mutations with strongly reduced CsrA binding to long mRNA showed that, same as in YFP, almost all cells switch into the ON state for CFP as well.

In a next step, switching into the ON state of strains containing the wild-type pColE2-P9 plasmid was analyzed. Here the two strains C_{REP1} and C_{REP2} with different copy-numbers of the reporter plasmid were used. They were studied with both glycerol and glucose supplemented medium (medium conditions used for competition see Appendix A) as the carbon source was shown to affect the single-cell expression dynamics (see Figure 4.6). With single cell time-lapse analysis it was shown that the additional wild-type plasmids accompanied by ssDNA production in the C_X strains has a big effect on post-transcriptional regulation via CsrA. This also had effects on the switching behavior of the C_X population that are shown in Figure 4.7 B. For high stress with

0.25 $\mu\text{g/ml}$ MitC almost all cells switch into the ON state for both C strains on either glycerol or glucose supplemented medium. Only C_{REP2} grown with glycerol showed reduced switching with only 71 % and 62 % of ON cells in YFP and CFP, respectively. For C_{REP1} and C_{REP2} with both carbon sources, the difference between YFP and CFP switching was below 10 %, reducing the difference compared to the S strain mutants, specifically S_{REP1} and S_{REP2} where the differences in switching were shown to be 21 % and 51 %. This means that in cells containing the wild-type pColE2-P9 plasmid, almost all cells producing the toxin released it within the time-scale of the measurement for these high induction level. For almost all mutations (S and C strain) and both carbon sources the cumulative fraction of cells in the ON state for both YFP and CFP stayed below 100 %. This emphasizes that it is important for the ColicinE2 operon to retain a small amount of cells that do not switch into the ON state and lyse, even at high stress levels. Those OFF cells could be able to reproduce and replenish the population.

For competition, induction levels were chosen smaller so that the colicin producers retain some of their growth but produce toxin in relevant amounts. The chosen induction levels were taken from previous studies of von Bronk *et al.* [10, 11] to facilitate different behavior for the C_X strains ranging from random switching without stress (0.00 $\mu\text{g/ml}$ MitC) to heterogeneous timing with intermediate stress (0.01 $\mu\text{g/ml}$, 0.1 $\mu\text{g/ml}$). In these conditions not all cells switch into the ON state and the C_X population can cooperate by division of labor between toxin producers and reproducers. In order to determine the amount of cells that release toxin and die, live-dead staining was performed for both growth conditions (glycerol or glucose supplemented medium) and induction levels corresponding to competition experiments as described in Chapter 3. Results for the fraction of dead cells for all used C_X strains for growth with glycerol or glucose are shown in Figure 4.8 A.

For all strains shown in Figure 4.8 A, the fraction of dead cells increased with increasing inducer concentration. Without stress only a small fraction of 1 % to 4 % of cells lyse and release toxin due to stochastic switching of the operon. When grown with glycerol as carbon source, medium stress of 0.01 $\mu\text{g/ml}$ MitC lead to fractions of dead cells between 20 % and 33 % where the amount of dead cells decreased with increasing median lysis time of the strains. The same happened for high induction with 0.1 $\mu\text{g/ml}$ MitC but with more than 80 % of dead cells for all C_X strains. Consequently, for high induction most of the cells released their toxin into the environment and less than 20 % of C cells were left to reproduce and populate space.

4. Results: Single-cell Expression Dynamics in the ColicinE2 System

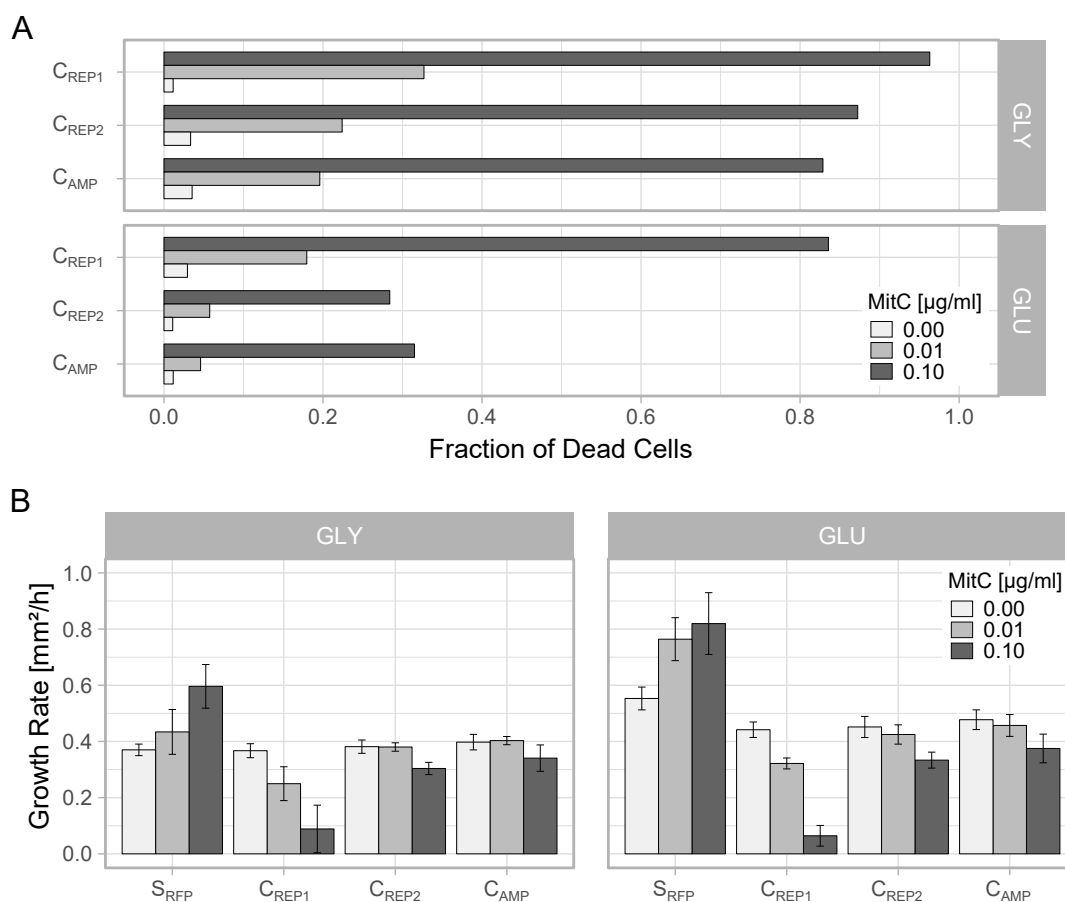


Figure 4.8

Cell lysis and growth rate of C_X strains and S_{RFP} depend on medium composition and induction level. A) Fraction of dead C_X cells after 3 h and B) effective area growth rates for plate expansion measurements dependent on MitC inducer concentration and medium composition. Increasing MitC levels of 0.00 µg/ml, 0.01 µg/ml and 0.10 µg/ml (light to dark gray). B) Error bars depict standard deviation. Significance analysis for the differences in GR without MitC are shown in C.2. Figure adapted from [51].

In contrast to that, when grown on glucose, the C_X strains showed higher diversity and when stress was present and less cells lysed than for medium containing glycerol. For both 0.01 µg/ml and 0.1 µg/ml MitC C_{REP1} displayed the highest dead fractions comparable to its behavior with glycerol. At high stress C_{REP2} and C_{AMP} however exhibited dead numbers in the range of around $(30 \pm 2)\%$ which was comparable to dead fraction of C_{REP1} at medium stress when grown on glycerol. For these two strains on glucose this enables them to increase the number of cells that can reproduce which could give them an advantage in competition. These high variations in dying rates for different strains which depend on medium composition and stress could lead to a variation in effective growth rates because only the non-lysing cells can grow and

contribute to area expansion of the whole population.

In a next step, the area growth rates (GR) of all strains used in competition experiments were analyzed in order to determine the contributions of switching to growth. Data for all strains, including the sensitive strain S_{RFP} were analyzed from control experiments for competition and fitted for linear 2D expansion from 20 h to 48 h (see Chapter 3). Resulting growth rates are shown in Figure 4.8 B for both media. In general, for glycerol as main carbon source growth is slower for each strain than its counterpart grown with glucose. In glycerol medium without stress the sensitive S_{RFP} strain and the reporter strains C_{REP1} and C_{REP2} grow without significant difference with a mean GR around $0.37 \text{ mm}^2/\text{h}$ (for results of significance analysis see Table C.2). In comparison, C_{AMP} is faster with a mean GR of $0.40 \text{ mm}^2/\text{h}$. The balance of growth rates shifted for glucose medium. Here, all colicin producing strains showed significantly smaller growth rates than S_{RFP} . Comparing the expansion of the various strains for increasing MitC inducer concentrations showed two major trends independently from the carbon source. First, with increasing stress S_{RFP} area growth increased, while the growth rates of all C_X strains decreased (Figure 4.8 B). Second, the decrease in growth rates was biggest for mutants that had the highest amount of dead cells in live-dead staining experiments, specifically C_{REP1} on glucose (Figure 4.8 A,B). This showed that indeed the switching behavior of a population containing the colicinE2 operon leads to variation in effective area growth. When more cells produce and release toxin, a smaller amount of the population is left to reproduce.

4.2.2. Toxin Amounts Being Released Depend on Toxin Release Time

In experiments observing the switching dynamics of all C_X strains a major effect plasmid composition on toxin release times was shown. Additionally, live-dead staining showed that the fraction of cell lysing was also dependent on the reporter plasmid and the CsrA composition within a cell. This led to experiments that determine what effects the delayed lysis can have on the toxin amount released by a population. Experiments to determine the amount of colicin released for all conditions and strains were performed indirectly by determining the extinct area caused by adding colicin extracted from all strains to S_{RFP} cells grown on M63-agar plates as described in the method section (see Chapter 3). After 16 h of incubation the area of extinction was analyzed and is plotted in mm^2 in Figure 4.9 A. Experiments with C_X strains con-

4. Results: Single-cell Expression Dynamics in the ColicinE2 System

taining a reporter plasmid showed that with increasing lysis time, the area of S_{RFP} that was extinct increased as well. This was true for cells grown on both glycerol and glucose as a carbon source. According to the lysis times, the extinct areas for each strain were larger when grown on glucose supplemented medium than compared to glycerol supplemented medium. Additionally, the wild-type colicin producing strain C_{WT} was analyzed and its toxin production was found to be higher than C_{REP1} and C_{REP2} for each medium. Its lysis time determined in single cell time-lapse experiments of approximately >150 min (see Figure 4.5) and increased toxin amount fits the trend observed for strains with a reporter plasmid. However it is smaller than the areas detected for the C_{AMP} strain.

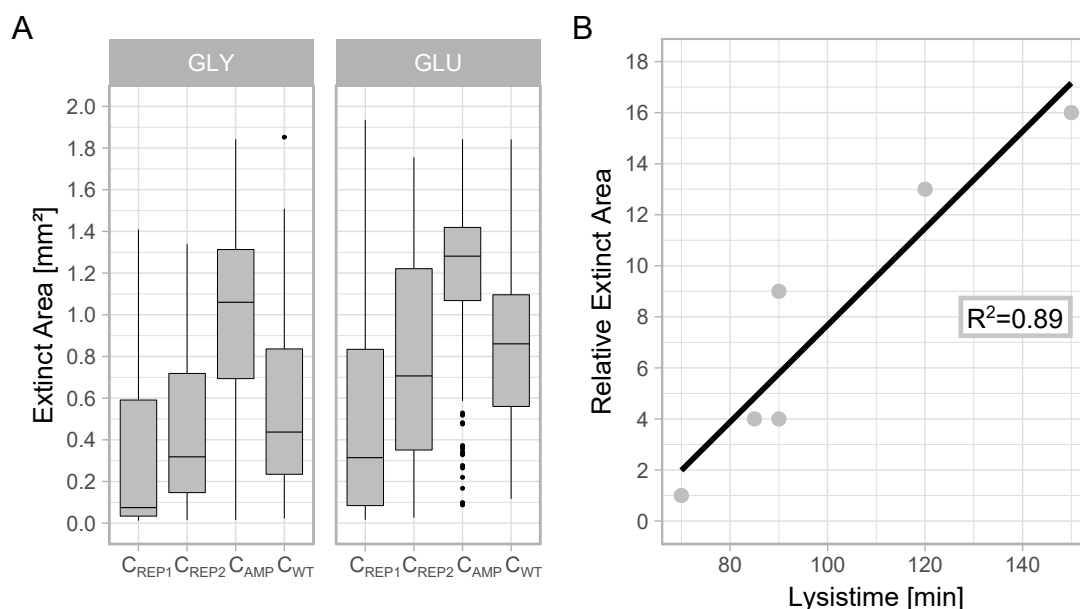


Figure 4.9

Connection between toxin amount being produced and toxin release time for different medium compositions. A) Toxin release by specific C strain leads to cell death of the S strain. Extinct S area after 16 h quantifies the toxin amount that is released per strain and medium. B) Relative toxin amounts compared to C_{REP1} on glycerol for corresponding lysis times (gray dots). Linear fit (black line) with high correlation ($R^2 \approx 0.89$). Figure adapted from [51].

To further characterize the influence of lysis time on toxin production, relative extinct areas were calculated depending on median extinct area of C_{REP1} grown on glycerol resulting colicin factors from 1 to 16 for the various C_X strains and media as shown in Table 4.1. These relative extinct areas were plotted depending on their lysis time and fitted with a linear fit function (Figure 4.9 B). This fit showed a high correlation of toxin amount to the lysis time with $R^2 = 0.89$, which means that with increasing lysis time, the amount of toxin being released increases linearly as well.

	Glycerol (GLY)				Glucose (GLU)			
	C_{REP1}	C_{REP2}	C_{AMP}	C_{WT}	C_{REP1}	C_{REP2}	C_{AMP}	C_{WT}
Median Extinct Area [mm ²]	0.08	0.32	1.06	0.44	0.31	0.71	1.28	0.86
Resulting Colicin Factor	1	4	13	6	4	9	16	11

Table 4.1

Extinct area and resulting colicin factor depend on C_X strain and the carbon source. Areas determined by extinction experiments in Figure 4.9 and their resulting factor of produced colicin in comparison to C_{REP1} on glycerol.

In the following, using combined experimental and theoretical analysis, the impact of lysis timing and toxin amount being released on competition outcome will be studied more closely in order to determine the effect of TED on colicin driven competition (see Chapter 5) The data obtained from single-cell and single-strain analysis (e.g. toxin amounts and GRs) will be used for theoretical modeling.

4.3. Discussion

4.3.1. Single-cell Toxin Dynamics

As a first step of this study, the aim was to identify factors controlling the dynamics of toxin production and release within the ColicinE2 operon after induction of the SOS response. A reporter strain with an artificial ColicinE2-like plasmid was used that contained all relevant regulatory elements, but containing fluorescent proteins instead of the colicin (YFP) and the protein causing cell lysis (CFP). Time-lapse fluorescence microscopy showed a time-delay between toxin production and release (*cea-cel* delay) for a reporter strain S_{REP1} . Mutations on different regulatory modules were then introduced to identify the relevant factors controlling colicin expression dynamics.

Starting with the transcriptional mutants (ΔLexA , LexA1 and LexA2) revealed transcriptional repression to be a possible mechanism causing delayed *cel* expression. Reduction of the delay in these mutants was caused by later onset times of the colicin. This shift could be caused by either changes in repression of the operon by changing the binding strength of LexA, or by the protein AsnC [77]. AsnC in combination with LexA was shown to control the onset of transcription of the colicin operon [77]. Mutations on the LexA binding sites of the SOS box could also affect the binding of

AsnC to the SOS sequence, as it binds within the same binding sites like LexA [3, 77]. Considering the observed loss of time delay in a strain containing the wild-type plasmid (C_{REP1}), the changes caused by the transcriptional module were not enough to explain this substantial change in TED.

Considering variation in the post-transcriptional module next, revealed that CsrA is the main player controlling the toxin release by modulation of lysis time. CsrA is a global regulatory protein affecting a plethora of target genes [6, 7]. It is a highly abundant protein within *Escherichia coli* with more than 10 000 proteins per cell [78]. However, Taniguchi *et al.* 2010 [74] showed that only a small number (~ 100) of these are free CsrA molecules. Consequently, the number of binding partners that sequester CsrA can have large effects on the abundance of free CsrA and thus the translation of the ColicinE2 operon. Two well studied CsrA sequestering components are the sRNAs CsrB and CsrC of the Csr system [71, 78, 79]. These two sRNAs can bind multiple CsrA molecules each and are the main binding partner of CsrA [78]. An additional CsrA sequestering element within the ColicinE2 system is the long mRNA produced by the operon upon SOS induction, which contains binding sites for CsrA [22]. In this study it was shown that CsrA can bind to long mRNA, which in turn reduced the abundance of free CsrA. Here, it was also shown that ssDNA, which can be produced by autonomous replication [65] of the pColE2-P9 plasmid (see Figure 3.5, can pose as an additional CsrA sequestering element. CsrA binding is specific to the GGA motif on the ssDNA hairpin with reduced binding affinity compared to mRNA. Gel shift analysis revealed a dual role of CsrA as not only being a mRNA binding protein, but also a ssDNA binding protein.

Incorporating the information gathered from binding assays and single-cell time-lapse experiments into theoretical analysis [72] revealed the importance of ssDNA for the ColicinE2 system. Only when ssDNA as sequestering element was present, the wild-type strain C_{WT} was able to lyse in the time-scale relevant of the measurements (5 h). Due to the small number of free CsrA molecules within a cell [74], ssDNA as an additional CsrA sequestering element, that was newly discovered in this thesis, is a relevant factor that can shorten the time-delay before cell lysis. Experimental and theoretical analysis of a mutant plasmid with reduced copynumber (S_{REP2} and C_{REP2}) revealed that reduction of long mRNA transcripts via reduction of plasmid copynumber shifts lysis to later time-points.

Following results that CsrA abundance plays a key role in ColicinE2 toxin production and release dynamics, three different C_{X} strains with varying binding sites for CsrA

were studied (C_{REP1} , C_{REP2} , C_{AMP}). Time-lapse data confirmed, that cell lysis depends on the amount of CsrA sequestering element, where cell lysis takes place later for low numbers of CsrA binding partners and thus low translation probability of the *cel* gene. Furthermore, variations in carbon source within the medium were shown to change the abundance of free CsrA within a cell [22]. When the main carbon source within the medium was changed to glucose instead of glycerol, variations of the lysis time of all tested C_X strains were observed. For glucose medium the abundance of CsrA was expected to increase by changing CsrD levels (see Chapter 2) and accordingly the lysis times were shifted to later time-points. This shows that indeed the variation of carbon source plays an important role in the control of ColicinE2 release.

4.3.2. Single-cell Dynamics Determine Single-strain Population Behavior

The population behavior of a single-strain population as result of single-cell dynamics was studied for variations in both the transcriptional and post-transcriptional module. For strains without the wild-type plasmid (S_X) the number of cells switching into the ON state for *cea* was bigger than for *cel*. Only mutations with big changes in CsrA binding or CsrA abundance showed comparable ON fractions for both proteins. The same was true for C_{REP1} and C_{REP2} where ON fractions were comparable for both proteins in both media. For strains containing the wild-type plasmid (C_X) live-dead staining experiments revealed that the fraction of cells that release the toxin by cell lysis depends on the stress induction level. Furthermore, the different strains showed that the fraction of lysed cells also depends on medium composition, such as carbon source. For glucose supplemented medium, most strains were observed to have reduced lysis fractions compared to glycerol medium. This correlation to carbon source might be due to the mode of action of the lysis protein. Pugslesy *et al.* [80, 81] showed that the lysis protein destroys the cell envelope by increasing permeability of the cell wall. This leads to the hypothesis that reduced cell lysis for cells grown on glucose is caused by a better repair rate of the cell envelope in energy rich medium. Changes in fractions of cells lysing within a population were then shown to lead to variation in area growth rates for the different induction levels, where lower lysis rates lead to higher area growth rates (Figure 4.8). Finally, population experiments showed that the amount of toxin being released is directly correlated to the lysis time of a cell. When a population exhibits late cell lysis, the amount of toxin released into the environment is large.

4.3.3. Summary

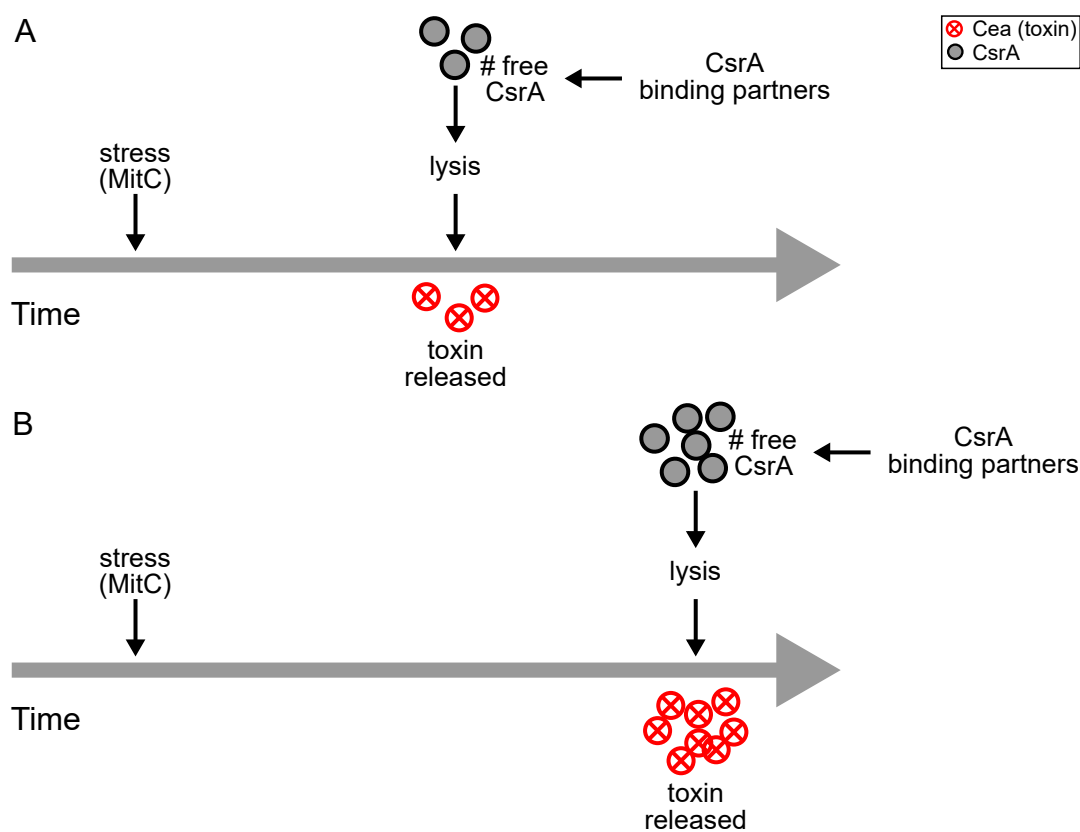


Figure 4.10

Number of free CsrA determines the time-point of cell lysis and the amount of toxin being released from the ColicinE2 operon. A) Small amounts of free CsrA lead early cell lysis with a low amount of toxin being released. B) Large number of free CsrA within a cell and consequent delayed cell lysis and an increased amount of toxin being released from the colicin operon. A,B) Amount of free CsrA is controlled by its binding partners.

In summary, it was shown here, that the main player regulating the dynamics of toxin production and release within the ColicinE2 system is the abundance of free CsrA within the cells. This abundance is regulated by the presence of CsrA binding partners within a cell sequestering free CsrA (Figure 4.10). Among others, sequestering elements were identified to be sRNAs CsrB and CsrC, the amount of long mRNA within a cell (dependent on plasmid copynumber) and ssDNA produced by autonomous replication of the wild-type plasmid. Even though the exact mechanism for toxin release within the ColicinE2 system is not fully understood [14, 82], the data presented here shows a correlation of lysis time and the amount of toxin released into the environment (see Figure 4.10). In turn, lysis time was shown to be dependent on

the amount of CsrA sequestering elements such as plasmid copynumber of plasmids containing CsrA binding sites. All sequestering elements are essential for regulation of toxin release and the single-cell response was shown to have a major impact on the population by modulating the effective area growth of a strain as well as toxin amounts released into the environment. As many other bacteriocin networks are also plasmid encoded [12] and under the control of the SOS response [2] and the global protein CsrA is part of genome-wide regulatory processes [6], many of the regulation factors identified in the ColicinE2 system might be essential for regulation of other systems as well.

5. Results: Toxin Expression Dynamics Shape Two Strain Bacterial Competition

The following chapter is based on the publication Weiss *et al.* 2020 (accepted): *Dynamics of ColicinE2 production and release determine the competitive success of a toxin-producing bacterial population* [51] and additional data from modeling.

In the previous chapter it was shown that TED differ for different reporter strains and nutrient conditions. Furthermore, changes in single-strain population behavior were observed for different strains and environmental conditions such as stress and carbon source of the medium. Consequently, these differences in TED and single-strain behavior will also influence competition of a C_X strain with a toxin-sensitive S_{RFP} strain (see Table 3.1). This will be discussed in detail in this chapter. Combined experimental and theoretical analysis for this bacterial competition is used to disentangle the main factors important for success of colicin producers. Competition is then characterized by inter-strain competition via toxin production of C cells and spacial exclusion by S cells. Furthermore, C cells can cooperate with one another by only parts of the population switching into the toxin producing state, while the rest continues to reproduce (see Chapter 2 Figure 2.7).

5.1. Competition Success of Toxin Producers is Coupled to Toxin Expression Dynamics

In a first step, long term range-expansion of two-strain competition was studied experimentally. For this, the above described sensitive strain S_{RFP} was combined with various C_X strains using both glycerol and glucose supplemented medium as it was shown from single-cell studies (Chapter 4) that toxin release times and amounts differ for the studied C_X strains and media. Competition was performed as described in Chapter 3 with a $C_X:S$ ratio of 1:100 and a starting volume of 5 nl. Mixed colonies were observed over a time of 48 h and competition outcomes were plotted in Figure 5.1 A and B for glycerol and glucose supplemented medium, respectively. Outcomes

5. Results: Toxin Expression Dynamics Shape Two Strain Bacterial Competition

were characterized according to the fraction of C_X strain in the final area covered by bacteria. Four major outcome groups were separated as follows:

- **S wins:** <10% C_X area
- **Coexistence:** 10% to 90% C_X area
- **C wins:** >90% C_X area
- **Extinction:** final area below detection limit

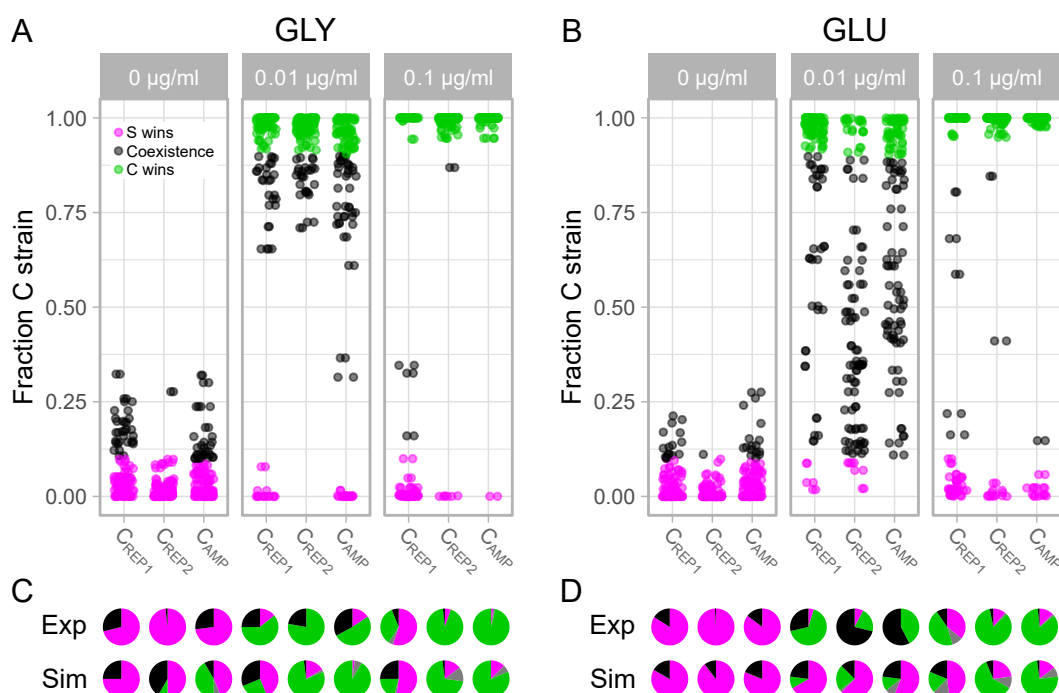


Figure 5.1

Experimental and simulation results of two-strain competition of C_X and S_{RFP} strain on different carbon sources. A,B) Final fraction of C_X on medium supplemented with glycerol (A) or glucose (B) for three different MitC inducer concentrations. C,D) Classified outcomes for competition experiments (Exp) and simulations (Sim) corresponding to the same MitC levels shown in A,B. Outcomes are classified as: S wins (<10% C, magenta), coexistence (10%-90% C, black) C wins (>90% C, green), extinction (no area detected due to toxin action, gray). Figure adapted from [51].

Initial conditions were chosen according to previous studies showing the importance of low C strain fractions at the beginning of interaction (single-cell interaction level) for coexistence of both C_X and S_{RFP} to be possible [10, 46].

By using three external stress levels from low to high MitC concentration, C cell toxin producer fractions were tuned according to Chapter 4 and previous studies by Mader *et al.* 2015 [13] from stochastic switching (no stress) to synchronous response (high

stress). In the absence of stress the sensitive strain was able to outcompete the colicin producer in most cases due to spacial exclusion. This was the case for all C_X strains in media containing glycerol or glucose as main carbon source (Figure 5.1 A,B). For medium stress levels the C_X strains release their toxin over a broad range of time with higher toxin producer fractions within the population. This shifted competition outcomes to higher numbers of C strain winning or in the case of glucose as carbon source, increased amounts of coexistence between S and C were detected. Finally, at high induction levels of 0.10 $\mu\text{g/ml}$ MitC a high number of C cells produced and released the toxin, which resulted in a high number of C wins outcomes for both media. Only the C wins fraction of C_{REP1} decreased in both media settings in comparison to their results for medium stress. One of the reasons for this decrease could be the high number of cell lysis for C_{REP1} at high induction level detected in Chapter 4 Figure 4.8 A, giving the S strain a disadvantage due to early lysis of C cells.

In the previous chapter it was shown that C_X strains with different plasmid composition lead to different lysis times and amount of toxin being released. The strains C_{REP2} and C_{AMP} showed later cell lysis than C_{REP1} and increased amounts of toxin being released into the environment. Increasing the time before cell lysis of the C_X strain in competition experiments had two major effects on competition. First, when toxin is released at later times, the sensitive S strain can grow longer without disruption by the toxin. Second, the C cells can release more toxin into the environment as the amount of toxin being released is directly correlated to lysis time. Using this information, a theoretical model was set up based on the described model by von Bronk *et al.* 2017 [10] (see Chapter 3). This model is a stochastic lattice-based model, that includes the measured values for switching rate into the toxin producing state, growth and toxin amounts, but also stochastic positioning and phenotypic heterogeneity within a C strain population. In a first step, the model was validated for values obtained for C_{REP1} with glycerol and a toxin effectivity of $s_S = \sigma_S \cdot n_{tox}$ of 1500 was chosen as basic value, which was the same as in von Bronk *et al.* 2017 and 2019 [10, 11] (see Chapter 3). Using this model, theoretical analysis for all strains and media combinations were performed by incorporating all values obtained by single cell analysis as well as growth rates (GRs) and toxin factors adapted from single-strain population measurements. All precise values for these simulations are listed in Table B.1. For C_{REP1} on glycerol the toxin amount being released was chosen as $n_{tox} = 1$ and was increased up to $n_{tox} = 16$. This value was obtained for C_{AMP} grown on glucose supplemented medium and according to relative toxin amounts being released compared to

5. Results: Toxin Expression Dynamics Shape Two Strain Bacterial Competition

C_{REP1} on glycerol leading to toxin factors shown in Table 4.1. Results of theoretical competition outcomes corresponding to 48 h of competition for all strains are shown in Figure 5.2 A and B for rates corresponding to glycerol and glucose measurements, respectively.

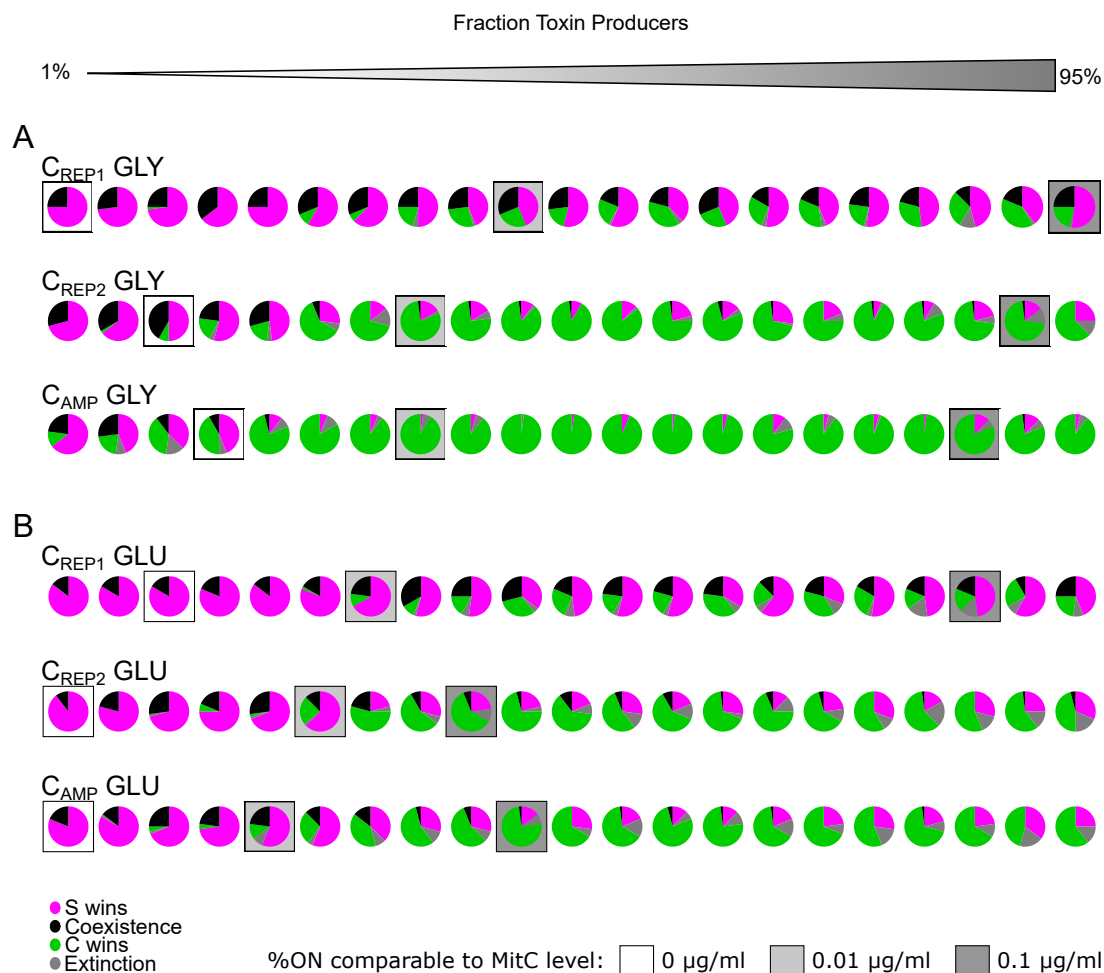


Figure 5.2

Numerical simulations of two-strain competition corresponding to experimental conditions for glycerol (A) and glucose (B). Simulations are run for increasing toxin producer fractions from left to right corresponding to 1% to 95% of C_X strains producing the toxin. Boxes around the pie charts correspond to toxin producer fractions that were obtained in live-dead experiments shown in Section 4.2.1 Figure 4.8 for the different inducer concentrations of MitC. The exact toxin producer fractions for all pie charts are given in Table B.2. This figure is adapted from [51].

Simulations were performed for a broad range of toxin producer fractions (details see Table B.2). For all simulations the amount of C winning increased with increasing C producer fraction until, at high toxin producer fractions, increased cell lysis lead to significant numbers of extinction outcomes in competition. Furthermore, S strain

success was detected for a broader range of toxin producers in the cases of glucose even though the amount of toxin released was bigger. One reason for this could be the increased GR of the S strain for glucose medium, giving it a bigger chance for spacial exclusion in competition.

Using the fractions of lysing cells measured above (Figure 4.8 A) the corresponding pie charts in Figure 5.2 were marked and compared to experimental results in Figure 5.1 B. For both low and high stress levels competition outcomes showed the same main results for experiments and theory. Although, at intermediate stress levels of 0.01 $\mu\text{g/ml}$ bigger discrepancies between experimental and theoretical results were detected. A variety of reasons could contribute to this discrepancy. One of them is the strong dependence on initial conditions of the competition experiments which are inherently noisy. Furthermore, at intermediate stress levels stochasticity in toxin expression dynamics plays an important role [13]. How this affects competition will be discussed more closely in Section 5.3.

Combining all these results indicates that for most cases competition outcome did not change for the various C_X strains despite their differences in toxin amount and release times. Consequently, either the broad range of release times does not have a significant effect on competition outcomes, or effects compensating the variation in release time come into play. However, many of these factors, e.g. toxin amount being produced and time-point of toxin release are connected within a cell. Thus theoretical analysis was performed to disentangle these factors and their impact on competition outcome.

5.2. The Importance of Toxin Release Time and Toxin Amount on Bacterial Competition

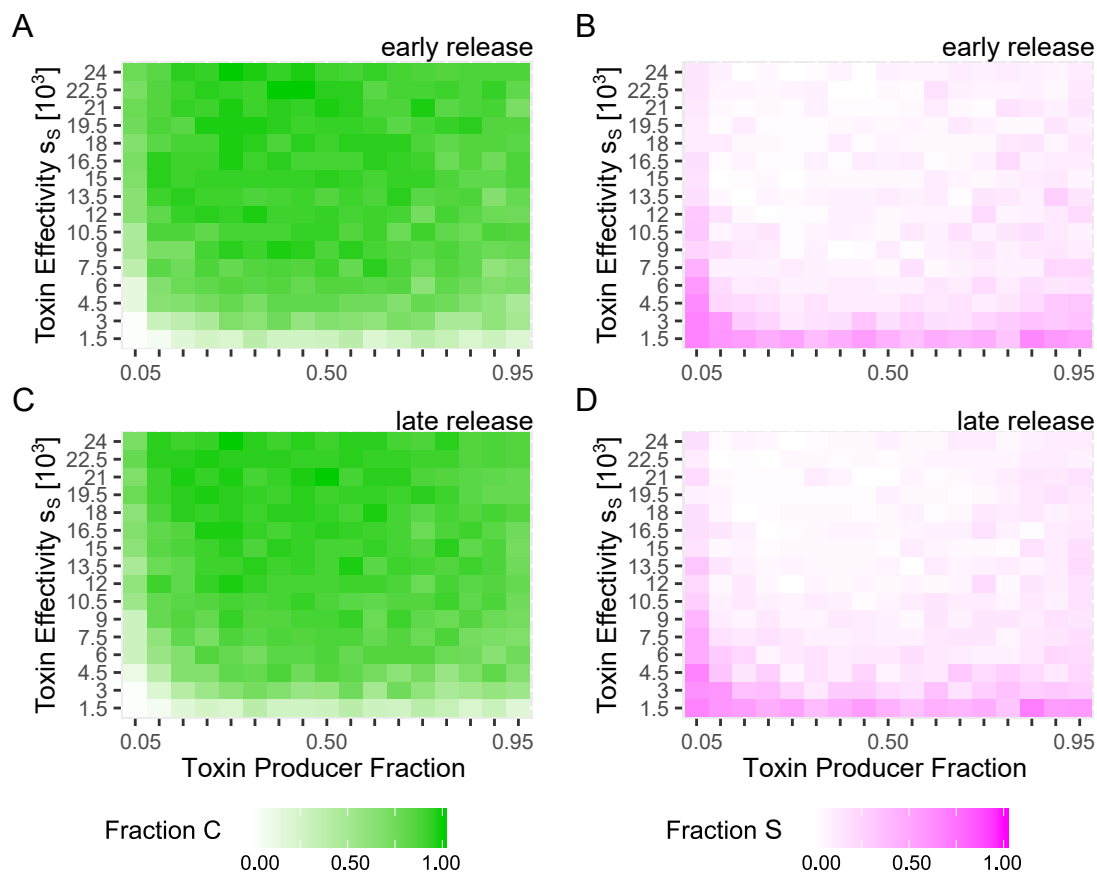
In general, as shown above, most results of the theoretical model are consistent with the overall trends shown in experiments. Thus, the model implemented above was used to disentangle the role of the biologically connected parameters of toxin amount and toxin release time for competition outcome. To do so, parameter sweeps for those two parameters were performed for varying toxin producer fractions to investigate the impact of both single variables on competition outcome.

5.2.1. Competition with Similar Single-strain Growth of S and C Strains

In a first step, the toxin effectivity s_S was varied from 1500 to 24 000 (see Chapter 4 and Table B.1) for a broad range of toxin producers (5 % to 95 %, details see B.1). As a starting point, simulations were performed with early and late release times, corresponding to d_{Con} rates on glycerol. GRs of S_{RFP} and C_{REP1} on glycerol medium, which showed no significant difference, were chosen to analyze the impact timing of toxin release and amount of toxin being released have on the competitive success of the C strain. In case of glycerol as main carbon source the GR of the sensitive strain shows no significant difference to the one of C_{REP1} leading to comparable growth for both strains used in simulations.

Phase diagrams of sweeps over toxin effectivities for 48 h are shown in Figure 5.3 for S and C fractions at early (A,B) and late (C,D) toxin release times. Theoretical results showed that independent of lysis time, the C strain was dominant in competition with the S strain as long as high enough amounts of toxin were produced. For comparable growth rates of competing strains (S and C) this was the case for $s_S > 1500$. For both lysis times, for toxin effectivities >1500 the fraction of C in the final area was bigger than the fraction of S strain (see Figure 5.3 A,C: C fraction; B,D: S fraction).

In a next step, the fixed toxin effectivities were chosen with 1500 and 19 500 that correspond to the lowest and highest toxin amounts detected for C_X strains grown on glycerol. Toxin producer fractions were varied again from 5 % to 95 % while toxin release times were modulated from 50 min to 1250 min (lysis rate $d_{Con} = 1/T_{lysis}$ evenly spaced). This corresponds to the minimal lysis time of the system as well as very late cell lysis with >20 h (see Chapter 3). Other rates, including growth rates were chosen


Figure 5.3

Phase diagrams of C fractions (A,C) and corresponding S fractions (B,D) in competition simulations for various toxin effectivities on glycerol. For each sweep over varying toxin effectivity an early and late release time comparable to glycerol experiments were chosen for the toxin with early release at 68 min (A, B) and late release at 120 min with GRs for medium supplemented with glycerol. This figure is adapted from [51].

for S_{RFP} and C_{REP1} grown on glycerol to only study the influence of variations in d_{Con} and s_S .

Phase diagrams for variations of lysis times are shown in Figure 5.4 for both S and C fraction at low (A,B) and high (C,D) toxin amounts. Results showed that at low toxin amounts released by colicin producers, only early release of the colicin at intermediate toxin producer fractions leads to competitive success of the C strain. Only in this regime the S strain showed reduced success compared to the C strain. In all other cases the S strain was dominant due to spacial exclusion (Figure 5.4 A,B). Contrary to this, when high toxin amounts were released, the results showed C strain dominance for a broad range of toxin release times and toxin producer fractions (see Figure 5.4 C,D). The S strain only had a change for competition success when colicin producers

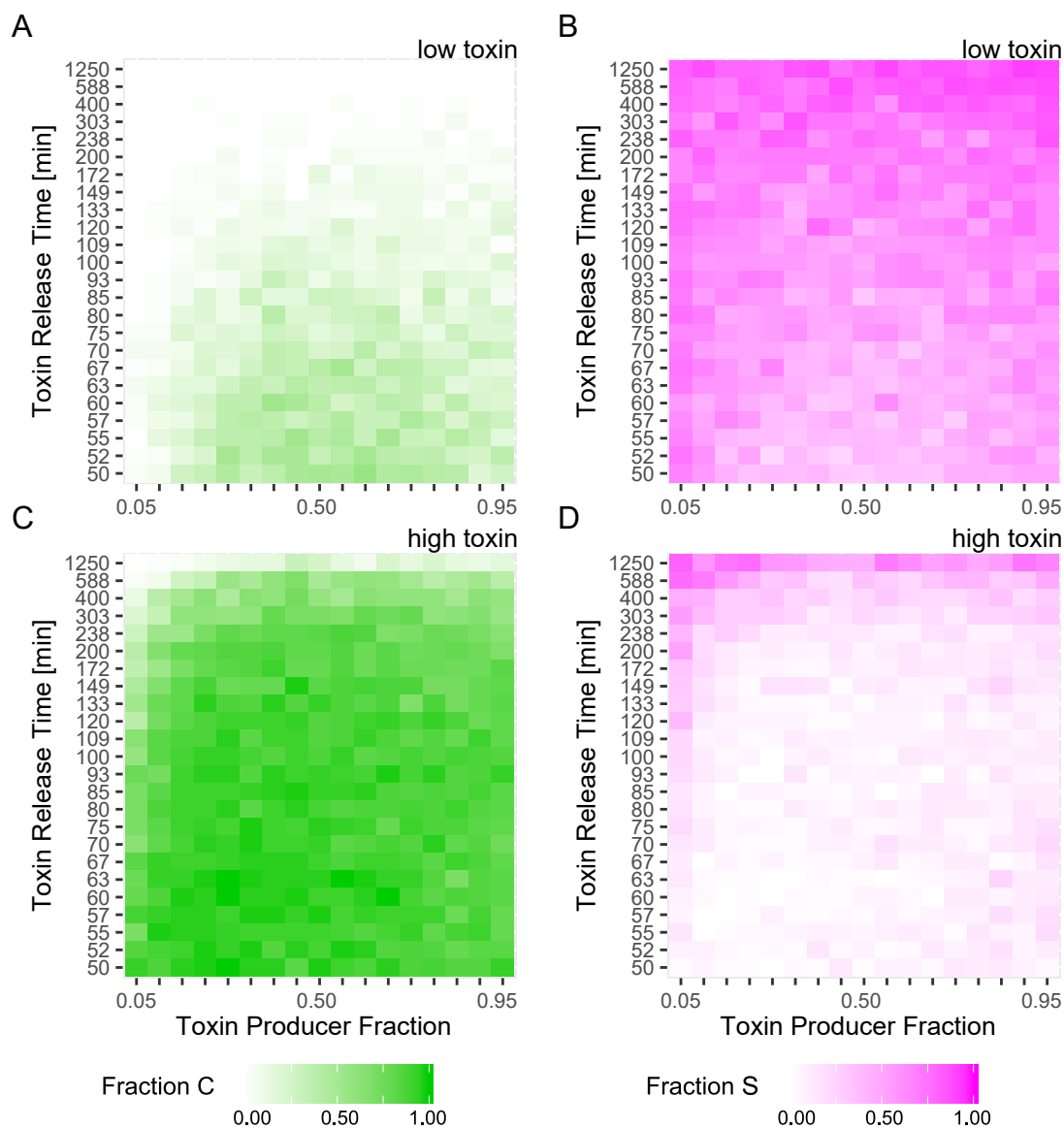
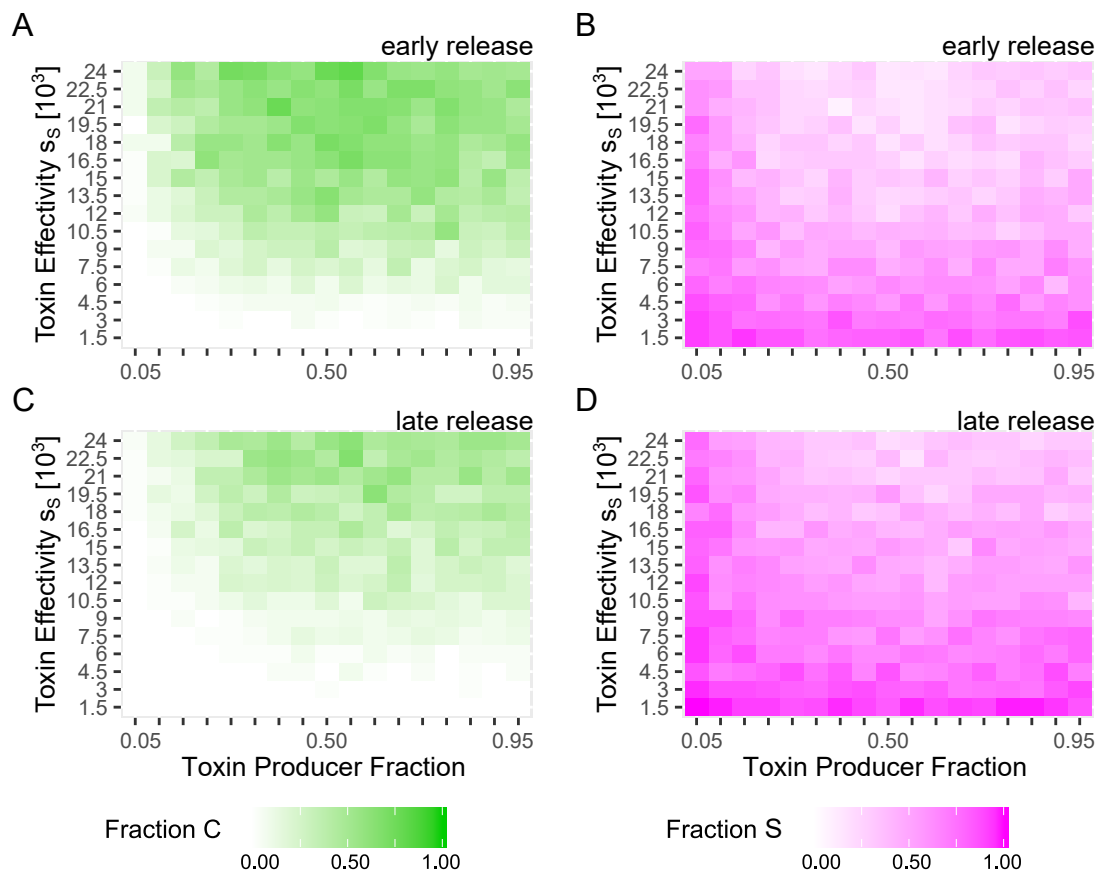


Figure 5.4

Phase diagrams of C fractions (A,C) and corresponding S fractions (B,D) in competition simulations for various toxin release times on glycerol. For each sweep over varying toxin release times a low and high toxin amount comparable to glycerol experiments were chosen for the low toxin amount at 1500 (A, B) and high toxin amount at 19 500 with growth rates for medium supplemented with glycerol. This Figure is adapted from [51].

released their toxin at extremely late times of 1250 min after switching into the ON state. These results for comparable growth of both strains showed that the amount of toxin being released seems to be the crucial factor for the competitive success of the C strain population.

5.2.2. Competition of a C Strain with a Faster Growing S Strain

**Figure 5.5**

Phase diagrams of C fractions (A,C) and corresponding S fractions (B,D) in competition simulations for various toxin effectivities on glucose. For each sweep over varying toxin effectivity an early and late release time comparable to glucose experiments were chosen for the toxin with early release at 90 min (A, B) and late release at 150 min with growth rates for medium supplemented with glucose. This figure is adapted from [51].

In the previous set of theoretical analysis growth rates were chosen to be comparable for both the sensitive and the colicin producing strain. However, this is not the case for glucose supplemented medium, where the S_{RFP} strain had a significantly faster growth rate than all C_X strains (see chapter 4). Thus, simulations were repeated with GRs corresponding to S_{RFP} and C_{REP1} on glucose supplemented medium.

Simulations were performed for toxin producer fractions from 5% to 95% and toxin effectivities of 1500 to 24000. Two sets were run first, with an early release time of toxin by the colicin producers of 90 min (Figure 5.5 A,B) and second, for late release times of 150 min (Figure 5.5 C,D) corresponding to C_X strains grown on glucose

medium. Phase diagrams for outcome fractions of the C (A,C) and S strain (B,D) are shown in Figure 5.5. For both early and late colicin release, a high amount of toxin was needed for colicin producers to succeed in competition. Beginning with toxin effectivities of around 9000 and medium toxin producer fractions, success of the C strain increased and S strain success decreased with increasing toxin amount and for a bigger range of toxin producer fractions. Similar to the simulation of competition on glycerol this showed that a threshold of toxin amount has to be reached for the C strain to have a competitive advantage. However, this toxin amount is higher for competition conditions on glucose, which could be due to the increased GR of S_{RFP} . Adjusting the parameter sweeps for toxin release time to glucose medium, low and high toxin amounts were adapted according to experiments for C_X strains on glucose to 6000 and 24000 for smallest and largest toxin amounts being released, respectively (see Table 4.1 and Table B.1). Phase diagrams for S strain and C strain fractions shown in Figure 5.6 (A,B: C fractions; C,D: S fractions) show reduced C strain success compared to results for glycerol. Here, for a low toxin amount being released per C cell, the C strain was only successful at a narrow range of early release times and intermediate toxin producer fractions. For other conditions the sensitive S strain was dominant. In comparison to results for high toxin amounts (Figure 5.6 C,D), a much broader spectrum of cases with C strain dominance was observed. Only at toxin producer fractions of 5% or for toxin release times bigger than 300 min high S fractions were detected in competition outcomes.

In general, due to the faster growth of the sensitive S strain on glucose supplemented medium, higher amounts of toxin need to be produced to facilitate success of colicin producers in competition. Nevertheless, the theoretical analysis for glycerol and glucose showed the same trends for the impact of the two biologically connected factors toxin amount and toxin release time on competition. Even though in experiments, the amount of toxin being released is directly correlated to the lysis time of colicin producers as shown in Figure 4.9 B ($R^2 = 0.89$), parameter sweeps within the model were able to disentangle the impact of the two factors. Of the two investigated parameters, production of higher amounts of toxin has a greater effect on $C_X:S$ competition than the timing of toxin release.

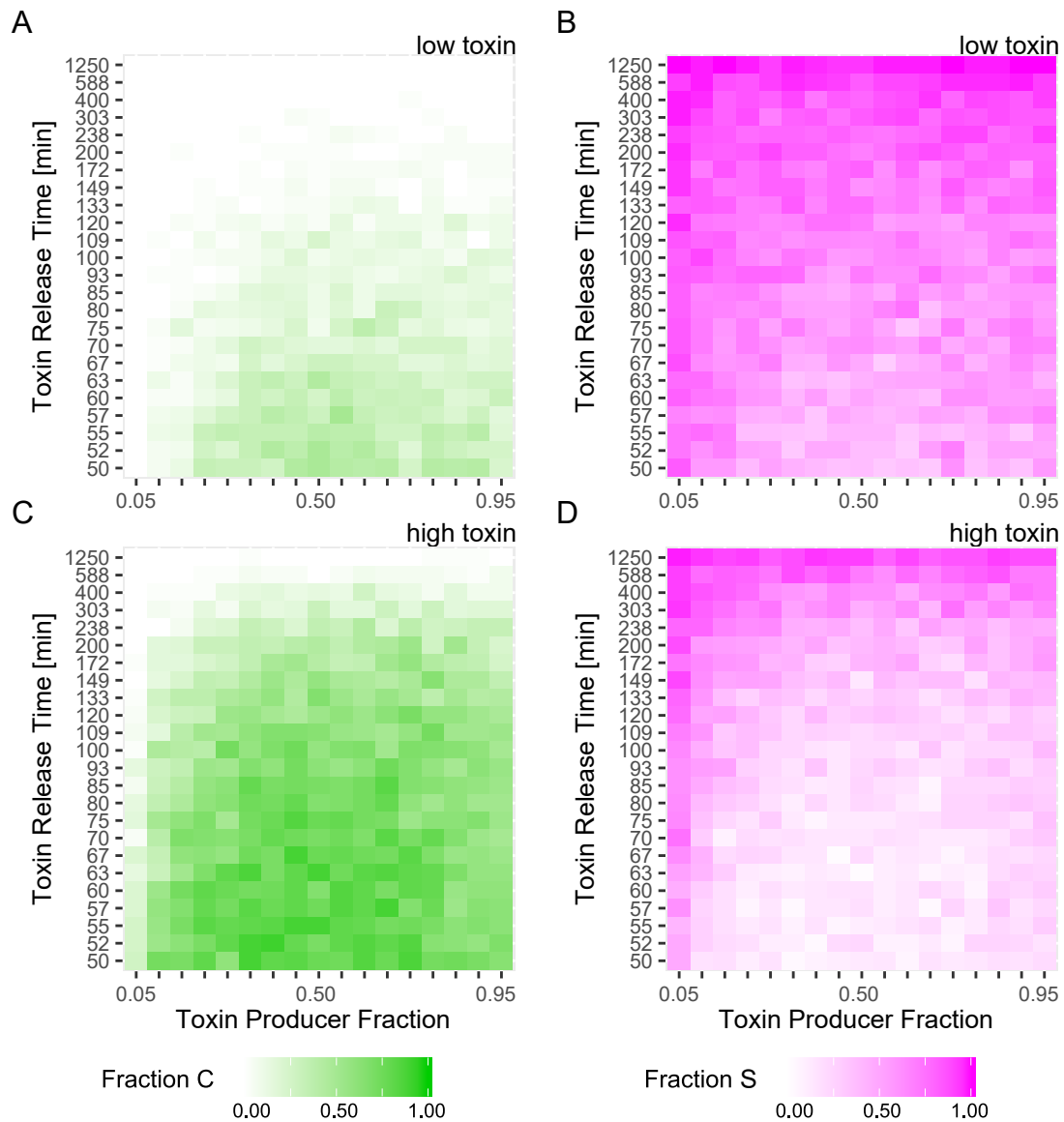


Figure 5.6

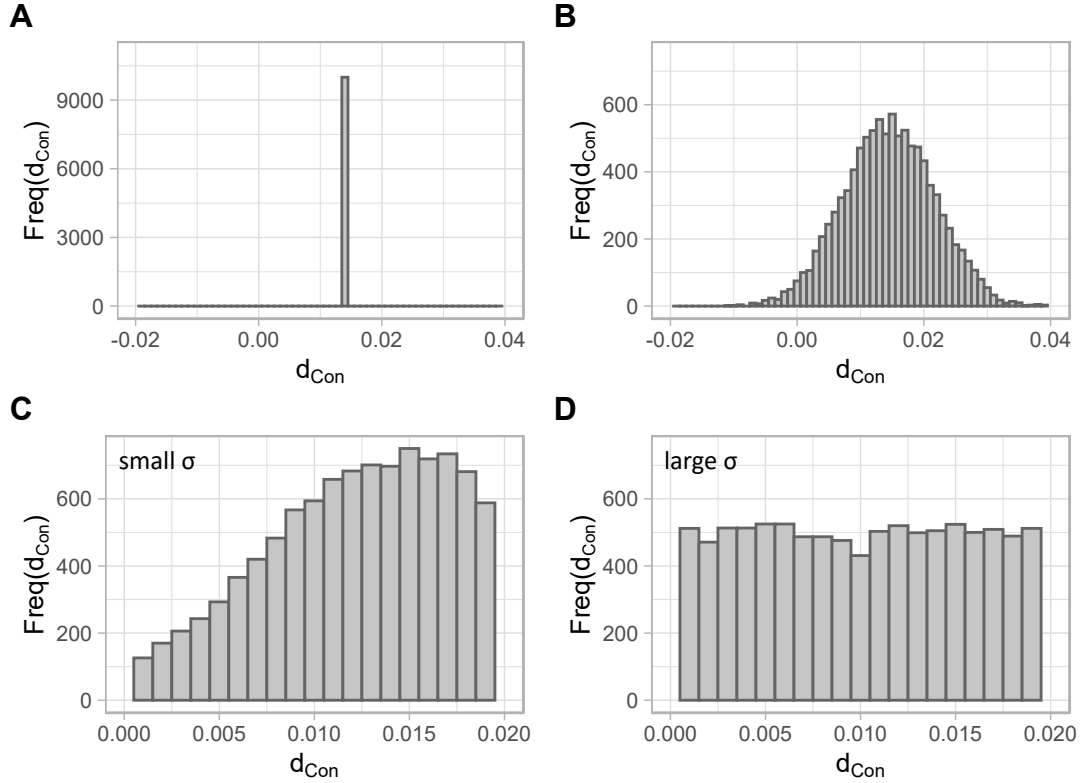
Phase diagrams of C fractions (A,C) and corresponding S fractions (B,D) in competition simulations for various toxin release times on glucose. For each sweep over varying toxin release times a low and high toxin amount comparable to glucose experiments were chosen for the low toxin amount at 6000 (A, B) and high toxin amount at 24 000 with growth rates for medium supplemented with glucose. This figure is adapted from [51].

5.3. Introduction of Time-fluctuations/ Increased Stochasticity in Two-strain Competition Model

As shown in Figure 5.1 B for intermediate stress levels, the theoretical model shows major discrepancies to experimental competition results. Mainly, the theoretical model underestimated C_X strain success at intermediate stress, especially for growth conditions on glucose medium. Even though stochasticity in switching between states is implemented in the model, the intermediate stress level of $0.01 \mu\text{g/ml}$ MitC was shown to be highly heterogeneous in switching time-point by Mader *et al.* 2015 [13]. Thus, high variation of lysis time in this stress regime could be a cause for discrepancies between experiment and simulation. In this section an approach to improve the model for heterogeneous regimes will be introduced.

5.3.1. Implementation of Noise in the Two-strain Bacterial Interaction Model

The response of the ColicinE2 system is highly heterogeneous, especially at intermediate induction levels. In order to increase heterogeneity in simulations the following changes on the switching rate $d_{C_{on}}$ of cells from ON state to cell lysis were made. In first simulations the lysis time extrapolated from measurements was used to calculate this switching rate for all C strains used. But, some discrepancies between simulation and experiment were evident mainly at medium stress induction levels. As already described above, Mader *et al.* 2015 [13] found that at intermediate stress levels heterogeneous timing in colicin production and release takes place. This means that the cells produce and release toxin over the complete time-course of the measurement. Stochasticity is already implemented into the system by random selection of a parameter that determines state transitions with probabilities depending on the transition rates. In these cases the transition rate from C_{on} to lysed C cells was chosen as constant which is shown in Figure 5.7 A. When allowing this rate to fluctuate around the mean, a normal distribution with $d_{C_{on}}$ as mean and a variable, but set standard deviation can be chosen as distribution of $d_{C_{on}}$ as shown in Figure 5.7 B. This leads to increased variability, especially for conditions where many cells are in the C_{on} state. At each time point, all C_{on} cells are randomly assigned a $d_{C_{on}}$ rate according to the fixed values of variation and mean.


Figure 5.7

Variation of d_{Con} rate distributions and biological restrictions. Frequency of d_{Con} shown for changes in σ . A) Constant d_{Con} rate extracted from time-lapse measurements. B) Normal distribution with set standard deviation around the d_{Con} rate with random noise ($W_{frac} = 0.5$). C/D) Restriction of the distribution to biological constrictions with varying width of distributions by increasing the standard deviations. C) Small ($W_{frac} = 0.5$) and D) high standard deviation ($W_{frac} = 5$).

However, the created d_{Con} distribution has to be limited to the following boundary conditions set by biological processes and mathematical constrictions. The upper limit of $d_{Con} = 0.2$ is chosen according to the time the ColicinE2 system needs to respond to the external stimulus. It was shown before, that this limit is at least 50 min to 60 min after induction, which means that the lysis time of cells cannot be smaller than 50 min to 60 min [77], leading to an upper limit of $d_{Con} = 0.02$. The lower limit is set as $d_{Con} = 0$ as rates smaller than that would require a negative lysis time. $d_{Con} = 0$ corresponds to $T_{lysis} \rightarrow \infty$.

The spread of the distribution is then modified by adapting the standard deviation as a measure of the switching rate with $\sigma = W_{frac} \cdot d_{Con}$, where the factor W_{frac} is the width factor as a fraction of d_{Con} . This means for $W_{frac} = 0.5$ the standard deviation of the d_{Con} distribution is 50% of the switching rate (see Figure 5.7 C). This width

modification is then adapted incrementally until at high values, all switching rates for d_{Con} occur with almost the same frequency at $W_{frac} = 5$ (shown in Figure 5.7 D).

5.3.2. Influence of Noise in Toxin Release on Bacterial Interaction

Incorporating this variability into the model, parameter sweeps over W_{frac} for values from 0 to 5 were performed in 0.5 steps, corresponding to a fixed switching rate ($\sigma = 0$) and high variability in switching rate (large σ)(see Figure 5.7). Heatmaps for simulations with conditions representing C_{REP1} on glycerol medium are plotted in Figure 5.8 for outcome fractions of C, S and coexistence (A-C).

These parameter sweeps showed that for increasing variability in d_{Con} in the intermediate switching regime C success was increased over a broader ranges of toxin producer fractions. Especially the C fraction increased for a broader range of toxin producer fractions and the amount of C winning increased. At the same time the fraction of coexistence was reduced for medium toxin producer fractions, while the amount of S fractions did not shift considerably.

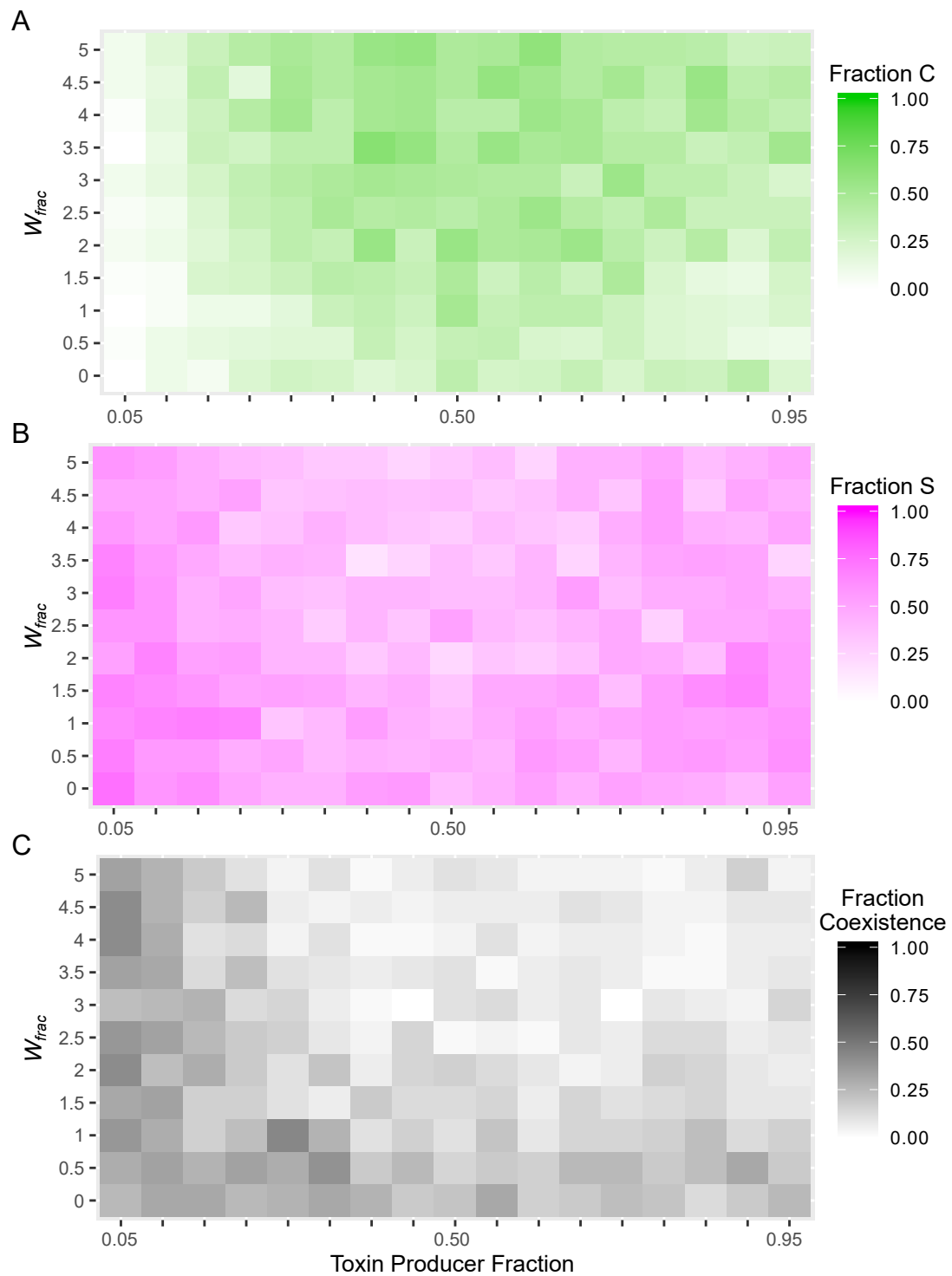


Figure 5.8

Theoretical analysis of parameter sweep over variability factor W_{frac} . Conditions of C_{REP1} -GLY rates for d_{Con} , growth rate and toxin amount. Heatmap of outcomes over a broad range of toxin producer fractions and distribution width factor W_{frac} for A) C fraction B) S fraction and C) Coexistence fraction.

5. Results: Toxin Expression Dynamics Shape Two Strain Bacterial Competition

Following the parameter sweeps, simulations for $W_{frac} = 5$ were performed for all C_X strains for both media corresponding to rates from Table B.1 comparable to Figure 5.2. The high variability of $W_{frac} = 5$ was chosen, as in these regimes all d_{Con} rates occur with comparable frequency (see Figure 5.7 D).

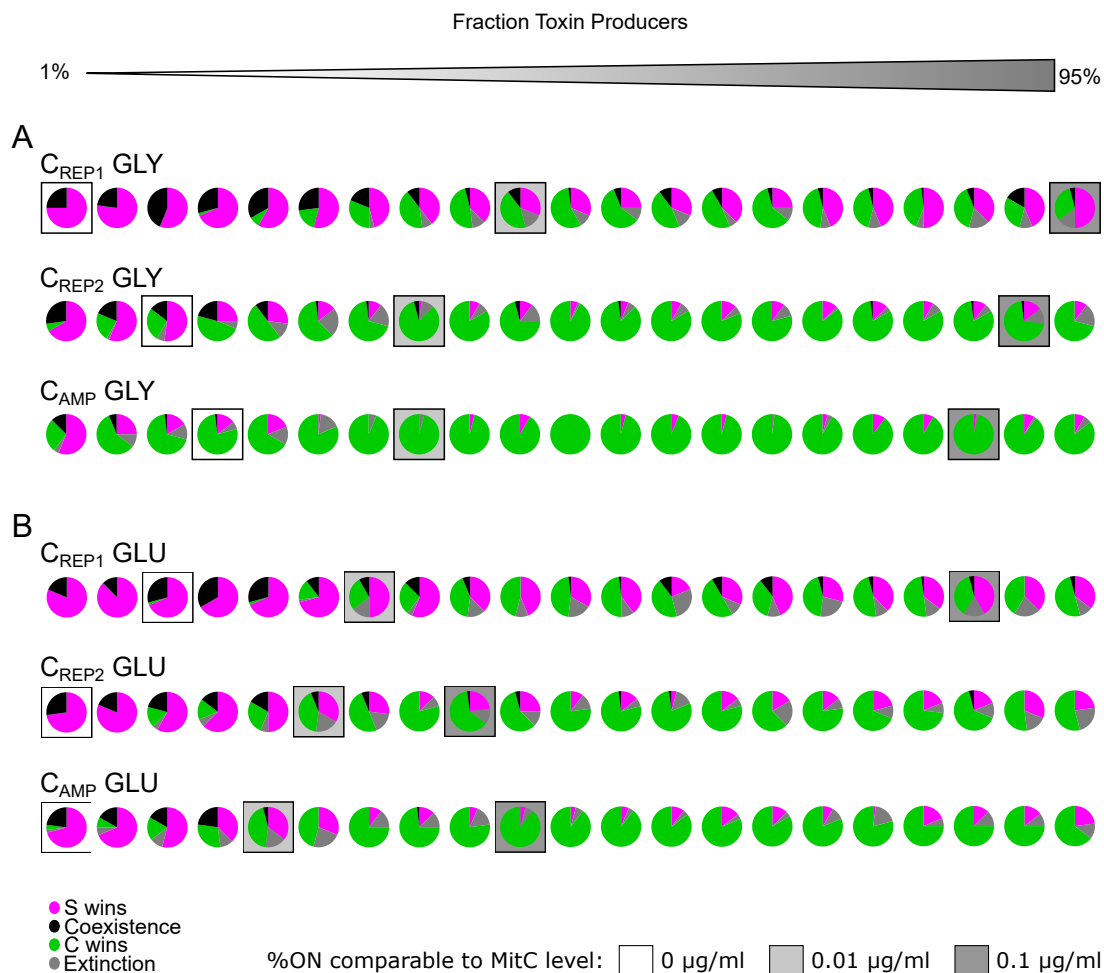


Figure 5.9

Numerical simulations of two-strain competition with variation in d_{Con} rate for glycerol (A) and glucose (B). For all pie charts shown, a high standard deviation was chosen with $\sigma = 5 \cdot \mu$. Simulations are run for increasing toxin producer fractions from left to right corresponding to 1% to 95% of C_X strains producing the toxin. Boxes around the pie charts correspond to toxin producer fractions that were obtained in live-dead experiments shown in Section 4.2.1 Figure 4.8 for the different inducer concentrations of MitC.

Pie charts for simulations with $W_{frac} = 5$ corresponding to all C_X strains on both glycerol and glucose are shown in Figure 5.9 A and B, respectively. Main trends in results of this theoretical analysis are comparable to results from previous simulations. At low toxin producer fractions, the simulation results do not seem to show any major

shifts as for small amounts of toxin producers, the variability in d_{Con} rate did not have much impact. The same was true when almost all C cells produced and released the toxin. However, at medium producer fractions the C wins outcome fraction increased for all conditions. Additionally, extinction became more dominant, especially when high amounts of toxin were produced and for high toxin producer fractions. Again, lysis data from live-dead staining was used to mark theoretical outcomes corresponding to experimental measurements.

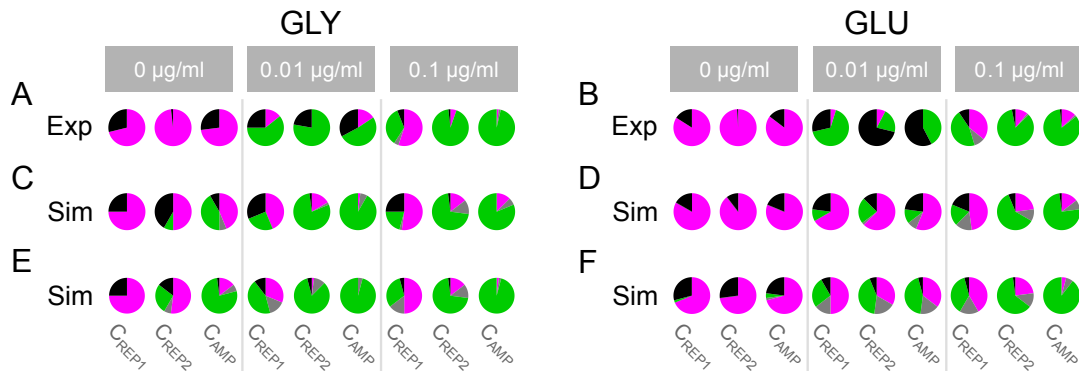


Figure 5.10

Comparison of experimental results of competition with original and adjusted simulations on glycerol (A,C,E) or glucose (B,D,F). A,B) experimental results for all MitC levels. C,D) Simulation outcomes with GRs corresponding to medium. E,F) Simulation outcomes for heterogeneity adjusted variability of d_{Con} (GRs corresponding to the respective medium). Outcomes are classified as: S wins (<10% C, magenta), coexistence (10%-90% C, black) C wins (>90% C, green), extinction (no area detected due to toxin action, gray).

A comparison of experimental results is shown in Figure 5.10 where experimental results (A,B) are compared with simulations with constant switching rate d_{Con} (C,D) and theoretical results for variable d_{Con} (E,F). Starting with medium supplemented with glycerol (A,C,E) the results of the model adapted for variations in d_{Con} fits experiments better especially at intermediate stress or when a small amount of toxin is produced. At low producer fractions (no stress) the strains displaying high toxin effectivity show big discrepancies. For glucose supplemented medium (Figure 5.10 B,D,F) the simulation results for variable d_{Con} generally better resemble the experimental results. At 0.01 µg/ml MitC the adjusted simulation still shows more C wins outcomes comparable to experiments, but still the high coexistence fractions were not reproducible. Instead increased amounts of extinction were detected for low stresses in all strains. The new simulation with high variability of d_{Con} rates especially at intermediate stresses, where heterogeneous switching takes place seems to be a better approximation for experimental results. But still, adjustments could be made in

the model to better describe the experiments over a broad range of lysis times, toxin amounts and toxin producer fractions.

5.4. Discussion

In order to investigate the impact of toxin expression dynamics on bacterial two strain competition, long-term competition experiments were performed according to von Bronk *et al.* [10, 11]. For experiments a toxin sensitive S strain (S_{RFP}) was combined with various C_X strains, where toxin production and release dynamics were known from Chapter 4. Experimental analysis of competition experiments showed that for different lysis times and toxin amounts of the three observed C_X strains (C_{REP1} , C_{REP2} and C_{AMP}) grown on either glycerol or glucose supplemented medium, no significant changes in competition outcome were detected. Comparing experimental and theoretical results showed good accordance for both low and high external stress levels (0.00 $\mu\text{g/ml}$ and 0.10 $\mu\text{g/ml}$). However, for intermediate stresses, increased discrepancies between experiments and theoretical results were detected. Reasons for this could be the noisy nature of these competition experiments that can not be incorporated into simulations. Furthermore, toxin released by the C strain was found to be able to induce its own production [83, 84]. This auto-inductive behavior is not included in the theoretical analysis either. Nevertheless, the same general trends were observed for theoretical and experimental results. At low stress, the S strain dominates competition against all C_X strains. When stress is present, an increased amount of C cells produce and release toxin, leading to better chances of success for the toxin producing strain.

As shown in Chapter 4, in the biological system toxin amounts and lysis times of colicin producers are strongly correlated. In a next step, the theoretical analysis was used to disentangle the relevance of these two factors for bacterial competition. This could lead to answer the question, if changes in C_X dynamics counteract each other concerning competition. For example, a later C cell lysis could lead to an advantage due to higher toxin amounts being released, but at the same time, the S strain has a longer time to grow and perform spacial exclusion of the C strain. In order to elucidate the importance of the two factors d_{Con} and n_{tox} for competition, parameter sweeps were performed varying the two factors in the theoretical model separately. Growth rate analysis of colicin producers and sensitive strains on both media showed that when grown on glycerol supplemented medium, the S and C_X strain have sim-

ilar growth rates, while for glucose medium, S grows significantly faster than all C_X strains. This constitutes a major difference between growth media, additional to the higher amounts of toxin being released for all C_X strains when grown on glucose. Theoretical results revealed that at low toxin amounts being released, C only wins a competition at early toxin release times. Similarly, for high toxin amounts C wins competition for a broad range of release times. Comparable trends were observed for both $GR(S) \approx GR(C_X)$ as well as $GR(S) > GR(C_X)$, but when S grows faster than C, higher amounts of toxin are needed for C to dominate the competition. This means, that early on delay of toxin release guarantees that more toxin is accumulated within a cell. Additional increase of lysis time has no major effect on competition. However, at optimal growth conditions (e.g. glucose supplemented medium), it could prevent cells from lysing without enough toxin being accumulated within the cell. The stability of the success of the C strain at intermediate and high stress under different conditions might be a biological trait caused by the complex regulation, ensuring a competitive advantage for the colicin producing population.

Even though experimental and theoretical results were shown to be in good accordance without stress and at high stress induction levels, discrepancies were detected at intermediate induction levels. Mader *et al.* 2015 [13] and von Bronk *et al.* 2017 [10] showed that especially at intermediate stress levels, heterogeneous toxin expression dynamics shape population behavior and accordingly the competition of toxin producers with a toxin-sensitive strain. Even though stochasticity was implemented in the theoretical model for all simulations, increased variability was added to increase the heterogeneity of d_{Con} rates derived from measured mean lysis times. For this adjusted model, higher C wins fractions were detected at intermediate stress induction levels mainly by reducing the number of coexistence outcomes, which fits better with experimental results for 0.01 $\mu\text{g/ml}$ MitC. This indicates that increased heterogeneity in toxin expression dynamics at medium stress level increases the competitive success of the toxin producers in the ColicinE2 system. Even though this increase in d_{Con} variability decreases discrepancies between experimental and theoretical results (Figure 5.10), additional modifications in the model might lead to an even better fit. For example, connecting the randomly chosen d_{Con} (from d_{Con} distribution) with a corresponding toxin amount for a fitting lysis time might further increase the accuracy of the model.

In summary, it was shown that experimentally changing the toxin dynamics of the ColicinE2 system does not significantly affect two-strain competition outcome. How-

ever, parameter sweeps within theoretical analysis revealed that the major factor for the competitive success of a colicin producing population (ColicinE2 system) is the increase of toxin accumulation before release while further delaying release time only prevents premature cell lysis. Combining these two strategies might be an important factor for the wild-type strain C_{WT} that shows lysis times and toxin amounts comparable to C_{AMP} (see Chapter 4 and [55]). Thus, considering other group A colicins with operon structures comparable to the ColicinE2 operon [14], this means that for lysis colicins increased lysis time can benefit competitive success of the colicin producers. However, not all colicins contain a lysis gene sequence [14]. For example, in group B colicins, lysis is mediated by temperate phages [85, 86]. Other colicins, such as group Z colicins [87] or Js colicins [88] show different mechanisms and genetic sequence order of cell lysis, e.g. lysis protein upstream of toxin sequence in colicin Js [88]. This leads to the assumption that tuning of toxin dynamics and specifically delaying cell lysis of colicin producers is a relevant biological trait for bacterial competition. Furthermore, as many SOS genes such as various colicins were shown to be expressed heterogeneously [18], similar to the ColicinE2 system, this heterogeneity could ensure increased success in competition.

6. Results: Noise Generation in the Toxin Expression System

This chapter is based on the publication Götz *et al.* 2020: *Gene expression noise in a complex artificial toxin expression system* [56].

Gene expression is an inherently noisy process [89] as both transcription and translation of a gene are influenced by stochastic fluctuations such as environmental conditions and or polymerase availability [29, 30]. In some cases noise is expected to be deleterious for the cell, however it can also benefit from noise in other cases [89, 90]. As shown in the previous chapter, variability in the dynamics of toxin production and release plays an important role for competition and increased variation in release times can boost the competitive success of the C strain population. In order to investigate how noise generation is controlled in the ColicinE2 system, single-cell fluorescence time-lapse measurements were performed as described in Chapter 4 with the S reporter strain that can not produce the toxin or lyse (Table 3.1). However, this strain contains all regulatory components of the ColicinE2 operon but the genes *cea* and *cel* are replaced with genes coding for the FPs YFP and CFP. This makes the S strain ideal to investigate the noise in this system. When stressed, the SOS response of the ColicinE2 system is triggered and the operon is transcribed. For investigation, three different noise types were chosen for analysis depending on the switching states that a toxin producing strain within the ColicinE2 system can be in.

- (i) **OFF state noise:** Noise of all cells with fluorescence intensity below the 5x initial FI switching threshold. As the response-time of the ColicinE2 system to stress is not immediate, during the first 1 h of the measurement, almost no cells switch into the ON state.
- (ii) **ON state noise:** Noise of cells that have switched into the ON state by crossing above the 5x initial FI threshold (see Figure 3.4). As only S strain mutants were analyzed for noise measurements, the number of ON cells reaches a maximum at the end of the measurement. Depending on the induction level and/or mutations this can be (almost) all observed cells within a population.

- (iii) **Population noise:** Noise of all cells observed (OFF and ON state) independent of their switching behavior. Hence, if all cells switch into the ON state during the measurement, noise of ON state and population noise are identical. And accordingly at early times, before switching, the OFF noise and population noise are the same.

Noise measurements were performed for the three different stress induction levels of 0.10 $\mu\text{g/ml}$, 0.25 $\mu\text{g/ml}$ and 0.40 $\mu\text{g/ml}$ MitC as described in Chapter 4. High stress induction levels were chosen to guarantee a high fraction of cells switching into the ON state and producing both YFP and CFP (see Chapter 3 and Figure 3.4). As a measure of noise, the coefficient of variation $CV = \sigma/\mu$ was chosen, which is described by the standard deviation and the mean of the measured fluorescence intensities of the single cells (see Chapter 3).

6.1. Quantification of Noise in Toxin Production and Release

Noise in the Reporter Strain S_{REP1}

In a first step, the noise of all three states was investigated for the S_{REP1} strain for all three induction levels separately. The corresponding CV over time is shown in Figure 6.1 for both YFP and CFP noise of all states.

Starting with the OFF state (Figure 6.1 A,B) the CV showed big fluctuations over time. No trend for change in CV was observed between the different MitC concentrations. This was the case for both YFP and CFP expression within the ColicinE2-based system (S_{REP1}). While for YFP expression the CVs for the various stresses fluctuated approximately from 0.5 to 1.0, CV changes in CFP were observed mostly from 0.25 to 0.75. This indicates that the basal noise of both FPs does not seem to be dependent on induction level or the time-point within the measurements. Thus, for basal noise the observation time of 45 min after induction was chosen, as at this time-point almost no cells have switched into the ON state leading to high numbers of OFF cells.

In the next step, ON noise of the S_{REP1} strain is shown as CV over time in Figure 6.1 C and D for YFP and CFP expression. For both cases CV values started for time-points later than 50 min due to the response time of the ColicinE2-based operon (see Chapters 3 and 4) and thus start of switching of S_{REP1} into the ON state. Both FPs

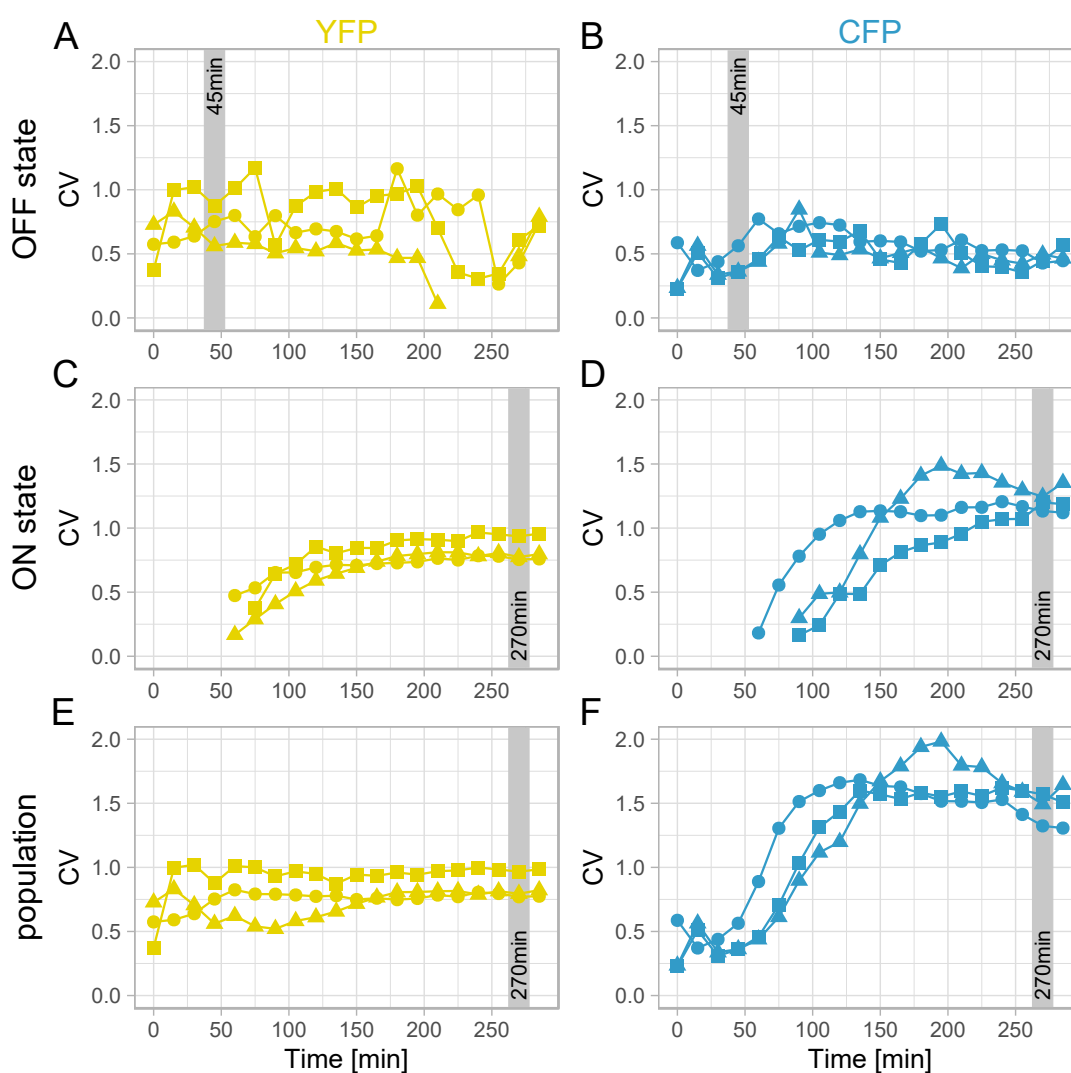


Figure 6.1

Coefficient of variation (CV) over time for three states of the S_{REP1} strain. A,B) OFF state, C,D) ON state, E,F) population noise over time for all three induction levels: $0.10 \mu\text{g/ml}$ (squares), $0.25 \mu\text{g/ml}$ (circles), $0.40 \mu\text{g/ml}$ (triangles). Noise in YFP (yellow) and CFP (blue) expression quantified by the coefficient of variation as described in Chapter 3. Gray areas mark the time-point chosen for further analysis of the corresponding states. Basal noise values at 45 min (OFF state) where most cells are in the OFF state (gray area). ON state and population noise were chosen at 270 min when the maximum amount of cells have undergone switching (gray are). Figure adapted from [56].

showed increasing CV over time and reached a steady-state value for late time-points when switching into the ON state is completed and almost all cells are in the ON state for the induction levels used in this study. CV increase for YFP was faster than for CFP as here, the CV converged to a steady state value at approximately 165 min to 180 min while in CFP this took until the end of the measurement with around

270 min. Again, no major differences between the CVs of the three different induction levels were observed. Therefore, for comparison of ON state noise 270 min was chosen (see gray area in Figure 6.1 C,D) as here most of the switching has taken place and a steady state of CV was reached for both FPs in the operon of the reporter plasmid. Finally, Figure 6.1 E and F show the population noise (CV over time) for YFP and CFP, respectively. Here, big differences between the fluorescent proteins were observed. The coefficient of variation for YFP fluorescence mainly stayed between 0.5 and 1.0 over the complete time-course. Fluctuations were bigger in the beginning and at later times CVs of all MitC levels converged to the same level (Figure 6.1 E). In contrast to this, population noise of CFP showed a big increase over time for all stresses. At the beginning, CVs were low with approximately 0.4 and increased drastically when switching into the ON state took place after 50 min to 150 min. In the end, the noise adjusted to a steady state and fluctuations between induction levels were small. Consequently, in order to separate the noise values of the various states from switching dynamics 270 min was defined as time-point of analysis for the population noise of both fluorescent proteins (see gray area Figure 6.1 E,F).

After setting the time-point for analysis for all three noise types (OFF, ON and population) a closer look into the single-cell fluorescent protein expression at all inductions levels is shown in Figure 6.2 for both YFP and CFP fluorescence intensity histograms. Plots are shown for the above specified times for all three noise types of 45 min for basal noise of the OFF state and 270 min for noise of the ON state and population noise. The different bar colors in the histogram correspond to the three stress levels used in the experiments.

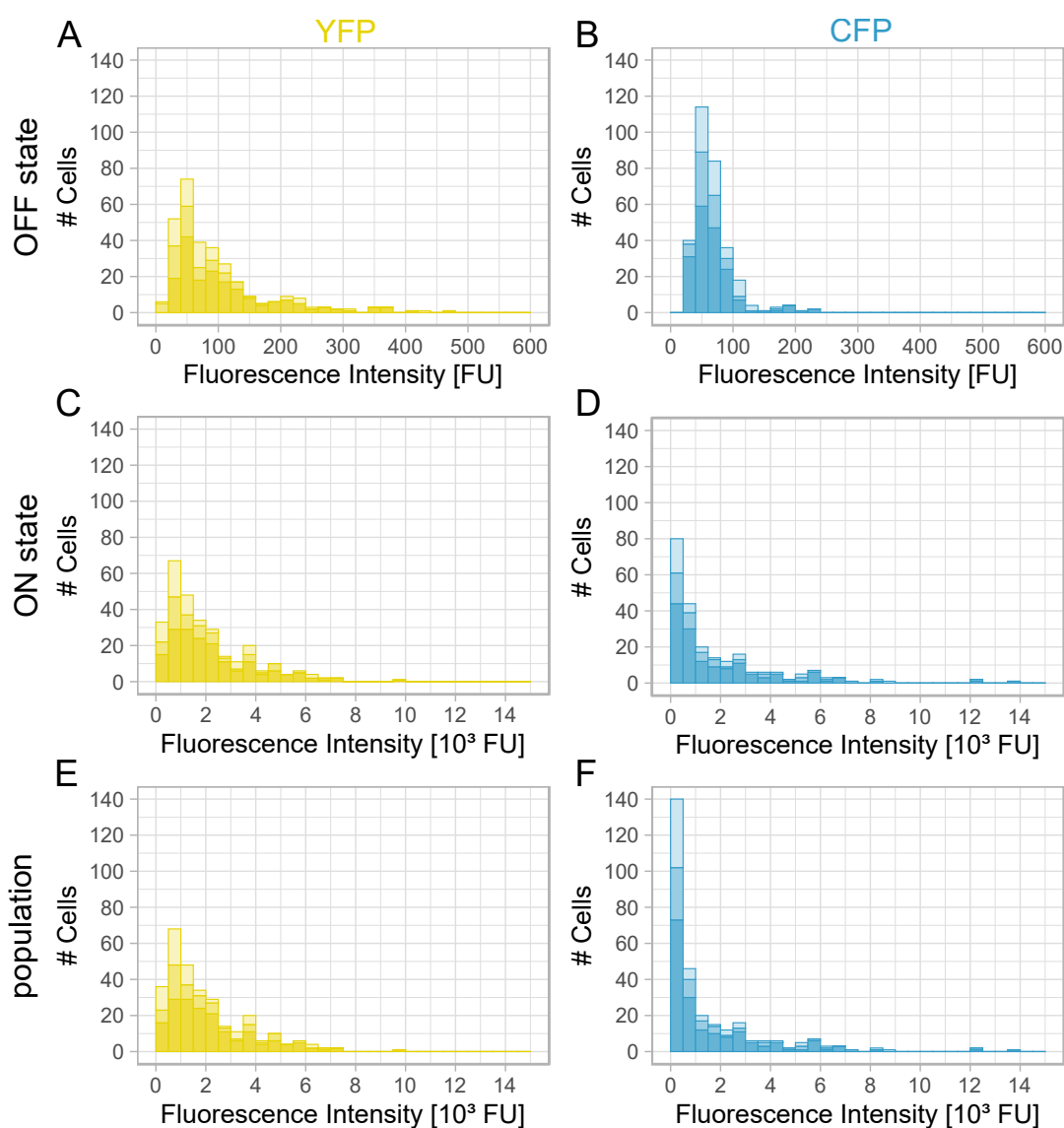


Figure 6.2

Fluorescence intensity histograms for three S_{REP1} strain states in YFP (yellow) and CFP (blue) at time-points shown in Figure 6.1. Plots for noise of OFF state (A,B), ON state (C,D) and population noise (E,F) are shown for all induction levels from 0.10 $\mu\text{g/ml}$ to 0.40 $\mu\text{g/ml}$ from light to dark bar color. Bar widths: 20 FU for basal noise Figure 6.2 A,B); 500 FU for ON state and population noise Figure 6.2 C-F. Figure adapted from [56].

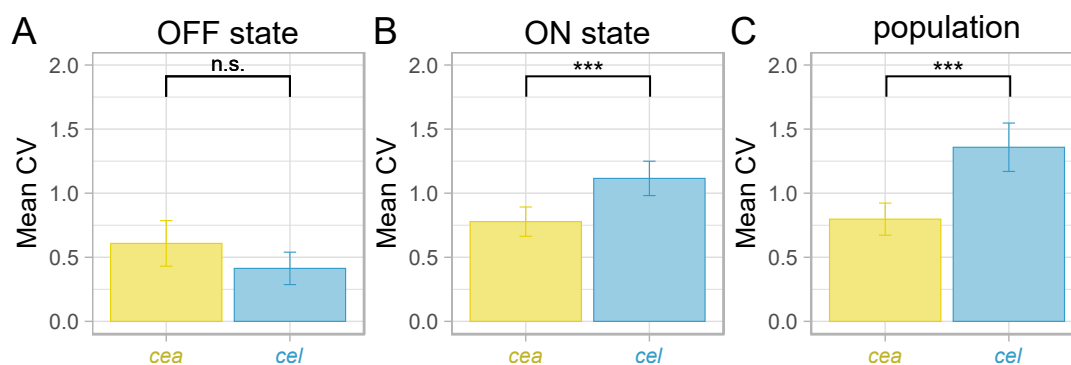
For OFF state noise (Figure 6.2 A,B), the distributions for YFP and CFP fluorescence intensities were lower than 600 FU with a peak of approximately 60 FU for both YFP and CFP expression. Both distributions showed a clear peak around the basal fluorescence of the FPs with an elongated tail for higher intensities. However, the histogram for CFP fluorescence showed a narrower distribution than the YFP fluorescence, leading to a smaller coefficient of variation (CV). For the ON state noise

and population noise of YFP and CFP expression higher fluorescence intensities than in the OFF state were detected for both proteins (see Figure 6.2 C-F). YFP noise between ON state and population noise did not show big differences, as most of the S_{REP1} cells switched into the ON state during the measurement. For the intensity of 1000 FU the highest number of cells are expressing YFP within that histogram range. Fluorescent protein expression in CFP showed variations between the noise types (ON and population) as for CFP, a reduced fraction of cells were shown to switch into the ON state (see Figure 4.7 A). For both, the ON and population noise, the largest amount of cells expressed CFP with low intensities up to 500 FU, which is less FI than shown for YFP expression. However, the tail of the CFP histograms was much longer and shifted to higher intensities. A combination of this could have caused the increase in noise for ON state and population CVs.

Additionally, to further elucidate the role of the stress induction level on the noise of the ColicinE2-based system, data for all MitC concentrations is shown in Figure 6.2 with different bar colors from light to dark for both YFP and CFP with increasing MitC concentration. Closer examination showed similar behavior for all induction levels for each noise type and fluorescent protein. Cell numbers vary due to different number of cells analyzed for each concentration (see Table 6.1). Nevertheless, the basic trends for the distributions for YFP and CFP expressions did not change.

Concluding, the data for the three different MitC induction levels shown in Figure 6.1 and Figure 6.2 showed that at these high stresses, none of the noise types showed major dependence on the MitC concentration. Thus, to increase the amount of data to identify the mechanisms regulating noise control of the ColicinE2 system, mean CVs from all measurement sets (0.10 $\mu\text{g/ml}$, 0.25 $\mu\text{g/ml}$ and 0.40 $\mu\text{g/ml}$) can be used for analysis as shown in Figure 6.3 for all noise types (ON, OFF and population noise).

Combining the noise information of all measurements and induction levels allows the comparison of noise types and proteins within the operon, determining if there are significant differences between noise in toxin production and release. For the OFF noise of the S_{REP1} strain (see Figure 6.3 A) no significant difference between noise of *cea* (YFP) and *cel* (CFP) was found. Both FPs showed mean CVs of around 0.5 for basal expression. Comparison of *cea* (YFP) noise showed no significant differences between the three noise types (see Table C.3). In comparison to that, *cel* (CFP) noise of the OFF state of S_{REP1} was significantly smaller than that of both other noise types. Its noise increased from around 0.41 to 1.12 and 1.36 for the ON state and population mean noise. This means that for *cel* expression noise, switching into the ON state

**Figure 6.3**

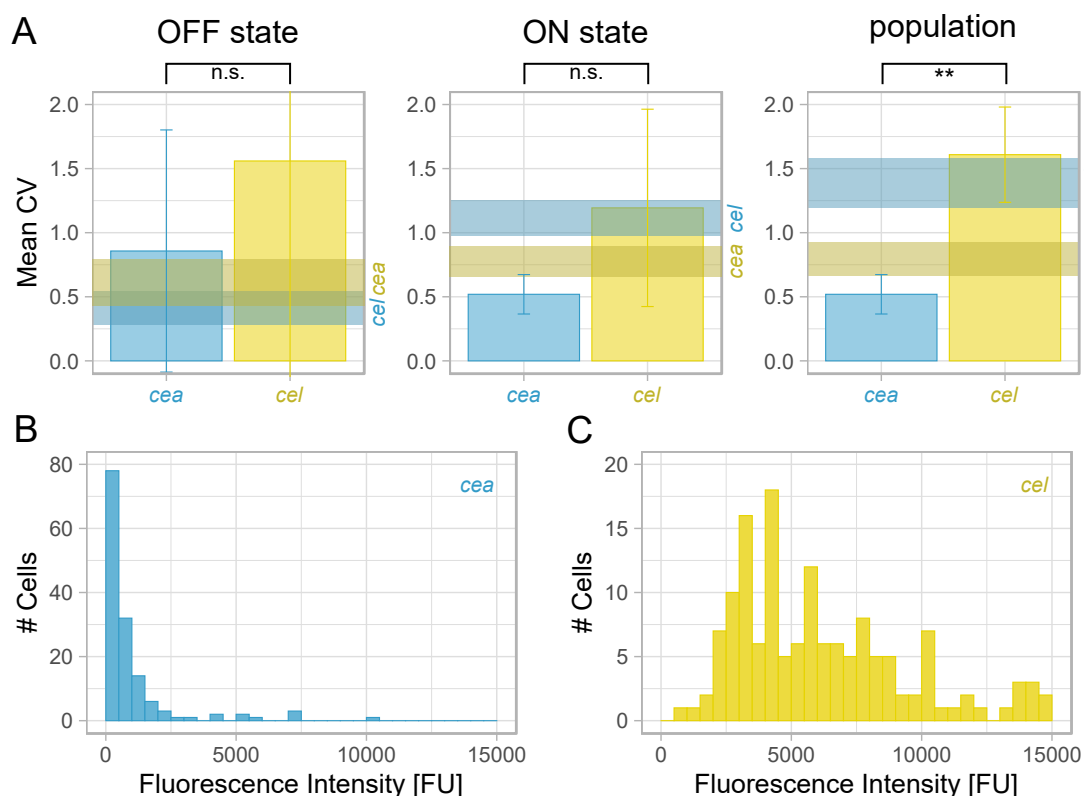
Mean CV of the S_{REP1} strain for OFF state, ON state and population noise. Noise *cea* (YFP, yellow) and *cel* (CFP, cyan) shown as mean CV at time-point chosen for specific state. A) OFF state, B) ON state C) population; Error bars depict the 95% confidence interval. Significance levels: n.s.: no significant difference, ***: $p < 0.001$. Significance analysis performed as described in Chapter 3. Detailed values from analysis shown Table C.3. Figure adapted from [56].

highly increased noise. The population noise was found to show the largest CV, which could be caused by the inclusion of ON and OFF cells within the population as for CFP not all cells switch into the ON state during the measurement of S_{REP1} (shown before in Chapter 4 Figure 4.7 A). For both, noise of the ON state and population noise, the mean CV of *cel* (CFP) was significantly larger than noise of *cea* (YFP) (see Figure 6.3 B,C). This indicated that the complex multi-layer regulation of *cel* expression in the ColicinE2 system could lead to an increase in its noise.

Control Experiments for Changes in Fluorescent Proteins

To elucidate whether the difference of noise in *cea* and *cel* expression was caused by the regulation steps of the system or the choice of fluorescent protein order within the reporter plasmid, a second strain with flipped FPs S_{FLIP} was studied. This mutant consists of a sensitive S strain containing a reporter plasmid with identical regulation mechanisms as the REP1 plasmid, but with interchanged order of the two fluorescent proteins within the operon. Thus, *cea* and *cel* were replaced by sequences coding for *cfp* and *yfp*, respectively (see Chapter 3, Table 3.1).

Mean noise of all three noise types of the S_{FLIP} strain is shown in Figure 6.4 A. In each bar plot, the mean CV values of S_{REP1} with confidence interval are included as shaded areas for comparison. Even though the 95% confidence intervals for the S_{FLIP} mutant were generally bigger than those measured for S_{REP1} similar trends were observed. The basal noise of both *cea* and *cel* did not show a significant difference.

**Figure 6.4**

Mean CV and population noise histogram of the S_{FLIP} strain with flipped order of the fluorescence proteins. Noise *cea* (CFP, cyan) and *cel* (YFP, yellow) shown as mean CV at time-point chosen for the specific state. A) OFF state, ON state and population noise; Error bars depict the 95 % confidence interval. Shaded area in yellow and blue mark the corresponding CV of each state of the S strain in YFP and CFP, respectively. Significance levels: n.s.: no significant difference, **: $p < 0.01$. Significance analysis performed as described in Chapter 3. Detailed values from analysis shown Table C.4. B,C) Population noise histograms of FIs at 270 min depicted for *cea* (blue, B) and *cel* (yellow, C). Figure adapted from [56].

The same was found for noise in the ON state despite the big difference in mean CV of approximately 0.67. One reason for this could be the big error in *cel* noise due to a reduced number of measurements for S_{FLIP} (see Table 6.1). Nevertheless, population noise of *cea* (CFP) is significantly smaller than of *cel*. Fluorescent intensity histograms corresponding to population noise single-cell data of S_{FLIP} are shown in Figure 6.4 B and C for *cea* (CFP) and *cel* (YFP). This fluorescence data showed the same trends for toxin and lysis protein compared to S_{REP1} but in the switched color. Due to the sequence change on the reporter plasmid, the illumination times had to be adjusted as described in detail in Chapter 3. Thus the mean values for both FPs shifted. However, *cel* intensities showed a much broader distribution than *cea* intensities. The same

trend for distribution widths was shown for S_{REP1} in Figure 6.2 E and F. Combining results for the strains S_{REP1} and S_{FLIP} shows that significant difference between *cea* and *cel* population noise is an effect caused by the ColicinE2 operon and its regulation rather than an inherent property of the fluorescent proteins.

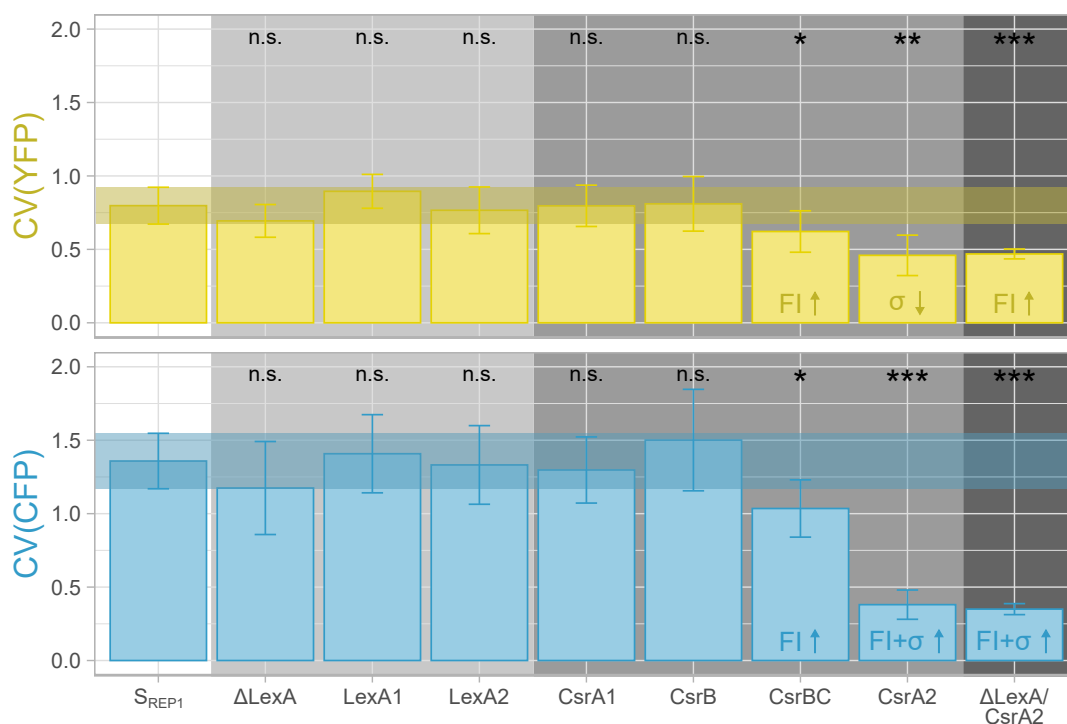
Strain	S	ΔLexA	LexA1	LexA2	CsrA1	CsrB	CsrBC	CsrA2	$\frac{\Delta\text{LexA}}{\text{CsrA2}}$	S_{FLIP}	S_{REP2}
MitC	0.10	0.10	0.10	0.10	0.10	0.10	0.10	0.10	0.10		0.10
Conc. Measured [$\mu\text{g/ml}$]	0.25	0.25	0.25	0.25	0.25	0.25	0.25	0.25	0.25	0.25	
	0.40	0.40	0.40	0.40	0.40	0.40	0.40	0.40	0.40		
Replicates N	8	9	11	10	9	6	7	7	7	3	3
Total Number of Cells X	310	301	431	382	434	314	312	348	247	143	93

Table 6.1

Overview over measured noise data with information on cell numbers and induction levels.

6.2. Noise Control in the ColicinE2 System

Using the quantification of noise in the S_{REP1} strain that is closest to the regulation mechanisms of the wild-type ColicinE2 operon, the aim of this study was to identify the influence of the complex regulation mechanisms of the ColicinE2 network on the noise of the system. This is one of the few examples of how noise is regulated in a plasmid encoded operon. To facilitate identification of noise regulating mechanisms, genetic modifications were introduced influencing multiple regulation steps on various levels, e.g. transcriptional regulation via LexA binding and post-transcriptional regulation via CsrA binding to mRNA. A list of the used genetic modifications is shown in Chapter 3 Table 3.1 including expected changes caused by genetic modifications. In order to be able to investigate the complete time-course of expression without cell lysis, only strains without the wild-type pColE2-P9 plasmid were studied. From now on, population noise was chosen as measure for the comparison between the different mutant strains, as all cells are included in the corresponding CV and a high number of cells express the operon. For identification of factors influencing noise, the noise values obtained for mutant strains were compared to S_{REP1} coefficient of variation with 95% confidence interval. Significance analysis was performed as described in Chapter 3 and detailed values are indicated in Appendix C by tables referenced in each figure caption.

**Figure 6.5**

Population noise measured in S_{REP1} strain and several strains carrying transcriptional and post-transcriptional genetic modifications. Mean noise of YFP (yellow) and CFP (blue) are shown in bar plots. Error bars depict the 95% confidence interval. Shaded area in yellow and blue mark the corresponding CV of the S strain in YFP and CFP, respectively. Background colors show changes on transcriptional level (light gray), post-transcriptional level (medium gray) and on both transcriptional and post-transcriptional level (dark gray). Significance levels: n.s.: no significant difference, *: $p < 0.05$, **: $p < 0.01$, ***: $p < 0.001$. Significance analysis performed as described in Chapter 3. Detailed values from analysis shown in Table C.5. Figure adapted from [56].

6.2.1. How Transcriptional Regulation Affects Noise Generation

Transcription of the ColicinE2 system is under the control of protein LexA that represses gene expression of the ColicinE2 operon when no stress is present by binding to the SOS box of the ColicinE2 operon (see Chapter 2 and Figure 2.1). In Chapter 4 it was shown that changes in the transcriptional regulation of the ColicinE2 system have an effect on gene expression dynamics (GED) of its proteins. To analyze how transcriptional regulation affects noise generation of the ColicinE2 system, three different mutations regarding the LexA binding site were introduced to analyze the influence of different transcriptional changes on noise of both YFP and CFP expression. Population noise of these mutants is given in Figure 6.5 (light gray background). In Chapter 4 it was shown, that both mutants LexA1 and LexA2 display increased LexA binding and thus reduced transcription of the operon. Contrary to that, in the

Δ LexA mutant, the complete LexA binding site was deleted and constitutive expression of the operon takes place, even without induction. Changes in noise were rather small and within the 95% confidence interval when compared to S_{REP1} . Small trends in CV changes of YFP were also seen for CFP expression noise. However, for all transcriptional mutations, no significant changes in population noise were detected for both YFP and CFP expression (Figure 6.5 and Table C.5).

6.2.2. How Post-transcriptional Regulation Affects Noise Generation

In a next set of experiments multiple post-transcriptional modifications were investigated. Detailed analysis of GED of the ColicinE2 system shown in Chapter 4 showed the importance of post-transcriptional regulation by the global regulatory protein CsrA for toxin expression dynamics (TED) in the ColicinE2 system. CsrA represses *cel* gene translation by binding to long mRNA produced after SOS induction of the ColicinE2 operon and is controlled by the abundance of CsrA sequestering elements like the sRNAs CsrB and CsrC (see Chapter 2). To investigate how this post-transcriptional regulation affects noise generation in the ColicinE2 system, post-transcriptional modifications were introduced on the two main different levels (see Table 3.1). Either by changing the sequence on the reporter plasmid to change the binding strength of CsrA to the transcribed mRNA. Or by changing the availability of CsrA within the cell by deleting the genetic sequence of one or both sRNAs. As shown in Chapter 4, the mRNA mutants CsrA1 and CsrA2 have slightly stronger and much weaker CsrA binding strength compared to S_{REP1} . The sRNA mutations change CsrA abundance and thus indirectly influence translation on the *cel* gene (CFP expression). The population noise of all post-transcriptional mutants is shown in Figure 6.5 (medium gray background). Regarding population noise, no significant changes in CV were found for CsrA1 and CsrB. For these mutants, changes in the genetic sequence only produce slight changes of the GED in the cell (Chapter 4). This is due to the fact that CsrA binding to mRNA of S_{REP1} is nearly optimal [4] and for the CsrB mutant, when one sRNA is deleted, compensating effects can take place that up-regulate the second sRNA, in this case CsrC [71]. Analog to the CsrB mutant, a double knock-out with deletion of both the CsrB and CsrC sequence was created (CsrBC). In this strain the abundance of free CsrA within the cell highly increased due to the lack of sRNA binding partners. A corresponding mutation without CsrA would require

dramatically changed growth conditions, as CsrA is an essential player in the central carbon metabolism (see Chapter 2). Thus, a mutant with much smaller CsrA binding strength to mRNA was created (CsrA2). Examination of population noise of these two mutants showed significant reduced CFP population noise in both mutants compared to S_{REP1}. For CsrBC, this was due to an increase in mean fluorescence intensity. For CsrA2, both mean FI μ and σ increased by a factor of 11 x and 3 x, respectively. This resulted in a much smaller CV for CsrA2 to approximately 0.38.

Surprisingly, for the two mutants CsrBC and CsrA2, which showed significant changes in CFP noise, also the YFP noise was significantly reduced. This was unexpected, as both mutations were only expected to influence post-transcriptional regulation of the operon. However, as these mutants produce substantial changes in CsrA abundance within a cell, this lead to the hypothesis that CsrA as a global regulatory protein [6, 7] could act as a global factor for noise control within the ColicinE2 system. To verify the effect of these mutations, a double mutant was created that combined the mutations that showed the biggest effect (transcriptional and post-transcriptional) creating the strain Δ LexA/CsrA2 (see Table 3.1). This mutant showed similar behavior to CsrA2, namely a significant decrease in population noise of both YFP and CFP.

To get a better insight into the mechanism that caused a significant change in either YFP and/or CFP expression, fluorescence intensity histograms of these mutants are shown in Figure 6.6. Starting with YFP expression, the distributions of FIs were compared for mutations causing significant changes in CVs. While the FI distribution of CsrBC showed a comparable width to S_{REP1}, the mean FI increased, which lead to a decrease in population noise. For CsrA2, the opposite was true, as the change of the mean FI was small, while the distribution width decrease was larger, shown by a narrower distribution in Figure 6.6 (YFP: CsrA2). Lastly, in the double mutant a FI distribution similar to S_{REP1}, but with increased mean FI from approximately 1900 FU to around 3200 FU was observed. Next, CFP histograms of fluorescence intensity are compared for the same mutants (Figure 6.6, CFP:right). For CsrBC, the distribution only showed small changes. Mainly, the mean FI increased due to a lower number of cells with intensities around a basal FI level. For both post-transcriptional mutations changing the mRNA binding to CsrA (CsrA2 and Δ LexA/CsrA2) a vast change in CFP distributions was found. Fluorescence intensities did not show a peak for small FIs, but rather a broad distribution accompanied by a much larger mean fluorescence. While the mean intensities for CsrA2 and Δ LexA/CsrA2 increased by a factor of 11 x and 9 x, σ changed by a factor of 3 x and 2 x, respectively.

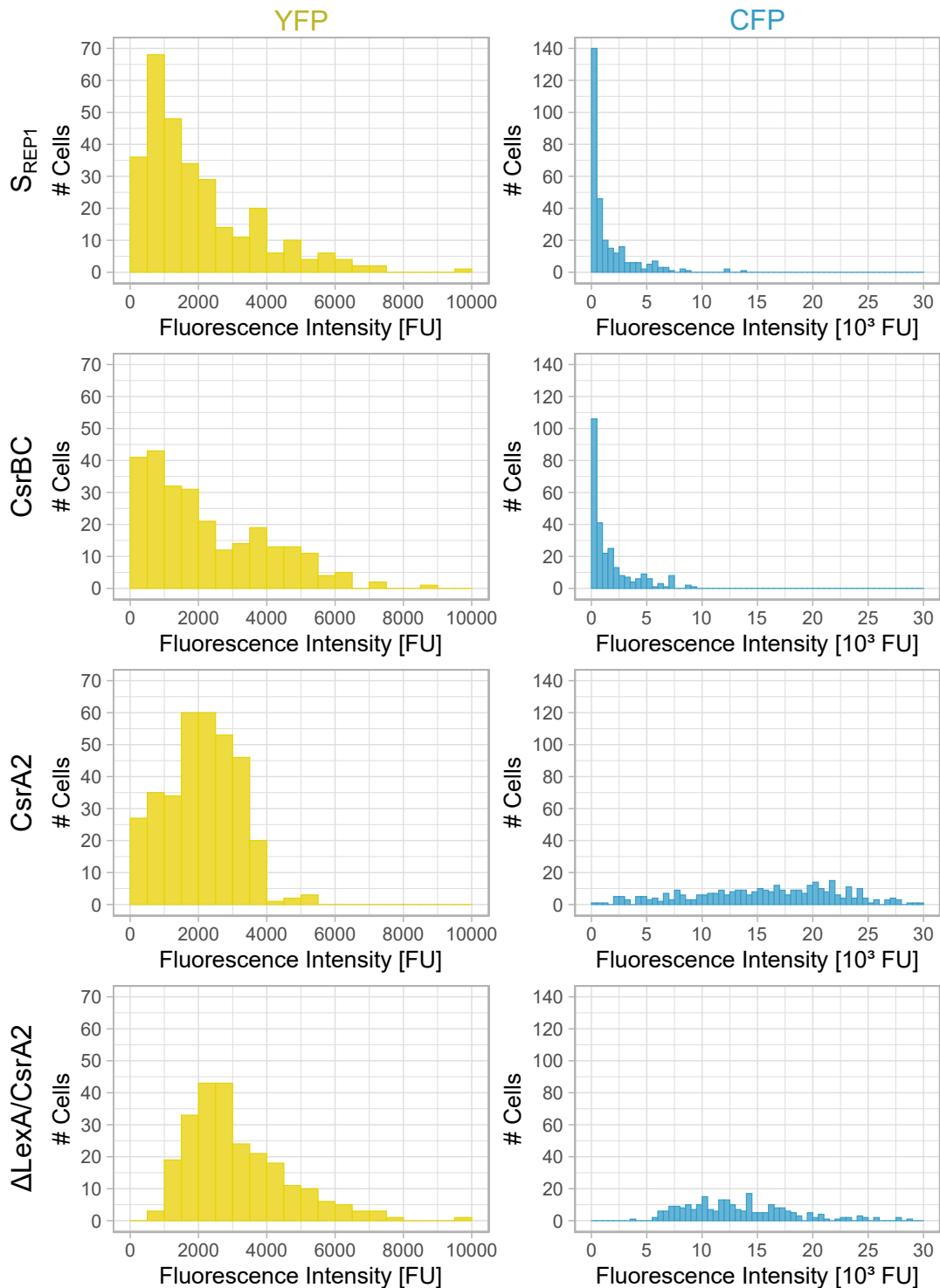


Figure 6.6

Histogram of FIs for mutant strains with significant changes in population noise as shown in Figure 6.5. Data includes all induction levels (0.10 $\mu\text{g}/\text{ml}$ to 0.40 $\mu\text{g}/\text{ml}$). Fluorescence intensities for YFP expression (left) and CFP expression (right) are depicted in yellow and blue, respectively. Time-points were chosen corresponding to the population noise time shown in Figure 6.1 E and F. Figure adapted from [56].

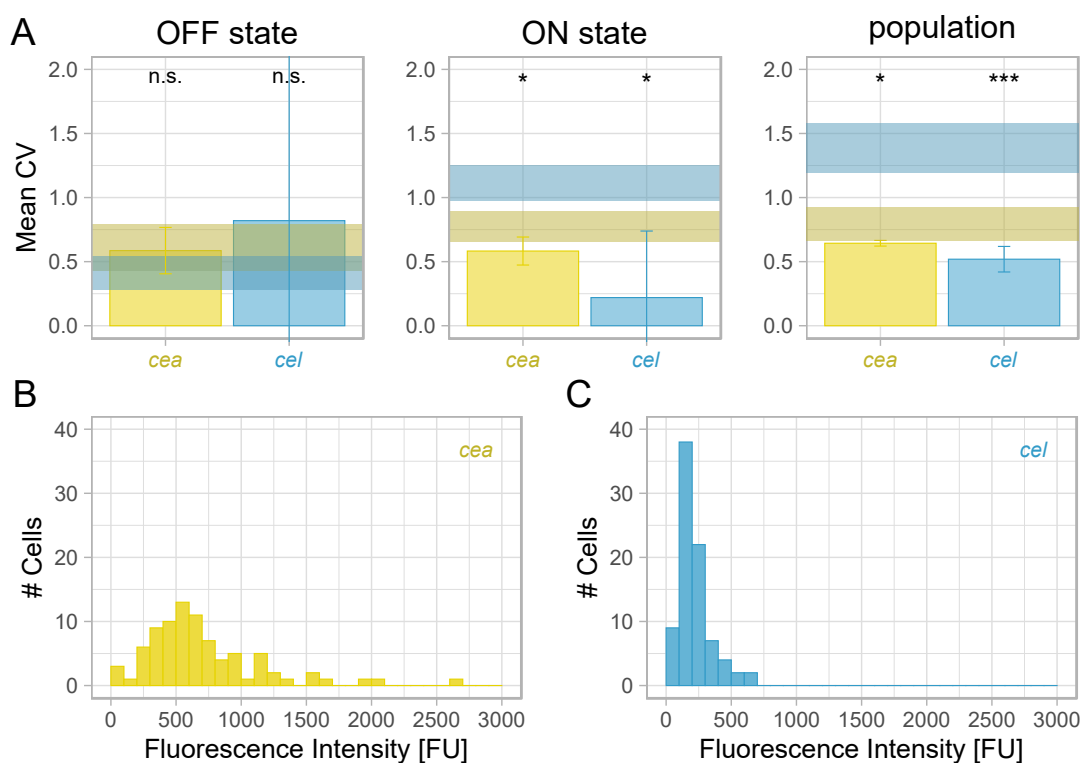
Taken together, this data indicated that changes in post-transcriptional regulation reduce the population noise of CFP (*cel*) within the ColicinE2 operon. One hypothesis is that CsrA could be a major player for noise control in the system.

In Chapter 4 it was shown that CsrA is a main player that regulated GED in the ColicinE2 system. It is controlled by abundance of CsrA sequestering elements like the sRNAs but also long mRNA produced by the ColicinE2 operon. The amount of long mRNA in turn is dependent on the copynumber of the plasmid containing the ColicinE2 operon. Thus, the copynumber of the plasmid was also shown to determine GED of the ColicinE2 system (see Chapter 4). To support the hypothesis that CsrA is a major player for noise control of the system, the global factor plasmid copynumber will be analyzed in the following, as it influences both the transcriptional level, by reducing the amount of DNA and in turn mRNA being produced, and the post-transcriptional level, by reducing the amount of long mRNA and additionally changing the abundance of free CsrA in the cell.

6.3. How Global Factors Influence Noise Generation

A global factor for noise generation in the expression of fluorescent proteins of the reporter strain is the plasmid copynumber of the reporter plasmid. The wild-type pColE2-P9 plasmid has a copynumber of ~ 20 copies per cell while the reporter plasmid pMO3 has an increased copynumber with ~ 55 copies per cell. Thus, to decrease this discrepancy and study the influence of the global factor copynumber on the noise response of the ColicinE2 system, a second reporter plasmid pMO8 was studied creating the strain $S_{\text{REP}2}$. As described in Chapter 3 (see Table 3.1) this plasmid has the same regulatory elements as pMO3, but the origin of replication was changed to facilitate a smaller copynumber of ~ 13 copies per cell. Due to the low number of plasmids per cell, $S_{\text{REP}2}$ was measured with longer illumination time and higher lamp-power to enable reliable detection of fluorescent proteins above the detection limit. Thus, fluorescence intensities of YPF and CFP between $S_{\text{REP}1}$ and $S_{\text{REP}2}$ are not directly comparable. However, this should not have a major impact on the noise of the system, as the CV compensates for changes in mean fluorescence.

Results for all noise types for $S_{\text{REP}2}$ are shown as mean CV and fluorescence histograms in Figure 6.7. The mean CV for each fluorescent protein was compared to the corresponding values obtained for $S_{\text{REP}1}$. For the OFF state, no significant differences between both *cea* (YFP) and *cel* (CFP) noise were found compared to the

**Figure 6.7**

Mean CV and population noise histograms of the $S_{\text{REP}2}$ strain with reduced plasmid copynumber. Noise *cea* (YFP, yellow) and *cel* (CFP, cyan) shown as mean CV at time-point chosen for specific state. A) OFF state, ON state and population noise; Error bars depict the 95% confidence interval. Shaded areas depict corresponding mean with confidence intervals for all states measured for the S strain. Significance levels: n.s.: no significant difference, *: $p < 0.05$, ***: $p < 0.001$. Significance analysis performed as described in Chapter 3 with the corresponding $S_{\text{REP}1}$ value. Detailed information for significance analysis shown Table C.6. B,C) Population noise histograms of FIs at 270 min depicted for *cea* (yellow, B) and *cel* (blue, C). Figure adapted from [56].

corresponding CVs of $S_{\text{REP}1}$. Additionally, the basal noise of *cea* was not significantly different from the basal noise of *cel* in $S_{\text{REP}2}$ (see Table C.6), which was the same as found for $S_{\text{REP}1}$. For ON state noise and population noise of $S_{\text{REP}2}$, all mean CVs (both YFP and CFP) were significantly smaller than the CVs obtained for $S_{\text{REP}1}$. This means that for a reduced copynumber of the reporter plasmid within a cell the noise of both *cea* and *cel* in the ColicinE2 operon decreased significantly. Direct comparison of noise of *cea* and *cel* of $S_{\text{REP}2}$ showed that the population noise of *cel* was significantly smaller than that of *cea*. This was opposed to $S_{\text{REP}1}$, where *cel* population noise was shown to be significantly larger than *cea* noise.

A closer look at histograms of the fluorescence intensities (Figure 6.7 B,C) showed narrower distributions for both *cea* and *cel*. Even though the mean FI of both proteins was smaller as well, the population noise is significantly smaller for both proteins.

Comparing the FI histograms of *cea* and *cel* displayed a broad distribution of FIs for *cea* with a peak around 500 FU, whereas the maximum FI corresponding to *cel* gene expression was detected at low intensities around 100 FU and maximum intensities below 1000 FU. This again showed that for higher amounts of free CsrA which is the case for reduced plasmid copynumber, *cel* noise in the ColicinE2 operon was reduced with a much narrower distribution of FIs. Population noise of *cea* and *cel* is reduced, but here noise in *cel* is smaller than in *cea* for ON and population noise. This data, in combination with the changes in noise in both *cea* and *cel* for mutations affecting the global regulator protein CsrA further supports the hypothesis that CsrA might act as a global regulator for noise in toxin production and release. Changes in global factors such as plasmid copynumber or CsrA abundance play a key role in the regulation of noise in the plasmid encoded ColicinE2 system.

6.4. Discussion

Studying noise generation within the ColicinE2 system was performed by single-cell time-lapse microscopy using a reporter strain with the *cea* and *cel* genes replaced with genes coding for the fluorescent proteins YFP and CFP, respectively. The coefficient of variation (CV) was chosen as a measure for noise of both proteins for three different states: OFF state, ON state and population noise. Starting with the reporter strain closest to the wild-type plasmid S_{REP1}, all noise types were compared for both FPs. Data showed no significant difference between basal noise (OFF state) of *cea* and *cel*. For all other states, noise in *cel* was bigger than noise in *cea*. This could be caused by an increase of long mRNA numbers at high inductions and late time-points ($t = 270\text{min}$) [14]. A higher amount of long mRNA has to be repressed by the constant numbers of CsrA, leading to higher noise values in gene expression.

In a next step, the impact of the two regulatory models (transcriptional and post-transcriptional regulation) on noise generation within the ColicinE2 system was analyzed using various mutant strains. Changes in LexA repression affect transcription of the entire operon [14]. The three tested transcriptional mutants (Δ LexA, LexA1 and LexA2) showed no significant changes in population noise (Figure 6.8). Post-transcriptional genetic modifications affected the carbon storage regulation (Csr) system [78, 91] either by changing the binding affinity of CsrA to long mRNA, or by deleting CsrA sequestering sRNAs [71, 78]. For small post-transcriptional changes (CsrA1, CsrB) no significant changes in *cel* population noise were detected. How-

ever, for big post-transcriptional mutations on sRNA binding partners [7] (CsrBC) or binding affinity of CsrA to the long mRNA construct (CsrA2, Δ LexA/CsrA2), the population noise of *cel* is strongly reduced compared to S_{REP1} (Figure 6.8). This shows that CsrA binding and CsrA availability within the cell control *cel* population noise. An additional factor for noise reduction in the CsrA2 mutants might be the missing stem loop structure containing the CsrA binding site of the long mRNA which strongly reduced the binding strength of CsrA to the mRNA (see Chapter 4). Dacheux *et al.* 2017 [92] showed that the presence of a stem loop structure can increase translation noise. Thus the lack of the second stem loop structure in CsrA could be a factor reducing its *cel* population noise.

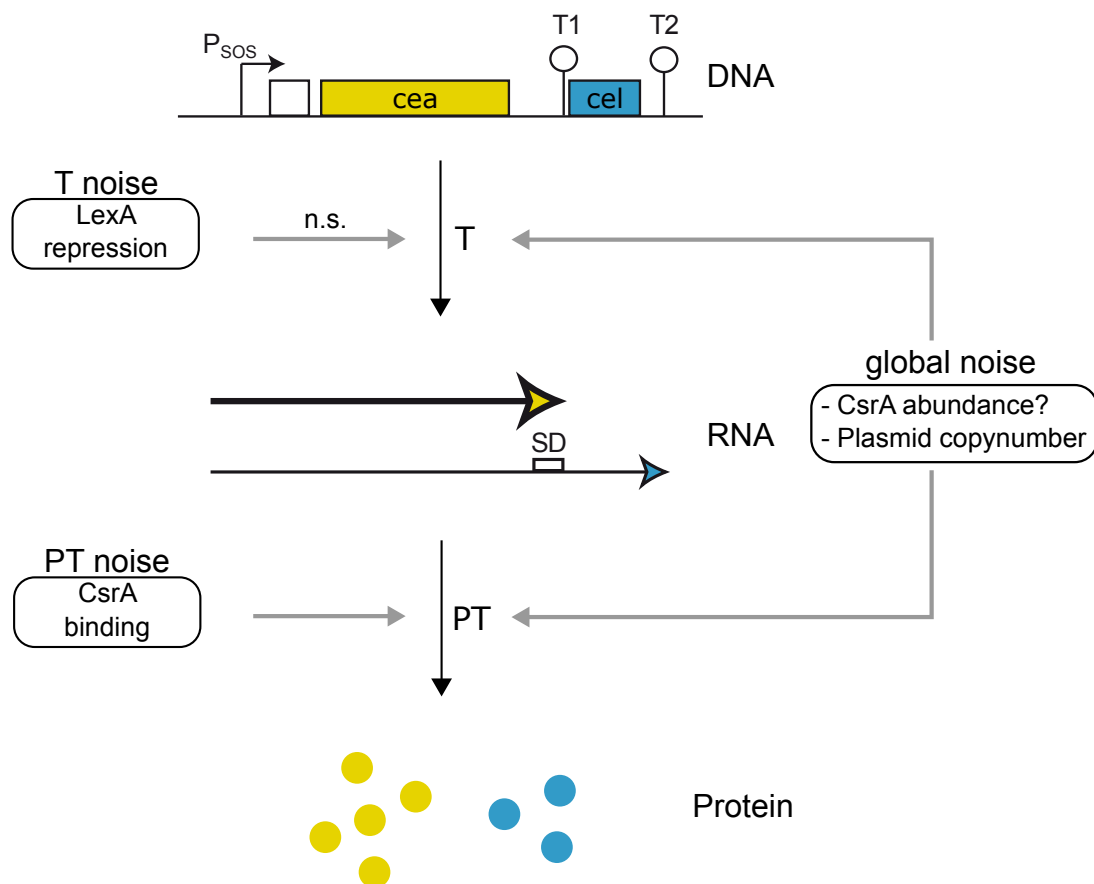


Figure 6.8

Factors contributing to noise control of the ColicinE2 system. T: transcriptional, PT= post-transcriptional. Black arrows show regulation mechanisms while gray arrows indicate elements that influence noise control of the system. Transcriptional changes in LexA repressions were shown to be not significant for noise in the system (n.s.). ?: denotes that CsrA could act either as a direct or a indirect global factor influencing noise control in our system. Figure adapted from [56].

Unexpectedly, for mutants with major post-transcriptional changes (CsrBC, CsrA2 and Δ LexA/CsrA2) *cea* population noise decreased as well. As global factors are known to influence noise on multiple steps of regulation [35], a hypothesis for the observed noise reduction in *cea* is that the global regulator protein CsrA affects noise of the entire ColicinE2-based operon. As described in Chapter 4, the concentration of free CsrA is directly affected by post-transcriptional mutations as they can change the abundance of CsrA [78] and CsrA is a protein controlling a multitude of regulatory processes within the cell [93]. For increased free CsrA abundance (CsrA2, CsrBC, Δ LexA/CsrA2) the noise of the entire operon (including *cea* and *cel* expression) is significantly reduced. This noise reduction is hypothesized to be caused by transcriptional changes on the global protein and transcription level. Different possible mechanisms might come into play to create this effect. CsrA is not only a post-transcriptional regulator of gene expression, but also a global negative regulator of transcription within bacterial cells [6]. Furthermore, mRNA stability can be increased by CsrA binding to the long mRNA of the ColicinE2-based operon, thus changing the *cea* expression noise. Additionally, indirect effects can take place when CsrA changes the abundance of other global proteins such as Hfq [23], a protein that initiates translation by binding to mRNA [94]. In addition, Hfq takes part in the regulation of bacterial reproduction [95]. Another biological mechanism involved might be an increased ribosomal density caused by strong *cel* translation rates in respective mutant strains. This could cause an increased stability of the long mRNA [96], which would again affect *cea* expression noise as well.

To further investigate the importance of global regulation factors [35, 64, 97] for noise control in the ColicinE2-based system a second S_{REP2} mutant with reduced plasmid copynumber, but otherwise identical plasmid structure as pMO3 was analyzed. Here, it was shown again, that changes on the global level can lead to a reduction of noise of the entire ColicinE2-like operon, as here both noise in *cea* and *cel* gene expression was significantly reduced (see Figure 6.8).

In summary, the data presented here showed that mainly changes in post-transcriptional regulation control noise generation of the ColicinE2-based system. This indicates that post-transcriptional regulation is an important part in noise control of the wild-type ColicinE2 system for population noise of toxin release as well as for the toxin amount being released. Several mutant strains for post-transcriptional changes and plasmid copynumber showed that noise is not minimized for the natural colicin operon. This indicates that there might be an optimal noise level that increases the variation of

toxin expression and release times increasing the competitive success of colicin producers. Comparable to this, in recent studies by Carey *et al.* 2018 [98], it was shown that up-regulation of noise enables bet-hedging strategies that help a bacterial population to succeed in diverse environments. Lastly, the ColicinE2-based system is controlled by global regulation factors such as LexA and CsrA which target a plethora of other genes and their expression. Thus, findings on population noise control gathered in this study could also be relevant for other protein expression systems under similar control.

7. Conclusion

In this thesis, the toxin producing ColicinE2 system of *Escherichia coli* was chosen as a bacterial model system to study the competitive behavior between a toxin producing and a toxin-sensitive strain. Control of toxin expression dynamics (TED) was studied and how these single-cell dynamics affect population dynamics and population fate in the context of bacterial competition. Expression and release of the toxin are encoded in an SOS induced operon, which in previous studies was shown to have external stress dependent response from stochastic to synchronous expression of the operon with increasing stress levels [13]. The ColicinE2 regulation constitutes a complex genetic network with regulation steps on various levels: Transcriptional regulation by LexA binding and repression of transcription of the operon without stress, additional post-transcriptional regulation of lysis gene translation via the global regulatory protein CsrA. This connects the ColicinE2 system to multiple other cellular processes that are also under control of these global proteins like e.g. the carbon metabolism of a cell, that changes the carbon storage regulation (Csr) system regulation [22]. Starting with single-cell time-lapse microscopy in combination with theoretical analysis, main components for regulation of expression and release dynamics were identified. Investigation of mutations in the transcriptional and post-transcriptional modules showed that a delay in release times compared to toxin expression start is mostly caused by the post-transcriptional repression of *cel* gene translation. Binding assays of CsrA to mRNA with sequences similar to the long mRNA of the ColicinE2 operon, showed strong binding of CsrA to the long mRNA transcript. Surprisingly, binding assays with similar ssDNA sequences also showed specific CsrA binding to ssDNA but with reduced binding strength than binding of CsrA to long mRNA. Here, it was also shown that during replication of the pColE2-P9 plasmid ssDNA is produced in high amounts, comparable to pColE3-CA38, where ssDNA accumulation within the cell was observed [65]. Binding of CsrA to this ssDNA therefore revealed a dual role of CsrA as an mRNA and ssDNA binding protein, but also showed the action of ssDNA as a new, yet unknown regulatory element, affecting CsrA abundance. Due to the strong binding affinity of CsrA to the long mRNA construct, *cel* gene translation

and cell lysis are also linked to the copynumber of the plasmid containing the colicin operon. Theoretical and experimental analysis identified the global regulatory protein CsrA as main player, specifically the abundance of free CsrA determines lysis gene translation and thus, the delay between toxin production and release present in the ColicinE2 system. Even though CsrA is a highly abundant protein within the bacterial cell [78], only a small number of free CsrA is present [74]. Therefore, even small changes in the extent of CsrA sequestering elements can have a big impact on the number of free CsrA molecules that are able to repress *cel* gene translation. Furthermore, the data presented in this thesis shows that the lysis time of colicin producing strains is coupled to the metabolic state of the cells due to changing CsrA abundances. Changing the level of observation from single-cell behavior to single-strain population dynamics showed that *cea* and *cel* switching is dependent on the post-transcriptional regulation. For early *cel* switching, a high amount of cells lyse which results in different effective growth rates of colicin producing strains. This constitutes an important parameter for competition. In addition, a positive linear correlation between lysis time and toxin amount being released were found, which means that for later cell lysis, a higher amount of toxin is released into the environment.

In a next step, it was investigated how the single-cell TED affect competition of the toxin producing strain with a toxin sensitive strain. The impact of delayed lysis time and thus higher toxin amounts on two-strain competition between a toxin-sensitive S strain and three different C_X strains was studied for two growth media (varying carbon source). Long-term competition experiments in combination with theoretical analysis were performed similar to von Bronk *et al.* [10, 11]. No significant change between competition outcomes of the three strains was observed. However, the theoretical analysis used in this study revealed that the two parameters lysis time and released toxin amount coupled in experiments were not equally important. In contrast, parameter sweeps revealed that the main factor for competition and lysis delay is the accumulation of a sufficient toxin amount. Even though simulation and experimental results showed good accordance without stress and at high stress, at intermediate induction levels larger discrepancies between theory and experiments were detected. Mainly in the model C wins fractions were underestimated. In earlier studies by Mader *et al.* 2015 it was shown that at medium stresses the ColicinE2 system expression is highly heterogeneous [13]. Therefore, when the model was adjusted for increased variability of the switching rate d_{Con} , increasing C wins fractions were found at intermediate induction levels. Even though the adjusted model does not entirely describe the ob-

served experimental results, this showed that heterogeneity in toxin expression and release dynamics on the single-cell level can have a big impact on competition outcome, increasing the success of colicin producers.

Based on the fact that variability can be an important feature increasing competitive success of the C strain, the noise of the ColicinE2 operon was investigated. The coefficient of variation of the FIs of a reporter strain S_{REP1} with regulation similar to the wild-type ColicinE2 operon and various mutants were compared to identify regulation mechanisms controlling noise generation within the system. Three types of noise were defined according to switching behavior as noise of the OFF state, ON state and population noise. For the strain closest to the wild-type colicin system OFF state noise of *cea* is bigger than for *cel*. For all other noise types, the noise of *cel* exceeds that of *cea*, showing that when cells switch into the toxin producing state, noise of toxin production is smaller than noise of toxin release. Analyzing the response of strains carrying different mutations in the transcriptional and post-transcriptional regulation modules showed that similar to the expression dynamics, CsrA is a main player regulating not only noise of *cel* gene expression but also acts as global factor reducing noise of the entire colicin operon including *cea* and *cel* noise. Comparing data of different mutant strains and plasmid copynumbers showed that the natural system does have a significant noise level, indicating the presence of an optimal noise level that helps to increase the success of the C strain in bacterial competition.

In conclusion, the main regulation factor of both TED and noise generation in the ColicinE2 system was found to be the global regulation protein CsrA. Availability of free CsrA controls cell lysis and with it the amount of toxin that is released by colicin producers. This abundance is coordinated by a multitude of CsrA sequestering elements and also connected to the metabolic state of a cell. Competition experiments for strains with different plasmid composition and for two media showed comparable competition results for a broad range of induction levels and lysis times. This could indicate that changes in TED with its complex regulation help to increase C strain success for varying conditions. Theoretical analysis showed that as long as enough toxin is produced C strain can succeed for both comparable growth of toxin producers and toxin-sensitive strains but also if the C strain has a disadvantage in competition due to a smaller growth rate. Expression and release of the colicin were shown to be highly noisy and the theoretical model showed that increased variability in release times at intermediate stresses can give the colicin producers an advantage in competition. As the ColicinE2 systems main regulators were determined to be global, chromosomally

7. Conclusion

encoded proteins like LexA and CsrA, the observed characteristics might be important regulation mechanisms for a multitude of genes like other colicins or many plasmid encoded systems. In summary, this thesis showed that many regulatory factors work together to tune single-cell TED that shape not only population fate of one strain, but can lead to long term competition success of the toxin producing population in varying environments.

8. Outlook

The main habitat of bacteria is within a biofilm produced by the bacteria themselves [99]. It protects bacteria from a plethora of different environmental stresses such as antibiotics [100, 101], shear stress [102, 103] and many others. In the case of biofilms expressions of matrix components like proteins or sugars on the single cell level shapes biofilm formation [104]. These components produced and secreted on the single-cell level of biofilm formation, making the population within it more resilient [105]. Within a biofilm the bacteria can cooperate to produce matrix components by division of labor. Dragoš *et al.* 2018 were able to show that when different mutants of *Bacillus subtilis* NCIB 3610 lacking genes for biofilm production were mixed, they were able to form a complete biofilm by collaboration through division of labor [44]. This is comparable to division of labor between producers and reproducers found for the ColicinE2 wild-type strain. This collaboration within a population can increase its success in long term competitions balancing the workload of the population by dividing the work between cells of the population. Thus, insight gained from the ColicinE2 system in this study could help to further understand the division of labor in other systems such as biofilm production [44] or secretion of enzymes [42].

In this study, competition between different *Escherichia coli* strains (sensitive and toxin producers) was studied as a result of the single-cell dynamics of the bacterial cells. A theoretical model was implemented, predicting competition outcome, which was also used to disentangle the roles of different parameters that are biologically connected and can not be addressed separately in experiments. The same could be used to describe competition between cells forming a biofilm. In the beginning they only secrete low amounts of matrix components, leading to similar 2D competition as implemented here, but only driven by differences in growth dynamics. Even the higher order interactions of three dimensional biofilm formation could be reduced to a 2D model system. This could be facilitated by adding the ability to grow on already occupied lattice space for biofilm formers, as they are able to grow in three dimensions due to biofilm formation. Additionally, protein release such as colicin production of the C strain in the model used here, could be adapted to include release of matrix com-

ponents that e.g. occupy space or increase the growth advantage of biofilm producers and not their competitors in simulations. For this, data obtained from single-cell production experiments as well as detailed colony identification of competition outcomes could be used.

With increasing problems of biofilm formation in unwanted places such as food industry [106] or hospitals (valves and implants) [105, 107], it is important to find new ways to destroy them in an efficient and reliable manner. For this, detailed knowledge of biofilm composition and the cause of its resistance against chemicals or antibiotics [100–102] and mechanical forces [103, 108] is needed. For example, Faclón-García *et al.* 2019 were able to show that topological changes caused by external treatments can make biofilms susceptible to penetration of chemicals and mechanical stress [109]. Characteristic properties such as surface wetting was changed by chemical treatments, leading to a decrease in biofilm resistance. Furthermore, erosion measurements performed by Klotz *et al.* 2019 [103] demonstrated that erosion resistance of a *Bacillus subtilis* NCIB 3610 strain is dependent on the presence of all matrix components. This underlines the importance of detailed insight into formation dynamics and spatial structure of biofilms to be able to efficiently destroy it. An additional way to increase the elimination of growing biofilms could be to infiltrate it with bacteria containing toxin expression systems such as ColicinE2 where the toxin could be adapted to kill biofilm formers specifically from within a formed biofilm.

All in all, information gained for two-strain competition could be used to get a better understanding of how protein expression dynamics can affect population fate in complex microbial systems. These could be other bacterial systems such as multi-strain bacterial communities found in nature e.g. on teeth [110, 111], in the gut [40] or in the ocean [112]. Taking into account the possibility of higher order interactions for increasingly complex systems, comparable models could be used [11]. Moreover, the general interaction dynamics of such fast growing systems can often be applied to higher order slower developing communities like forests or higher order population dynamics in nature [113]. The action of global influence factors for stability of a given system as well as noise as an active mechanism increasing competitive success of toxin producers could be applied for a multitude of biological processes.

A. Media and Buffers

A.1. M63 Medium

M63 Basic

For 500 ml Medium:

- 500 ml ddH₂O
- 6.8 g KH₂PO₄
- 1 g (NH₄)₂SO₄
- 9 µl FeSO₄ × 7H₂O (1M)

Adjust pH = 7.00 using KOH and autoclave

M63 Complete

For 500 ml Medium; add to autoclaved basic medium:

- 0.2 % Casein (10 ml of pre-autoclaved 10 % stock)
- 1 µg/ml Thiamin (500 µl of sterile filtered stock)
- 500 µl MgSO₄ (1 M)
- 0.5 % glycerol or 0.25 % glucose

M63 Competition

For competition experiments, medium was supplemented with 0.2 % arabinose for induction of fluorescence of the S_{RFP} strain. Additionally, 100 µg/ml ampicillin were added for selection.

A.2. Buffers

A.2.1. TAE Gel Electrophoresis

Gel and Running Buffer

50x TAE Buffer

For 1 l buffer:

- 242 g Tris base (40 mM)
- 842.9 ml ddH₂O
- 100 ml EDTA (0.5 M pH = 8.0)
- 57.1 ml Acetic Acid

Dilute 50 x with water in ratio 1 : 50 to prepare 1 x buffer.

Concentrations 1 x TAE buffer:

- 2 M Tris
- 2 M Acetic Acid
- 50 mM EDTA

TAE-Agarose gel

Mix TAE buffer with 1% Agarose (Biozym Scientific, Germany) and heat until the powder is completely dissolved without grains. Then cast gel with appropriate number of lanes.

A.2.2. Gel Shift Binding Assay

RNA/ssDNA Folding

Folding buffer:

- 10 mM Tris-HCl
- 1 mM EDTA
- 200 mM KCl
- 20 mM MgCl₂

Folding was performed for 3.5 min at 85 °C for ssDNA and 90 °C for ssDNA.

Binding and Gel Shift

A two-fold dilution series of CsrA was prepared according starting with 6.6 μM and 33 μM starting concentrations for RNA and ssDNA, respectively.

For each lane 10 μl CsrA dilution was combined to create final concentrations in binding reactions as follows:

- 5 nM DNA/RNA
- 15 μl Tris-HCl
- 0.5 mM EDTA
- 250 mM NaCl
- 50 mM KCl
- 5 mM MgCl₂
- 3.25 ng/μl yeast RNA
- 4 U RNase inhibitor (Ambion)
- 10 % glycerol (loading buffer)

Final CsrA concentrations for binding are shown in Table A.1.

Binding-partner	Lane #	1	2	3	4	5	6	7	8	9	10	11	12	13	14	15
DNA	CsrA [nM]	0	3300	1650	825	412	206	103	51	25	12	6,4	3,2	1,6	0,8	0,4
RNA	CsrA [nM]	0	16670	8335	4167.5	2083	1041	520	260	130	65	32	16	8	4	2

Table A.1

CsrA concentrations used for gel shift analysis measurements.

A. Media and Buffers

Mixtures were incubated at 37°C for 30 min, then gel shift measurements were performed using a 4-20% Mini-PROTEAN precast gel (bio-rad) in Tris/Glycine buffer (bio-rad) running it at room temperature for 1 h with 85 V. For imaging a Chemi-Doc™ MP Imaging System (bio-rad) was used.

B. Simulation Parameters

Carbon source	C_X strain	rS	rC_X	dC_{on}	n_{tox}
GLY	C_{REP1}	0.0682	0.0676	0.0145	1500
GLY	C_{REP2}	0.0682	0.0703	0.0118	6000
GLY	C_{AMP}	0.0682	0.0732	0.0083	19500
GLU	C_{REP1}	0.1019	0.0814	0.0111	6000
GLU	C_{REP2}	0.1019	0.0832	0.0111	13500
GLU	C_{AMP}	0.1019	0.0879	0.0067	24000

Table B.1

Competition simulation parameters for all mutants and growth media extracted from single cell and population data discussed in Chapter 4.

	1	2	3	4	5	6	7	8	9	10	
Frac ON	0.010	0.020	0.030	0.040	0.050	0.106	0.163	0.219	0.275	0.331	
	11	12	13	14	15	16	17	18	19	20	21
	0.388	0.444	0.500	0.556	0.613	0.669	0.725	0.781	0.838	0.894	0.950

Table B.2

Toxin producer fractions for pie charts from 1% to 95%. In Figure 5.2 and Figure 5.9 the complete range was used for simulations. For parameter sweeps only values of 5% and larger were used. Switching rates were then calculated as shown in Equation (3.7).

C. Details for Significance Analysis

C.1. Significance Analysis for Chapter 4

Comparison switching times of different C_X strains and growth conditions

	Sample A	Sample B	Sample Size A	Sample Size B	U-Value	p-Value	
T_{ONcea}	$C_{REP1-GLY-T_{ONcea}}$	$C_{REP2-GLY-T_{ONcea}}$	85	66	3152	0.1937	n.s.
	$C_{REP1-GLY-T_{ONcea}}$	$C_{REP1-GLU-T_{ONcea}}$	85	98	2218	5.14E-08	***
	$C_{REP1-GLU-T_{ONcea}}$	$C_{REP2-GLU-T_{ONcea}}$	98	95	6567	8.35E-07	***
	$C_{REP2-GLY-T_{ONcea}}$	$C_{REP2-GLU-T_{ONcea}}$	66	95	2767	0.2065	n.s.
T_{ONcel}	$C_{REP1-GLY-T_{ONcel}}$	$C_{REP2-GLY-T_{ONcel}}$	78	58	1167	1.47E-06	***
	$C_{REP1-GLY-T_{ONcel}}$	$C_{REP1-GLU-T_{ONcel}}$	78	89	1899	4.63E-07	***
	$C_{REP1-GLU-T_{ONcel}}$	$C_{REP2-GLU-T_{ONcel}}$	89	86	3180	0.05366	n.s.
	$C_{REP2-GLY-T_{ONcel}}$	$C_{REP2-GLU-T_{ONcel}}$	58	86	1997	0.04314	*
T_{lysis}	$C_{REP1-GLY-T_{lysis}}$	$C_{REP2-GLY-T_{lysis}}$	89	66	1511.5	1.27E-07	***
	$C_{REP1-GLY-T_{lysis}}$	$C_{AMP-GLY-T_{lysis}}$	89	61	12.5	<2.2E-16	***
	$C_{REP1-GLY-T_{lysis}}$	$C_{REP1-GLU-T_{lysis}}$	89	94	1490	1.85E-14	***
	$C_{REP2-GLY-T_{lysis}}$	$C_{AMP-GLY-T_{lysis}}$	66	61	149.5	<2.2E-16	***
	$C_{REP2-GLY-T_{lysis}}$	$C_{REP2-GLU-T_{lysis}}$	66	93	2431.5	0.02253	*
	$C_{AMP-GLY-T_{lysis}}$	$C_{AMP-GLU-T_{lysis}}$	61	69	1109	3.04E-06	***
	$C_{REP1-GLU-T_{lysis}}$	$C_{REP2-GLU-T_{lysis}}$	94	93	4373	0.9967	n.s.
	$C_{REP1-GLU-T_{lysis}}$	$C_{AMP-GLU-T_{lysis}}$	94	69	298	<2.2E-16	***
	$C_{REP2-GLU-T_{lysis}}$	$C_{AMP-GLU-T_{lysis}}$	93	69	297.5	<2.2E-16	***
$C_{REP1-GLY}$	$C_{REP1-GLY-T_{ONcea}}$	$C_{REP1-GLY-T_{ONcel}}$	85	78	1972	8.20E-06	***
	$C_{REP1-GLY-T_{ONcea}}$	$C_{REP1-GLY-T_{lysis}}$	85	89	1093	4.16E-16	***
	$C_{REP1-GLY-T_{ONcel}}$	$C_{REP1-GLY-T_{lysis}}$	78	89	1942	8.27E-07	***
$C_{REP2-GLY}$	$C_{REP2-GLY-T_{ONcea}}$	$C_{REP1-GLY-T_{ONcel}}$	66	58	449	2.23E-13	***
	$C_{REP2-GLY-T_{ONcea}}$	$C_{REP2-GLY-T_{lysis}}$	66	66	289	<2.2E-16	***
	$C_{REP2-GLY-T_{ONcel}}$	$C_{REP2-GLY-T_{lysis}}$	58	66	910	4.46E-07	***
$C_{REP1-GLU}$	$C_{REP1-GLU-T_{ONcea}}$	$C_{REP2-GLU-T_{ONcel}}$	98	89	2705	7.52E-06	***
	$C_{REP1-GLU-T_{ONcea}}$	$C_{REP1-GLU-T_{lysis}}$	98	94	777	<2.2E-16	***
	$C_{REP1-GLU-T_{ONcel}}$	$C_{REP1-GLU-T_{lysis}}$	89	94	1460	2.48E-14	***
$C_{REP2-GLY}$	$C_{REP2-GLU-T_{ONcea}}$	$C_{REP1-GLU-T_{ONcel}}$	95	86	1096	<2.2E-16	***
	$C_{REP2-GLU-T_{ONcea}}$	$C_{REP2-GLU-T_{lysis}}$	95	93	414	<2.2E-16	***
	$C_{REP2-GLU-T_{ONcel}}$	$C_{REP2-GLU-T_{lysis}}$	86	93	2166	1.12E-07	***

Table C.1

Significance analysis for time-lapse analysis of switching times in C strains. ***: $p < 0.001$, **: $p < 0.01$, *: $p < 0.05$, n.s.: not significant. A Mann-Whitney-Wilcoxon test was performed to test for significant differences between the distributions.

Analysis of differences in growth rate of C_x strains for different growth conditions

	Sample A	Sample B	Sample Size A	Sample Size B	U-Value	p-Value
t.test	GR S _{RFP} -GLY	GR C _{REP1} -GLY	13	13	x	0.741
	GR S _{RFP} -GLY	GR C _{REP2} -GLY	13	13	x	0.202
	GR S _{RFP} -GLY	GR C _{AMP} -GLY	13	14	x	0.007
wilcox.test	GR S _{RFP} -GLU	GR C _{REP1} -GLU	14	12	168	2.07E-07
	GR S _{RFP} -GLU	GR C _{REP2} -GLU	14	12	162	6.21E-06
	GR S _{RFP} -GLU	GR C _{AMP} -GLU	14	12	156	5.63E-05

Table C.2

Significance analysis for fluorescence time-lapse analysis of area growth rates without stress shown in Figure 4.8.

C.2. Significance Analysis for Chapter 6

Significance analysis for different CV of S_{REP1}

Sample A	Sample B	Sample Size A	Sample Size B	t-Value	p-value	
CV(OFF,YFP)	CV(OFF,CFP)	8	8	2.1114	0.0550	n.s.
CV(ON,YFP)	CV(ON,CFP)	8	8	-4.5303	0.0005	***
CV(Pop,YFP)	CV(Pop,CFP)	8	8	-5.8515	0.0001	***
CV(Pop,YFP)	CV(ON,YFP)	8	8	0.2717	0.7898	n.s.
CV(Pop,YFP)	CV(OFF,YFP)	8	8	2.0580	0.0609	n.s.
CV(ON,YFP)	CV(OFF,YFP)	8	8	1.9008	0.0817	n.s.
CV(Pop,CFP)	CV(ON,CFP)	8	8	2.4801	0.0281	*
CV(Pop,CFP)	CV(OFF,CFP)	8	8	9.8329	3.6640E-07	***
CV(ON,CFP)	CV(OFF,CFP)	8	8	9.0074	3.4450E-07	***

Table C.3

Significance analysis noise of states in the S_{REP1} strain shown in Figure 6.3. A t-test was performed for all comparisons.

Significance analysis for different CV of S_{FLIP}

Sample A	Sample B	Sample Size A	Sample Size B	t-Value	p-value	
CV(OFF,cea)	CV(OFF,cel)	3	3	1.5645	0.2115	n.s.
CV(ON,cea)	CV(ON,cel)	3	3	3.6958	0.0587	n.s.
CV(Pop,cea)	CV(Pop,cel)	3	3	11.6500	0.0023	**
CV(Pop,cea)	CV(ON,cea)	3	3	2.0890	0.1315	n.s.
CV(Pop,cea)	CV(OFF,cea)	3	3	0.1224	0.9129	n.s.
CV(ON,cea)	CV(OFF,cea)	3	3	-0.8499	0.4619	n.s.
CV(Pop,cel)	CV(ON,cel)	3	3	N.A	N.A.	
CV(Pop,cel)	CV(OFF,cel)	3	3	-1.5185	0.2621	n.s.
CV(ON,cel)	CV(OFF,cel)	3	3	-1.5185	0.2621	n.s.

Table C.4

Significance analysis noise of states in the S_{FLIP} strain shown in Figure 6.4. A t-test was performed for all comparisons.

Population noise comparison of S_{REP1} with mutant strains

	Sample A	Sample B	Sample Size A	Sample Size B	t/U-Value	p-value	
t.test	S _{REP1} , YFP	Δ LexA, YFP	8	9	1.4444	0.1697	n.s.
t.test	S _{REP1} , YFP	LexA1, YFP	8	11	-1.3194	0.2052	n.s.
t.test	S _{REP1} , YFP	LexA2, YFP	8	10	0.3571	0.7258	n.s.
t.test	S _{REP1} , YFP	CsrA1, YFP	8	9	0.0129	0.9899	n.s.
t.test	S _{REP1} , YFP	CsrB, YFP	8	6	-0.1405	0.8911	n.s.
t.test	S _{REP1} , YFP	CsrBC, YFP	8	7	2.2459	0.0432	*
wilcox.test	S _{REP1} , YFP	CsrA2, YFP	8	7	53	0.0022	**
t.test	S _{REP1} , YFP	Δ LexA/CsrA2, YFP	8	7	6.0041	0.0003	***
t.test	S _{REP1} , CFP	Δ LexA, CFP	8	9	1.1571	0.2686	n.s.
t.test	S _{REP1} , CFP	LexA1, CFP	8	11	-0.3456	0.7340	n.s.
t.test	S _{REP1} , CFP	LexA2, CFP	8	10	0.1863	0.8547	n.s.
t.test	S _{REP1} , CFP	CsrA1, CFP	8	9	0.4838	0.6357	n.s.
t.test	S _{REP1} , CFP	CsrB, CFP	8	6	-0.9121	0.3872	n.s.
t.test	S _{REP1} , CFP	CsrBC, CFP	8	7	2.8652	0.0133	*
t.test	S _{REP1} , CFP	CsrA2, CFP	8	7	10.9130	5.4880E-07	***
t.test	S _{REP1} , CFP	Δ LexA/CsrA2, CFP	8	7	12.4050	2.8440E-06	***

Table C.5

Significance analysis for population noise all mutants comparison to the S_{REP1} strain shown in Figure 6.5. Used test types are listed in the first column. t-values listed for t-tests, U-values listed for wilcoxon-tests.

Significance analysis for different CVs of S_{REP2} and S_{REP1}

	Sample A	Sample B	Sample Size A	Sample Size B	t/U-Value	p-value	
t.test	S_{REP1} CV(OFF,YFP)	S_{REP2} CV(OFF,YFP)	8	3	0.2570	0.8030	n.s.
wilcox.test	S_{REP1} CV(ON,YFP)	S_{REP2} CV(ON,YFP)	8	2	22	0.0485	*
t.test	S_{REP1} CV(Pop,YFP)	S_{REP2} CV(Pop,YFP)	8	3	2.8900	0.0229	*
t.test	S_{REP1} CV(OFF,CFP)	S_{REP2} CV(OFF,CFP)	8	3	-1.1493	0.3647	n.s.
wilcox.test	S_{REP1} CV(ON,CFP)	S_{REP2} CV(ON,CFP)	8	2	16	0.0444	*
t.test	S_{REP1} CV(Pop,CFP)	S_{REP2} CV(Pop,CFP)	8	3	10.0960	7.7030E-06	***

Table C.6

Significance analysis for each state and CV of S_{REP2} compared to the S_{REP1} strain shown in Figure 6.7. Used test types are listed in the first column. t-values listed for t-tests, U-values listed for wilcoxon-tests.

Acronyms

Notation	Description
BF	Bright Field
CFP	Cyan Fluorescent Protein (mCerulean)
Csr	Carbon storage regulation
CV	Coefficient of Variation
FI	Fluorescence Intensity
FP	Fluorescent Protein
GED	Gene Expression Dynamics
GFP	Green Fluorescent Protein
GR	Growth Rate
IQR	InterQuartile Range
MitC	Mitomycin C
ODE	Ordinary Differential Equation
ORI	ORIGIN of replicaion
RFP	Red Fluorescent Protein (mCherry)
rpm	rounds per minute
ssDNA	single-stranded DNA
TED	Toxin Expression Dynamics

Acronyms

Notation	Description
WT	Wild-Type
YFP	Yellow Fluorescent Protein (mVenus)

List of Figures

1.1.	How single-cell gene expression affects multi-strain dynamics	3
2.1.	Gene regulation of the ColicinE2 system	7
2.2.	CsrA binding modulates <i>cel</i> gene translation and time-point of cell lysis	9
2.3.	Illustrations of deterministic and stochastic gene expression	11
2.4.	Noise types and influences	12
2.5.	Quantification of noise	14
2.6.	Bacterial interaction mechanisms	16
2.7.	Colicin driven two-strain interaction	19
3.1.	Reporter plasmids configuration	22
3.2.	Time-lapse Microscopy Setup	27
3.3.	Comparison of S and C strain data curves	28
3.4.	Analyzed parameters in single cell measurements	30
3.5.	Agarose gel for ssDNA detection	32
3.6.	Protein binding assay to RNA and ssDNA	33
3.7.	Bacteria spotting and competition	35
3.8.	Area detection for population experiments.	38
3.9.	Two-Strain Interaction Parameters	40
3.10.	Lattice configuration and transitions for simulation.	41
4.1.	Expression of the FP from the reporter genes in several mutant strains	46
4.2.	Times of switching into the ON state of both reporter genes in several mutant strains	48
4.3.	Biochemical network involved in the post-transcriptional regulation of ColicinE2	50
4.4.	Delay times and measured binding strengths for variations in CsrA binding efficiency	53
4.5.	Theoretical modelling shows importance of ssDNA as binding partner for CsrA	56

4.6. Toxin expression dynamics are dependent on post-transcriptional regulation via CsrA	58
4.7. Fraction of cells switching into the ON state for YFP and CFP in various S_X and C_X strains.	60
4.8. Cell lysis and growth rate of C_X strains and S_{RFP} depend on medium composition and induction level	62
4.9. Connection between toxin amount being produced and toxin release time	64
4.10. Number of free CsrA determines the time-point of cell lysis and the amount of toxin being released from the ColicinE2 operon	68
5.1. Experimental and simulation results of two-strain competition of C_X and S_{RFP} strain on different carbon sources	72
5.2. Numerical simulations of two-strain competition corresponding to experimental conditions	74
5.3. Phase diagrams of C and S fractions in competition simulations for various toxin effectivities on glycerol.	77
5.4. Phase diagrams of C and S fractions in competition simulations for various toxin release times on glycerol.	78
5.5. Phase diagrams of C and S fractions in competition simulations for various toxin effectivities on glucose	79
5.6. Phase diagrams of C and S fractions in competition simulations for various toxin release times on glucose.	81
5.7. Variation of d_{Con} rate distributions and biological restrictions	83
5.8. Theoretical analysis of parameter sweep over variability factor W_{frac}	85
5.9. Numerical simulations of two-strain competition with high variation in d_{Con} rate	86
5.10. Comparison of experimental results of competition with original and adjusted simulations	87
6.1. Coefficient of variation (CV) over time for three states of the S_{REP1} strain	93
6.2. Fluorescence intensity histograms for three S_{REP1} strain states at chosen times-points	95
6.3. Mean CV of the S_{REP1} strain for OFF state, ON state and population noise	97
6.4. Mean CV and population noise histogram of the S_{FLIP} strain with flipped order of the fluorescence proteins	98

6.5. Population noise measured in S_{REP1} strain and several strains carrying transcriptional and post-transcriptional genetic modifications	100
6.6. Histogram of FIs for mutant strains with significant changes in population noise	103
6.7. Mean CV and population noise histograms of the S_{REP2} strain with reduced plasmid copynumber	105
6.8. Factors contributing to noise control of the ColicinE2 system	107

List of Tables

3.1. Overview of the strains used in this study	23
3.2. Classification of Competition Outcomes	39
3.3. Fixed parameters for competition model	43
4.1. Extinct area and resulting colicin factor depend on C_X strain and the carbon source	65
6.1. Overview over measured noise data with information on cell numbers and induction levels	99
A.1. CsrA concentrations used for gel shift analysis measurements	119
B.1. Competition simulation parameters for all mutants and growth media .	121
B.2. Toxin producer fractions for pie charts	121
C.1. Significance analysis for time-lapse analysis of switching times in C strains.	123
C.2. Significance analysis for time-lapse analysis of area growth rates without stress	124
C.3. Significance analysis for noise of states in the S_{REP1} strain	125
C.4. Significance analysis for noise of states in the S_{FLIP} strain	125
C.5. Significance analysis for population noise all mutants compared to the S_{REP1} strain	126
C.6. Significance analysis for each state and CV of S_{REP2} compared to the S_{REP1} strain	127

Bibliography

1. Butala, M., Hodošček, M., Anderluh, G., Podlesek, Z. & Žgur-Bertok, D. Intradomain LexA rotation is a prerequisite for DNA binding specificity. *FEBS Letters* **581**, 4816–4820 (2007).
2. Gillor, O., Vriezen, J. A. C. & Riley, M. A. The role of SOS boxes in enteric bacteriocin regulation. *Microbiology* **154**, 1783–1792 (2008).
3. Fornelos, N., Browning, D. F. & Butala, M. The Use and Abuse of LexA by Mobile Genetic Elements. *Trends in Microbiology* **24**, 391–401 (2016).
4. Dubey, A. K., Baker, C. S., Romeo, T. & Babitzke, P. RNA sequence and secondary structure participate in high-affinity CsrA-RNA interaction. *Rna*, 1579–1587 (2005).
5. Yang, T. Y., Sung, Y. M., Lei, G. S., Romeo, T. & Chak, K. F. Posttranscriptional repression of the *cel* gene of the *ColE7* operon by the RNA-binding protein CsrA of *Escherichia coli*. *Nucleic Acids Research* **38**, 3936–3951 (2010).
6. Esquerré, T. *et al.* The Csr system regulates genome-wide mRNA stability and transcription and thus gene expression in *Escherichia coli*. *Scientific reports* **6**, 25057 (2016).
7. Romeo, T. & Babitzke, P. Global Regulation by CsrA and Its RNA Antagonists. *Microbiology Spectrum* **6**, 1–14 (2018).
8. Timmermans, J. & Van Melderren, L. Conditional Essentiality of the *csrA* Gene in *Escherichia coli*. *J. Bacteriol.* **191**, 1722–1724 (2009).
9. Vakulskas, C. A. *et al.* Antagonistic control of the turnover pathway for the global regulatory sRNA CsrB by the CsrA and CsrD proteins. *Nucleic Acids Research* **44**, 7896–7910 (2016).
10. Von Bronk, B., Schaffer, S. A., Götz, A. & Opitz, M. Effects of stochasticity and division of labor in toxin production on two-strain bacterial competition in *Escherichia coli*. *PLoS Biology* **15**, 1–25 (2017).

11. Von Bronk, B., Götz, A. & Opitz, M. Locality of interactions in three-strain bacterial competition. *Physical Biology* **16** (2019).
12. Riley, M. a. & Wertz, J. E. Bacteriocins: Evolution, Ecology, and Application. *Annual Review of Microbiology* **56**, 117–137 (2002).
13. Mader, A. *et al.* Amount of Colicin Release in Escherichia coli Is Regulated by Lysis Gene Expression of the Colicin E2 Operon. *Plos One* **10**, e0119124 (2015).
14. Cascales, E. *et al.* Colicin Biology. *Microbiology and Molecular Biology Reviews* **71**, 158–229 (2007).
15. Riley, M. & Gordon, D. The ecology and evolution of bacteriocins. *Journal of Industrial Microbiology* (1996).
16. Little, J. W. & Mount, D. W. The SOS regulatory system of Escherichia coli. *Cell* **29**, 11–22 (1982).
17. Butala, M., Žgur-Bertok, D. & Busby, S. J. W. The bacterial LexA transcriptional repressor. *Cellular and Molecular Life Sciences* **66**, 82–93 (2009).
18. Kamenšek, S., Podlesek, Z., Gillor, O. & Žgur-Bertok, D. Genes regulated by the Escherichia coli SOS repressor LexA exhibit heterogenous expression. *BMC Microbiology* **10**, 283 (2010).
19. Seyll, E. & Van Melderen, L. The ribonucleoprotein Csr network. *International Journal of Molecular Sciences* **14**, 22117–22131 (2013).
20. Babitzke, P. & Romeo, T. CsrB sRNA family: sequestration of RNA-binding regulatory proteins. *Current Opinion in Microbiology* **10**, 156–163 (2007).
21. Vakulskas, C. a., Potts, A. H., Babitzke, P., Ahmer, B. M. M. & Romeo, T. Regulation of Bacterial Virulence by Csr (Rsm) Systems. *Microbiology and Molecular Biology Reviews* **79**, 193–224 (2015).
22. Timmermans, J. & Van Melderen, L. Post-transcriptional global regulation by CsrA in bacteria. *Cellular and Molecular Life Sciences* **67**, 2897–2908 (2010).
23. Baker, C. S. *et al.* CsrA inhibits translation initiation of Escherichia coli hfq by binding to a single site overlapping the Shine-Dalgarno sequence. *Journal of Bacteriology* **189**, 5472–5481 (2007).
24. Hardy, K. G. & Meynell, G. G. "Induction" of colicin factor E2-P9 by mitomycin C. *Journal of Bacteriology* **112**, 1007–1009 (1972).

-
25. Weng, M.-w. *et al.* Repair of mitomycin C mono- and interstrand cross-linked DNA adducts by UvrABC: a new model. *Nucleic Acids Research* **38**, 6976–6984 (Nov. 2010).
 26. Pavliotis, G. A. *Stochastic processes and applications diffusion processes, the Fokker-Planck and Langevin equations* (Springer, 2014).
 27. Elowitz, M. B., Levine, A. J., Siggia, E. D. & Swain, P. S. Stochastic gene expression in a single cell. *Science* **297**, 1183–1187 (2002).
 28. Singh, A. & Soltani, M. Quantifying intrinsic and extrinsic variability in stochastic gene expression models. *PLoS ONE* **8** (2013).
 29. Raj, A. & van Oudenaarden, A. Nature, Nurture, or Chance: Stochastic Gene Expression and Its Consequences. *Cell* **135**, 216–226 (2008).
 30. Swain, P. S. Efficient attenuation of stochasticity in gene expression through post-transcriptional control. *Journal of Molecular Biology* **344**, 965–976 (2004).
 31. Fu, A. Q. & Pachter, L. Estimating intrinsic and extrinsic noise from single-cell gene expression measurements. *Statistical Applications in Genetics and Molecular Biology* **15**, 447–471 (2016).
 32. Singh, A. Transient Changes in Intercellular Protein Variability Identify Sources of Noise in Gene Expression. *Biophysical Journal* **107**, 2214–2220 (2014).
 33. Ozbudak, E., Thattai, M., Kurtser, I., Grossman, A. & van Oudenaarden, A. Regulation of noise in the expression of a single gene. *Nat Genet* (2002).
 34. Anufrieva, O., Sala, A., Yli-harja, O. & Kandhavelu, M. Real-time observation of bacterial gene expression noise. *Nano Communication Networks* **8**, 68–75 (2016).
 35. Bar-Even, A. *et al.* Noise in protein expression scales with natural protein abundance. *Nature Genetics* **38**, 636–643 (2006).
 36. Mundt, M., Anders, A., Murray, S. M. & Sourjik, V. A System for Gene Expression Noise Control in Yeast. *ACS Synthetic Biology* **7**, 2618–2626 (2018).
 37. Pedazra, J. M. & Oudenaarden, A. V. Noise Propagation in Gene Networks. *Science* **307**, 1965–1969 (2005).
 38. Friedman, J. & Gore, J. Ecological systems biology: The dynamics of interacting populations. *Current Opinion in Systems Biology* **1**, 114–121 (2017).

39. Von Bronk, B., Götz, A. & Opitz, M. Complex microbial systems across different levels of description. *Physical Biology* (2018).
40. Rakoff-Nahoum, S., Foster, K. R. & Comstock, L. E. The evolution of cooperation within the gut microbiota. *Nature* **533**, 255–259 (2016).
41. Oliveira, N. M., Niehus, R. & Foster, K. R. Evolutionary limits to cooperation in microbial communities. *Proceedings of the National Academy of Sciences of the United States of America* **111**, 17941–17946 (2014).
42. Folse, H. J. & Allison, S. D. Cooperation, competition, and coalitions in enzyme-producing microbes: Social evolution and nutrient depolymerization rates. *Frontiers in Microbiology* **3**, 1–10 (2012).
43. Waters, C. M. & Bassler, B. L. QUORUM SENSING: Cell-to-Cell Communication in Bacteria. *Annual Review of Cell and Developmental Biology* **21**, 319–346 (2005).
44. Dragoš, A. *et al.* Division of Labor during Biofilm Matrix Production. *Current Biology* **28**, 1903–1913.e5 (2018).
45. Hibbing, M. E., Fuqua, C., Parsek, M. R. & Peterson, S. B. Bacterial competition: Surviving and thriving in the microbial jungle. *Nature Reviews Microbiology* **8**, 15–25 (2010).
46. Weber, M. F., Poxleitner, G., Hebisch, E., Frey, E. & Opitz, M. Chemical warfare and survival strategies in bacterial range expansions. *Journal of The Royal Society Interface* **11**, 20140172–20140172 (2014).
47. Fredrickson, A. G. & Stephanopoulos, G. Microbial competition. *Science* **213**, 972–979 (1981).
48. Lemon, D. J., Schutzman, D. A. & Garza, A. G. Bacterial surface spreading is more efficient on nematically aligned polysaccharide substrates. *Journal of Bacteriology* **200**, 1–17 (2018).
49. Ghoul, M. & Mitri, S. The Ecology and Evolution of Microbial Competition. *Trends in Microbiology* **24**, 833–845 (2016).
50. Kerr, B., Riley, M. A., Feldman, M. W. & Bohannan, B. J. Local dispersal promotes biodiversity in a real-life game of rock-paper-scissors. *Nature* **418**, 171–174 (2002).

-
51. Weiß, A. S., Götz, A. & Opitz, M. Dynamics of ColicinE2 production and release determine the competitive success of a toxin-producing bacterial populatio. *Scientific Reports*. (accepted).
 52. Kremers, G.-j., Goedhart, J., Munster, E. B. V. & Gadella, T. W. J. Cyan and Yellow Super Fluorescent Proteins with Improved Brightness , Protein Folding , and FRET Förster Radius. *Biochemistry*, 6570–6580 (2006).
 53. Kremers, G. J., Goedhart, J., Van Den Heuvel, D. J., Gerritsen, H. C. & Gadella, T. W. J. Improved green and blue fluorescent proteins for expression in bacteria and mammalian cells. *Biochemistry* **46**, 3775–3783 (2007).
 54. Markwardt, M. L. *et al.* An improved cerulean fluorescent protein with enhanced brightness and reduced reversible photoswitching. *PLoS ONE* **6** (2011).
 55. Götz, A. *et al.* CsrA and its regulators control the time-point of ColicinE2 release in Escherichia coli. *Scientific Reports* **8**, 6537 (2018).
 56. Goetz, A., Mader, A., von Bronk, B., Weiss, A. S. & Opitz, M. Gene expression noise in a complex artificial toxin expression system. *PLOS ONE* **15**, e0227249 (2020).
 57. Lewis, L. K., Harlow, G. R., Gregg-Jolly, L. A. & Mount, D. W. *Identification of high affinity binding sites for LexA which define new DNA damage-inducible genes in Escherichia coli*. 1994.
 58. De Henestrosa, A. R. F. *et al.* Identification of additional genes belonging to the LexA regulon in Escherichia coli. *Molecular microbiology* **35**, 1560–1572 (2000).
 59. Gutiérrez, P. *et al.* Solution Structure of the Carbon Storage Regulator Protein CsrA from Escherichia coli. *Journal of Bacteriology* **187**, 3496–3501 (2005).
 60. Hiszczyńska-Sawicka, E. & Kur, J. Effect of Escherichia coli IHF mutations on plasmid p15A copy number. *Plasmid* **38**, 174–179 (1997).
 61. Edelstein, A., Amodaj, N., Hoover, K., Vale, R. & Stuurman, N. Computer Control of Microscopes Using MicroManager. *Current Protocols in Molecular Biology* (2010).
 62. Youssef, S., Gude, S. & Radler, J. O. Automated tracking in live-cell time-lapse movies. *Integr. Biol.* **3**, 1095–1101 (2011).
 63. Schneider, C. A., Rasband, W. S. & W. Eliceiri, K. NIH Image to ImageJ: 25 years of image analysis. *Nature methods* **9.7** (2012).

64. Pedraza, J. M. & van Oudenaarden, A. Noise propagation in gene networks. *Science* **307**, 1–12 (2005).
65. Morales, M., Attai, H., Troy, K. & Bermudes, D. Accumulation of single-stranded dna in Escherichia coli carrying the colicin plasmid pColE3-CA38. *Plasmid* **77**, 7–16 (2015).
66. Pagano, J. M., Clingman, C. C. & Ryder, S. P. Quantitative approaches to monitor protein-nucleic acid interactions using fluorescent probes. *Cold Spring Harbor Laboratory Press*, 14–20 (2011).
67. Von Bronk, B. *Stochastic processes and interaction dynamics in bacterial competition* PhD thesis (Ludwig-Maximilians-Universität München, Oct. 2018).
68. Gray, L. A mathematician looks at Wolfram’s new kind of science. *Notices-American Mathematical Society* **50**, 200–211 (2003).
69. Walser, H. *Statistik für Naturwissenschaftler* 1. Auflage (Haupt Bern, 2011).
70. Vimberg, V., Tats, A., Remm, M. & Tenson, T. Translation initiation region sequence preferences in Escherichia coli. *BMC molecular biology* **8**, 100 (2007).
71. Weilbacher, T. *et al.* A novel sRNA component of the carbon storage regulatory system of Escherichia coli. *Molecular Microbiology* **48**, 657–670 (2003).
72. Lechner, M., Schwarz, M., Opitz, M. & Frey, E. Hierarchical Post-transcriptional Regulation of Colicin E2 Expression in Escherichia coli. *PLoS Computational Biology* **12**, 1–20 (2016).
73. Lechner, M. F. *Stochasticity and Heterogeneity in Growing Bacterial Populations* PhD thesis (Ludwig-Maximilians-Universität München, 2017).
74. Taniguchi, Y. *et al.* Quantifying E. coli proteome and transcriptome with single-molecule sensitivity in single cells. *Science* **329**, 533–539 (2010).
75. Dickey, T. H., Altschuler, S. E. & Wuttke, D. S. Single-stranded DNA-binding proteins: Multiple domains for multiple functions. *Structure* **21**, 1074–1084 (2013).
76. Mu Ya Liu, Yang, H. & Romeo, T. The product of the pleiotropic Escherichia coli gene csrA modulates glycogen biosynthesis via effects on mRNA stability. *Journal of Bacteriology* **177**, 2663–2672 (1995).

-
77. Kamensek, S. *et al.* Silencing of DNase Colicin E8 Gene Expression by a Complex Nucleoprotein Assembly Ensures Timely Colicin Induction. *PLOS Genetics* **11**, e1005354 (2015).
 78. Gudapaty, S. *et al.* Regulatory Interactions of Csr Components : the RNA Binding Protein CsrA Activates *csrB* Transcription in *Escherichia coli*. *Journal of Bacteriology* **183**, 6017–6027 (2001).
 79. Liu, M. Y. & Romeo, T. The global regulator CsrA of *Escherichia coli* is a specific mRNA-binding protein. *Journal of bacteriology* **179**, 4639–42 (1997).
 80. Pugsley, a. P. & Schwartz, M. Colicin E2 release: lysis, leakage or secretion? Possible role of a phospholipase. *The EMBO journal* **3**, 2393–2397 (1984).
 81. Pugsley, a. P., Goldzahl, N. & Barker, R. M. Colicin E2 production and release by *Escherichia coli* K12 and other Enterobacteriaceae. *Journal of general microbiology* **131**, 2673–2686 (1985).
 82. James, R., Kleanthous, C. & Moore, G. R. The biology of E colicins: Paradigms and paradoxes. *Microbiology* **142**, 1569–1580 (1996).
 83. Pugsley, A. P. Autoinduced synthesis of colicin E2. *MGG Molecular & General Genetics* **190**, 379–383 (1983).
 84. Mavridou, D. A., Gonzalez, D., Kim, W., West, S. A. & Foster, K. R. Bacteria Use Collective Behavior to Generate Diverse Combat Strategies. *Current Biology* **28**, 345–355.e4 (2018).
 85. Nedialkova, L. P. *et al.* Temperate phages promote colicin-dependent fitness of *Salmonella enterica* serovar Typhimurium. *Environmental Microbiology* **18**, 1591–1603 (2016).
 86. Van Raay, K. & Kerr, B. Toxins go viral: Phage-encoded lysis releases group B colicins. *Environmental Microbiology* **18**, 1308–1311 (2016).
 87. Micenková, L. *et al.* Colicin Z, a structurally and functionally novel colicin type that selectively kills enteroinvasive *Escherichia coli* and *Shigella* strains. *Scientific Reports* **9**, 1–12 (2019).
 88. Šmajš, D. & Weinstock, G. M. Genetic organization of plasmid ColJs, encoding colicin Js activity, immunity, and release genes. *Journal of Bacteriology* **183**, 3949–3957 (2001).

89. Sanchez, A., Choubey, S. & Kondev, J. Regulation of Noise in Gene Expression. *Annual Review of Biophysics* **42**, 469–491 (2013).
90. Raj, A., Rifkin, S. A., Andersen, E. & Van Oudenaarden, A. Variability in gene expression underlies incomplete penetrance. *Nature* **463**, 913–918 (2010).
91. Suzuki, K., Babitzke, P., Kushner, S. R. & Romeo, T. Identification of a novel regulatory protein (CsrD) that targets the global regulatory RNAs CsrB and CsrC for degradation by RNase E. *Genes and Development* **20**, 2605–2617 (2006).
92. Dacheux, E. *et al.* Translation initiation events on structured eukaryotic mRNAs generate gene expression noise. *Nucleic Acids Research* **45**, 6981–6992 (2017).
93. Romeo, T. Global regulation by the small RNA-binding protein CsrA and the non-coding RNA molecule CsrB. *Molecular Microbiology* **29**, 1321–1330 (1998).
94. Vassilieva, I. M. & Garber, M. B. The regulatory role of the Hfq protein in bacterial cells. *Molecular Biology* **36**, 785–791 (2002).
95. Valentin-Hansen, P. *Structure, function and RNA binding mechanisms of the prokaryotic Sm-like protein hfq* 147–162 (Springer, 2012).
96. Edri, S. & Tuller, T. Quantifying the effect of ribosomal density on mRNA stability. *PLoS ONE* **9** (2014).
97. Jones, D. L., Brewster, R. C. & Phillips, R. Promoter architecture dictates cell-to-cell variability in gene expression. *Science* **346**, 1533–1536 (2014).
98. Carey, J. N. & Goulian, M. A bacterial signaling system regulates noise to enable bet hedging. *Current Genetics*, 1–6 (2018).
99. Flemming, H. C. & Wingender, J. The biofilm matrix. *Nature Reviews Microbiology* **8**, 623–633 (2010).
100. Stewart, P. S. Mechanisms of antibiotic resistance in bacterial biofilms. *International Journal of Medical Microbiology* **292**, 107–113 (2002).
101. Høiby, N., Bjarnsholt, T., Givskov, M., Molin, S. & Ciofu, O. Antibiotic resistance of bacterial biofilms. *International Journal of Antimicrobial Agents* **35**, 322–332 (2010).
102. Grumbein, S., Opitz, M. & Lieleg, O. Selected metal ions protect *Bacillus subtilis* biofilms from erosion. *Metallomics : integrated biometal science* **6**, 1441–50 (2014).

-
103. Klotz, M. *et al.* Importance of the biofilm matrix for the erosion stability of *Bacillus subtilis* NCIB 3610 biofilms. *RSC Advances* **9**, 11521–11529 (2019).
 104. Kesel, S. *et al.* Matrix composition determines the dimensions of *Bacillus subtilis* NCIB 3610 biofilm colonies grown on LB agar. *RSC Adv.* **7**, 31886–31898 (2017).
 105. Hall-Stoodley, L., Costerton, J. W. & Stoodley, P. Bacterial biofilms: From the natural environment to infectious diseases. *Nature Reviews Microbiology* **2**, 95–108 (2004).
 106. Aris, A. Z., Kam, R. C. Y., Lim, A. P. & Praveena, S. M. Concentration of ions in selected bottled water samples sold in Malaysia. *Applied Water Science* **3**, 67–75 (2013).
 107. Gupta, P., Sarkar, S., Das, B., Bhattacharjee, S. & Tribedi, P. Biofilm, pathogenesis and prevention—a journey to break the wall: a review. *Archives of Microbiology* **198**, 1–15 (2016).
 108. Irsfeld, M., Prüß, B. M. & Stafslie, S. J. Screening the mechanical stability of *Escherichia coli* biofilms through exposure to external, hydrodynamic shear forces. *Journal of Basic Microbiology* **54**, 1403–1409 (2014).
 109. Falcón García, C. *et al.* Topographical alterations render bacterial biofilms susceptible to chemical and mechanical stress. *Biomaterials Science* (2019).
 110. Kilian, M. *et al.* The oral microbiome - An update for oral healthcare professionals. *British Dental Journal* **221**, 657–666 (2016).
 111. Eriksson, L., Lif Holgersson, P. & Johansson, I. Saliva and tooth biofilm bacterial microbiota in adolescents in a low caries community. *Scientific Reports* **7**, 1–12 (2017).
 112. Fuhrman, J. A., Cram, J. A. & Needham, D. M. Marine microbial community dynamics and their ecological interpretation. *Nature Reviews Microbiology* **13**, 133–146 (2015).
 113. Grilli, J., Barabás, G., Michalska-Smith, M. J. & Allesina, S. Higher-order interactions stabilize dynamics in competitive network models. *Nature* **548**, 210–213 (2017).

Danksagung

Ich möchte mich nun bei allen bedanken, die mich in den letzten Jahren meiner Doktorarbeit unterstützt haben, ganz besonders bei...

...**PD Dr. Madeleine Opitz** für die großartige Betreuung, dein Organisationstalent, die ständige Motivation und Unterstützung. Vor allem auch dafür das du immer für die Arbeitsgruppe da warst, auch wenn du super viel zu tun hattest und andere Verpflichtungen hattest.

...**Prof. Dr. Joachim Rädler** für die Möglichkeit die Doktorarbeit hier am Lehrstuhl in einer so tollen Atmosphäre schreiben zu können.

...**Prof. Dr. Erwin Frey** und **Prof. Oliver Lieleg** für die tolle Zusammenarbeit in unseren Kollaborationen. Vielen Dank auch an **Matthias Lechner** für die Kollaboration, die unser Paper erst so richtig komplett gemacht hat. And thank you **Caro** for the nice collaboration on the biofilm project.

...der gesamten **AG Opitz** und vor allem allen Master- und Bachelorstudenten, HiWis und Praktikanten. Ich habe so viel gelernt durch euch und hoffe ihr hattet ebenso viel Freude an der gemeinsamen Zeit im Labor und drumherum, wie ich es mit euch hatte!

...**Benedikt** für die tolle Einführung in die theoretischen Aspekte unserer Forschung und die Entspanntheit im Labor, wenn ich mal wieder Hektik verbreitet habe.

...**Gerlinde, Susi** und **Charlott** - danke, dass ihr immer eine offene Tür hattet, ohne euch würde der Lehrstuhl niemals so rund laufen.

...dem gesamten **Lehrstuhl** für das tolles Arbeitsklima. Meinen **Bürokollegen** für die entspannte Stimmung und vor allem **Daniel**, dass du immer all die IT-Fragen beantworten konntest und die vielen Besprechungen dir nie zu viel waren.

Außerdem möchte ich mich bei meinen Freunden und meiner Familie bedanken. Zunächst meiner **Mutter**, die mich immer unterstützt und mich zu dem Menschen gemacht hat, der ich heute bin. Meiner **Schwester Stefanie**, die mir wirklich jederzeit mit Rat und Tat zur Seite steht, vor allem jetzt in der Endphase der Doktorarbeit bei der Korrektur der Doktorarbeit, trotz des eigenen Stresses. Meinem Freund **Alexander**, du bist seit mehr als 11 Jahre mein Ruhepol und bester Freund. Meinen **Strick-Omis**, vielen Dank für die erholenden Abende und langen Gesprächsrunden, egal ob beim Basteln oder Kochen, mit euch ist es immer toll.

